DEVELOPMENT OF NANOTECHNOLOGY-BASED DRUG DELIVERY AND IMAGING SYSTEM TO THE WHITE ADIPOSE TISSUE VASCULATURE USING WISTAR RAT MODEL

Ntevheleni Thovhogi

A thesis submitted in fulfilment of the requirements for the degree of
Philosophiae Doctor in the Faculty of Science
Department of Biotechnology
University of the Western Cape

Supervisor: Dr Abram M Madiehe
Co-supervisor: Dr Mervin M Meyer

May 2013

DST/MINTEK
N!C
Nanotechnology Innovation Centre

MRC
SOUTH AFRICA
SOUTH AFRICAN MEDICAL RESEARCH COUNCIL

ABSTRACT

Development of nanotechnology-based drug delivery and imaging systems to the white adipose tissue vasculature using a Wistar rat model

N. Thovhogi

PhD thesis, Department of Biotechnology, Faculty of Science, University of the Western Cape

Obesity is a complex metabolic disease of excessive fat accumulation. It is a worldwide epidemic affecting billions of people and its pharmacological management is hampered by drug toxicity and undesirable side effects. Therefore, a need still exists for the development of safe medication for treatment of obesity. Nanotechnology involves the use of small particles at atomic and molecular scale. It has application in medical diagnostics, drug delivery and molecular imaging. Various nanoparticles (NPs) functionalized with different biomolecules have been successfully used in many therapeutic and research applications due to their versatility, ease of chemical synthesis, low toxicity and unique properties. Examples of NPs used in this study are Gold nanoparticles (GNPs) and Quantum dots (QDs). GNPs and QDs are extensively used as drug delivery, labelling and imaging tools in biomedical research.

Nanotechnology offers a new potential useful avenue for solving the problem of toxicity of anti-obesity drugs. This could be achieved through targeted drug delivery. In this study, rats were fed a high fed diet (HFD) to induce obesity. The streptavidin conjugated GNPs and QDs were functionalized with biotinylated adipose-homing

peptide (AHP) and/or anti-obesity drug (Gallic acid). Functionalization was characterized using agarose gel electrophoresis, UV-vis spectroscopy and transmission electron microscopy. The binding-specificity and targeting ability of AHP was evaluated *in vitro* and *in vivo*. The apoptotic effect of AHP functionalized-drug loaded GNPs (AHP-GA-GNPs) was tested *in vitro* using APOP*ercentage* ^{TM} and Caspase-3 activation assays.

The *in vitro* data indicated that the binding was specific to prohibitin (PHB) expressing cells (MCF-7 and Caco-2), and that the binding was temperature dependent. PHB was confirmed as a target for AHP after overlaying AHP-FITC and anti-prohibitin antibody staining. Cellular uptake was detected on the cells treated with AHP-functionalized NPs as compared to unfunctionalized NPs. The GA and AHP-GA-GNPs reduced cellular viability and induced apoptosis through activation of Caspase-3. The *Ex-vivo* studies using primary endothelial cells (ECs) isolated from the WAT of lean and obese Wistar rats showed that the binding of AHP was receptor mediated, and specific to receptors differentially expressed in ECs from obese WAT.

The *in vivo* studies showed that, treatment of obese rats with AHP-functionalized NPs resulted in targeted delivery of the NPs to the WAT as compared to those treated with unfunctionalized NPs. Qualitative analysis using fluorescence microscopy and IVIS Luminar XR, live-imaging system showed that the unfunctionalized NPs accumulated mostly in the organs of the reticuloendothelial system, namely: liver, spleen, lungs and kidneys. In contrast, AHP-functionalized NPs accumulated mostly in the WATs as compared to the rest of the organs of the obese rats. Uptake and binding of the NPs

to the tissues was quantitatively confirmed by the inductive coupled plasma-optical emission spectroscopy (ICP-OES).

In conclusion, this study reports the 1) successful functionalization of GNPs and QDs with AHP, 2) use of AHP-functionalized GNPs and QDs as delivery and imaging agents to the WAT, and 3) potential use of AHP-functionalized drug-loaded GNPs in the treatment of obesity.

KEYWORDS:

Obesity; White adipose tissue; Nanotechnology; Drug delivery; Targeting peptides; Live imaging; Gold nanoparticles; Quantum dots; Gallic acid; Anti-obesity.

UNIVERSITY *of the*
WESTERN CAPE
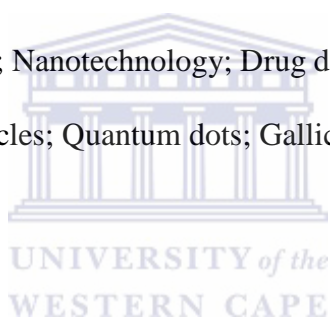
May 2013

University of the Western Cape

Private Bag X17, Bellville 7535, South Africa

Telephone: +27-21- 959 2255/959 2762

Fax: +27-21- 959 1268/2266

UNIVERSITY *of the*
WESTERN CAPE

FACULTY OF NATURAL SCIENCE

PLAGIARISM DECLARATION

I declare that ***Development of nanotechnology based drug delivery and imaging system to the white adipose tissue vasculature using a Wistar rat model*** is my own work, that it has not been submitted for any degree or examination in any other university and that all the sources I have used or quoted have been indicated and acknowledged by complete references.
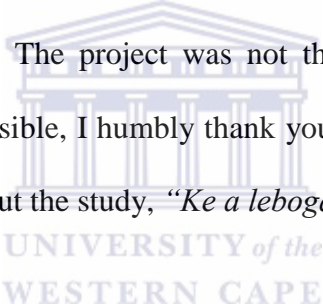
Ntevheleni Thovhogi   **10** May 2013

Signed ……………………………

xx

ACKNOWLEDGEMENTS

I would like to express my sincere gratitude for the valuable assistance I received from the following people. Their contributions towards the success of this study were perceived.

- ❖ *Above all, I want to acknowledge God almighty for giving me strength, wisdom, good health and his everlasting love, "To God be the Glory".*

- ❖ Dr Abram Madiehe, Thank you for your supervision, mentoring and motivations. I learned a lot from you, not only in the lab but also in my personal development. The project was not the easiest, but you pulled me through to make it possible, I humbly thank you for the guidance and support you provided throughout the study, *"Ke a leboga"*

- ❖ Dr Mervin Meyer, Thank you for your motivations, inputs, guidance and encouragements. Your belief in me and commitment to my success have been invaluable.The opportunity of letting me explore and network with other researchers, local and international is also acknowledged, *"Baie dankie"*.

- ❖ Dr Amanda Skepu, I thank you for the wonderful work you did towards the accomplishment of this study. You were such a passionate supporter and an honest source of feedback, your guidance and mentoring contributed immensely.

- ❖ Dr Martin Onani, I want to thank you for your encouragement, motivations and guidance.

- ❖ Mrs Peggy Mobo. I thank you for all the guidance and assistance throughout the study, especially your assistance with animal experiments, I greatly appreciate it.

- ❖ Joritha van Heerden and Elizabeth Bok, thank you for taking care of the animals. All the maintenance and animal experiments were possible because of your assistance.

- ❖ Mr Andrew Tomboer, Eloise Braaf and Bridget Daniels, your administrative skills towards this project did not go unrecognized. You never said "no" when I needed help, and for that I say thank you.

- ❖ To my fellow students: Nicole Sibuyi, Kwazi Gabuza, Paul Mushonga, Rumbidzai Mudzonga, Mustafa Drah, Margaret Mazyambe, Ira Fortuin and Charlene Kimar. Thank you for all the support and motivations. Working with you guys was a wonderful experience.

- ❖ To the colleagues at the Medical Research Council (MRC), Diabetes Research Group and Nanotechnology Innovation Centre (NIC), University of the Western Cape, Biolabel Unit, the past and present, your support, motivations and encouragements was recognized. You were such a wonderful group, thank you so much.

May God richly bless you all!

CONFERENCE CONTRIBUTIONS

1. **Ntevheleni Thovhogi,** Mervin Meyer, Abram Madiehe, Imaging of white adipose tissue using peptide functionalized gold NPs and quantum dots, the 3rd DST/Mintek, Nanotechnology Innovation Center (NIC) Annual Conference, New Life Science Building Auditorium, University of the Western Cape, South Africa, 22-23 November 2010, **Oral Presentation (1st prize, PhD category)**.

2. **Ntevheleni Thovhogi,** Mervin Meyer, Abram Madiehe, *In vivo* vascular targeting and imaging of the white adipose tissue using peptide functionalized NPs, Faculty of Science, Annual Biotechnology open day, University of the Western Cape (UWC), South Africa, 3rd September 2011, **Oral presentation.**

3. Abram Madiehe, **Ntevheleni Thovhogi,** Mervin Meyer, Targeted delivery to and imaging of white adipose tissue using peptide-functionalized gold NPs and quantum dots, Fourth European Foundation for Clinical Nanomedicine (CLINAM) Conference, Messeplatz 21, Basel, Switzerland, 23-25 May 2011, **Poster presentation.**

4. **Ntevheleni Thovhogi,** Mervin Meyer, Abram Madiehe, Vascular targeting and imaging of the white adipose tissue using peptide functionalized quantum dots, Medical Research Council (MRC) Research day, Cape Town, South Africa, Auditorium, South Africa, 19-20 October 2011, **Oral presentation.**

5. **Ntevheleni Thovhogi,** Mervin Meyer, Abram Madiehe, Biodistribution and imaging of white adipose tissue using peptide functionalized gold NPs and quantum dots, the 4th DST/Mintek, Nanotechnology Innovation Center (NIC) Annual Conference, Mintek Auditorium, Johannesburg, South Africa, 22-23 November 2011, **Oral presentation.**

6. **Ntevheleni Thovhogi,** Mervin Meyer, Abram Madiehe, Imaging and Biodistribution of Peptide Functionalized Quantum Dots in the White Adipose Tissue Vasculature, South African Nanotechnology initiative (SANI), Nano Africa 2012, The 4th International conference of nanoscience and nanotechnology, University of Free State, Bloemfontein, South Africa,1-4th April, 2012, **Poster presentation (1st prize, PhD category).**

7. **Ntevheleni Thovhogi,** Mervin Meyer, Abram Madiehe, Biodistribution and vascular targeting of the white adipose tissue using peptide functionalized NPs. The 6th international conference of Nanotoxicology, Beijing china**,** 4-7th September 2012**, Poster presentation.**

8. **Ntevheleni Thovhogi,** Mervin Meyer, Abram Madiehe, Biodistribution and vascular targeting of the white adipose tissue using peptide functionalized NPs, the 5th DST/Mintek, Nanotechnology Innovation Center (NIC) Annual Conference, Medical Research Council (MRC), Cape Town, South Africa, 21-22nd September 2012, **Poster presentation (Complementary award, PhD category).**

DEDICATION

This thesis is dedicated to my family

A winner never quits, and a quitter never wins!

"If you cannot do great things yourself, remember you may do small things in a great way"

"NAPOLEON HILL"

TABLE OF CONTENTS

LIST OF FIGURES

CHAPTER 1

CHAPTER 2

CHAPTER 3

CHAPTER 4

CHAPTER 5

UNIVERSITY *of the*

WESTERN CAPE

LIST OF TABLES

CHAPTER 1

CHAPTER 2

CHAPTER 4

ABBREVIATIONS

%	Percentage
μ	Micro
μL	Microlitre
Abs	Absorbance
ACC	Acetyl CoA carboxylase
ADAMTS	A disintegrin and metalloproteinase with thrombospondin motifs
AHP	Adipose homing peptide
Au	Gold
BAT	Brown adipose tissue
BMI	Body mass index
BPD-DS	Biliopancreatic duodenal switch
BSA	Bovine serum albumin
CASPASE	Cysteine aspartic acid-specific proteases
CCD	Charged-coupled device
Cd	Cadmium
CdS	Cadmium Sulphide
CdSe	Cadmium selenide
CHO	Chinese Hamster Ovary
Conc	Concentration
CTAB	Cetyl trimethyl ammonium bromide
CVD	Cardiovascular diseases

DAPI	Diamidino-2-phenylindole
DHLA	Dihydrolipoic acid
dL	Decilitre
DR	Diet resistance
DMEM	Dulbecco's Modified Eagle Medium
DMSO	Dimethylsulphoxide
EC	Endothelial cell
ECs	Endothelial cells
EDC-	1-Ethyl-3-(3-dimethylaminopropyl)carbodiimide
EDTA	Ethylenediaminetetraacetic acid
EGF	Endothelial growth factor
ELISA	Enzyme linked immuno sorbent assay
EPI	Epididymal
FA	Fatty acid
FACS	Fluorescence activated cell sorter
FAS	Fatty acid synthase
FBS	Foetal Bovine serum
FDA	Food and Drug Administration
FFA	Free fatty acid
FGF	Fibroblast growth factor
FITC	Fluorescein isothiocyanate
FSC	Forward scatter
g	Gram
GA	Gallic acid

GNPs	Gold nanoparticles
HDL	High density lipoprotein
HF	High fat
HFD	High fat diet
HGF	Hepatocytes growth factor
HIV	Human immunodeficiency virus
hr	Hour
ICP-MS	Inductively coupled plasma-mass spectroscopy
ICP-OES	Inductively coupled plasma-optical emission spectroscopy
IL-6	Interleukin-6
LAGB	Laparoscopic gastric banding
LF	Low fat
LSG	laparoscopic sleeve gastrectony
ME	Malic enzyme
Mes	Mesenteric
Min	Minute
MMP	Matrix metalloproteinases
MPS	Mononuclear phagocytic system
MRC	Medical Research Council
MS	Mass Spectroscopy
NaCl	Sodium chloride
NEFA	Non-esterified fatty acid
NPs	Nanoparticles

°C	Degree Celsius
OD	Optical density
PBS	Phosphate buffered saline
PDGF	Platelet-derived growth factor
PECAM-1	Platelet endothelial cell adhesion molecule-1
PEG	Poly ethylene glycol
PEG-SH	Thiolated poly ethylene glycol
Peri	Perirenal
PERI	Perirenal
pH	Potential of hydrogen
PHB	Prohibitin
PHB-1	Prohibitin-1
PHB-2	Prohibitin-2
PIGF	Placental growth factor
PL	Photoluminescence
QDs	Quantum dots
RES	Reticuloendothelial system
Retro	Retroperitoneal
RIRC	Research and International Relations Committee
RT	Room temperature
RYGP	Roux-en-Y gastric bypass
SMCC	Succinimidyl-4-(*N*-maleimidomethyl)cyclohexane-1-carboxylate
SPR	Surface plasmon resonance

SQ	Subcutaneous
SSC	Side scatter
STV	Streptavidin
TBE	Tris-borate-EDTA
TBE	Tris borate EDTA
TEM	Transmission electron microscopy
TF	Tissue factor
TGF	Transforming growth factor
TGs	Triglycerides
TNF-α-	Tumor necrosis factor-α
TSP	Thrombospondin
UVP	Ultra-violet products
UV-Vis	Ultraviolet-visible
V	Volts
v/v	Volume per volume
VEGF	Vascular endothelial growth factor
WAT	White adipose tissue
WC	Waist circumference
WHpR	Waist to hip ratio
WHR	Waist to height ratio
WST-1	Water soluble tetrazolium-1
ZnS	Zinc sulphide

CHAPTER 1

1. Literature review

1.1 Obesity

Obesity is a complex metabolic disease of excessive fat accumulation in adipose tissue (Belsing and Rasmussen, 2004; Kissler and Settmacher, 2013). It is a worldwide epidemic affecting billions of people and now recognized as a major public health problem in industrialized as well as in developing countries (Langin, 2006; Kissler and Settmacher, 2013). It occurs through a long-standing imbalance between energy intake and energy expenditure, which leads to the excess accumulation of fat in various adipose tissues and organs (Belsing and Rasmussen, 2004; Bertolini *et al*., 2012).
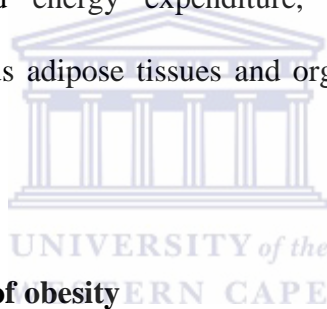
1.2. Causes and prevalence of obesity

Obesity is caused by the accumulation of adipose tissue to excess and to an extent that impairs both physical and psychosocial health. It is characterized by increased storage of fatty acids in an expanded adipose tissue mass (Galic *et al*., 2009). Obesity is caused by either genetic or environmental factors (Dubnov *et al*., 2003; Loos and Bouchard, 2003; Phan-Hug *et al*., 2012). The environmental factors include consumption of high fat diets, lack of physical exercise, and psychological factors. To date, about 250 chromosome loci found on all but the Y chromosome are thought to influence the genetic predisposition for obesity (Dubnov *et al*., 2003). The growing prevalence of obesity is apparently not due to genetic changes, but rather to the

environmental effects acting on a genetic susceptibility. The obsession of getting 'more for their money' leads consumers to increase food intake. The palatability of high fat foods leads to a higher caloric intake for the same portion size. These factors combine to increase total energy intake throughout the day, (Rosmond and Bjontore, 2000; Dubnov *et al*., 2003; Lavie *et al*., 2009). Obesity is a major health problem in developed countries, and is rapidly becoming an important health problem in developing countries (Dizdar and Alyamac, 2004).

In 2005, prevalence of obesity in developed countries, such as the United States, was as high as 26.6 % in men and 32.2 % in women above age 20 years (Goedecke *et al*., 2005). In 2010, the World Health Organisation (WHO) showed that, 400 million adults were classified as obese and 1.6 billion as overweight worldwide (WHO, 2010). The WHO, also predict that by 2015, approximately 2.3 billion adult will be overweight and more than 700 million will be obese (WHO, 2006). Presently, WHO projects that by 2025, 60 % of death worldwide will be caused by obesity related diseases (WHO, 2010). The prevalence of obesity among children, adolescents and adults has been dramatically increasing during the last decades. Thus, obesity is acquiring the characteristics of an authentic pandemia and it has been recognized as one of the major global health problems (Mokdad *et al*., 2003 and Huxley *et al*., 2010).

Table 1.1 shows obesity epidemic in both adult males and female worldwide. Globally, women are generally more prone to becoming obese than men (WHO, 2010). The prevalence of obesity (Body mass index (BMI) $\geq$ 30 kg/m^2) and overweight (BMI = 25 – 29.9 kg/m^2) has been increasing steadily since the past

decade in both males and females (Racette *et al*., 2003). It was estimated in 2010, that the prevalence of obesity for adults (>15 years) was higher in the USA for males and females with 44.2 % and 48.3 %, respectively. However, obesity is not only a problem of developed countries but is becoming an increasing problem in countries undergoing epidemiological transition, such as South Africa, Mexico and South American countries (Goedecke *et al*., 2005). In South Africa, 68.5 % and 36.8 % of women were considered overweight and obese, while 39.3 % and 7.6 % of men were overweight and obese respectively (WHO, 2010). However, obesity and its co-morbidities negatively affect the lives of many South Africans and the consequent burden of disease contributes to the increasing cost of health care, both at a state level and in the private sector (Goedecke *et al*., 2005).

UNIVERSITY *of the*
WESTERN CAPE

Table 1.1. Obesity rates among adults and epidemiology of obesity worldwide.

The OECD Health Data 2011; (http://dx.doi.org/10.1787/888932523956)
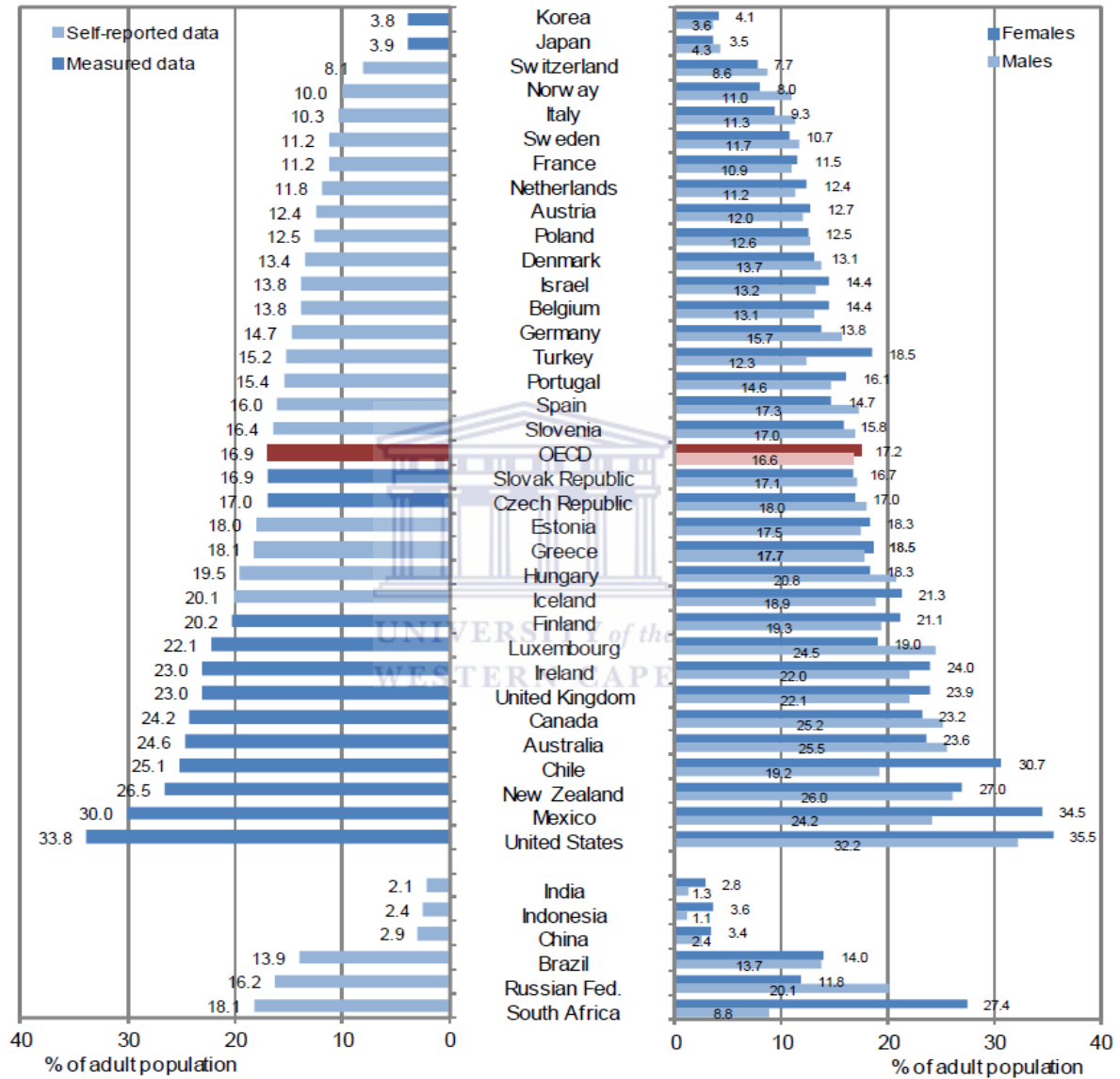
1.3. Measurement of obesity

Measures of central adiposity, namely waist circumference (WC), waist-to-hip ratio (WHpR), a newly described index and a waist to- height ratio (WHR), have been adopted as more accurate predictors of obesity-related cardiovascular risk and have replaced Body mass index (BMI) in several ways for clinical diagnosis of metabolic syndrome (Lavie *et al*., 2009; Sahin *et al*., 2011).

1.3.1. Body mass index (BMI)

Obesity is a result of excess body fat. A simple and useful measure to define obesity is the ratio of weight and height squared (kg/m^2) known as the BMI (Lavie *et al*., 2009). Presently, approximately 2.8 million adult deaths are associated with pathological BMI increase, bringing excess obesity to the fifth leading life threat. The BMI is the indicator most commonly used for determining obesity. It is used to define severity of overweight and obesity across populations. A BMI can be categorized as underweight (≤ 18.5 kg/m^2), normal weight (18.5 to 24.9 kg/m^2), overweight (25 to 29.9 kg/m^2), obese (30 to 34.9 kg/m^2), or severely obese (>35 kg/m^2) (Formiguera and Canton, 2004; Leitzmann *et al*., 2006; Lavie *et al*., 2009; Kissler and Settmacher, 2013)

Table 1.2. Classification of BMI

(Formiguera and Canton, 2004; Leitzmann *et al*., 2006)

BMI range – kg/m^2	Classification	Health Risk
<18.5	Underweight	Risk of developing problems such as nutritional deficiency and osteoporosis
18.5 -24.9	Normal	Low Risk (healthy range)
29-29.9	Overweight	Moderate risk of developing heart disease, high blood pressure, stroke, diabetes
>30.0-34.9	Obesity I	High risk of developing heart disease, high blood pressure, stroke, diabetes
35-39.9	Obesity 11	High risk of developing heart disease, high blood pressure, stroke, diabetes
>40	Extreme obesity	High risk of developing heart disease, high blood pressure, stroke, diabetes

1.3.2. The waist circumference

There are two main types of obesity regarding the fat distribution pattern: **Android or central obesity,** with the majority of fat depots located in the abdominal area, thus both subcutaneous and visceral, and **Gynoid or peripheral obesity** where the fat depots are mainly located subcutaneously in the lower body (hips and lower extremities). The difference between both types is fundamental, because the metabolic and cardiovascular complications of obesity are almost exclusively related to visceral fat depots. Because of its high correlation with visceral adipose tissue (Despres *et al*., 2001; Sahin *et al*., 2011), a measure as simple as the waist circumference is a good way to assess cardiovascular risk. A waist girth over **88 cm** for women and above **102 cm** for men indicates a high cardiovascular risk (Formiguera and Canton, 2004).

1.3.3. The waist-to-hip ratio (WHpR)

The WHpR is still a useful measure to be considered in obesity evaluation (Lavie *et al*, 2009), although its use has decrease during the last five or seven years as a measure of fat distribution. In patients with severe and very severe forms of obesity (class II and III obesities), with waist circumferences clearly beyond the upper risk limits, the WHpR is the best way to evaluate the fat distribution pattern, (Formiguera and Canton, 2004; Kissler and Settmacher, 2013)

1.4. Obesity as a health risk factor of other diseases

Unhealthy diet and physical inactivity can contribute to many chronic diseases and conditions. The increases in overweight and obesity in adults are widely projected to continue to heighten the burden of obesity-related morbidity and mortality in the coming decades (Swinburn *et al*., 2011). Obesity is associated with hyperinsulinemia, insulin resistance and abnormalities in lipid metabolism (Konyanda *et al*., 1997; Kahn and Flier, 2000; Qatanani and Lazar, 2007; Lavie *et al*., 2009).

As shown in Figure 1.1, obesity is strongly associated with a number of chronic diseases: hyperlipidemia, hypertension, diabetes (type 2 diabetes), coronary atherosclerotic heart disease, gout, restrictive lung disease, gall bladder disease, cancer, degenerative arthritis, infertility and cancer which includes uterine, breast, gallbladder, colon and prostate cancer, (Sidik and Ahmad, 2004). It is also associated with metabolic abnormalities such as impaired glucose tolerance, dyslipidaemia with elevated triglyceride levels, decreased high-density lipoprotein (HDL), cholesterol concentration and increased proportion of small dense lipoparticles (Prieto-Hontoria *et al*., 2011). Therefore, health consequences of obesity are huge and varied, ranging from an increased risk of premature death to several non-fatal but debilitating diseases that have adverse effects on quality of life (Lavie *et al*., 2009; Prieto-Hontoria *et al*., 2011).
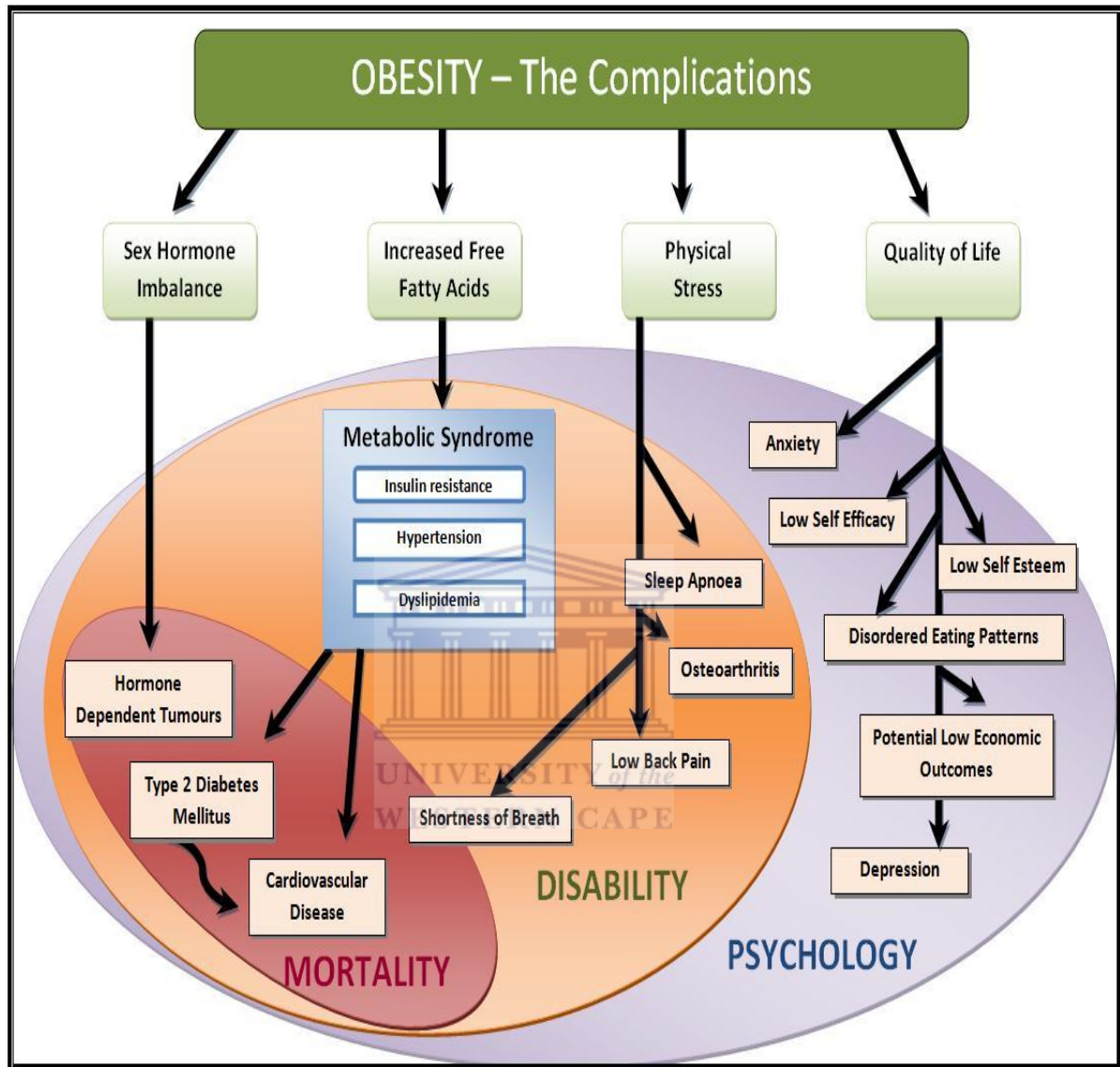
Figure 1.1. Schematic representation for obesity complications.

The figure shows obesity as a health risk factor for chronic disease of lifestyle (http://health-care-org.blogspot.com/2013/01/being-modest-obese-might-not-present.html)

1.5. Management of obesity

Obesity cannot be cured, but only managed (Dubnov *et al*., 2003). The conventional management of obesity includes lifestyle modification, pharmacotherapy (antiobesity drugs) and surgery. Management of obesity starts with comprehensive lifestyle management (i.e, healthy diet, physical activity and behavior modification) (Sidik and Ahmad, 2004; Phan-Hug *et al*., 2012).

1.5.1. Behavioural changes, physical activity and healthy diet

As obesity cannot be cured, there is a need for life-long changes in certain habits; behavior has a major role in the maintenance of the newly reduced body weight. The goal of changing everyday behavior is to reduce food intake and increase energy loss. A major cause for the weight gain is again lack of sufficient physical activity (Dubnov *et al*., 2003). Increased physical activity is therefore an important component of lifestyle modification (Donnelly *et al*.,2004) The type of exercise recommended for weight loss is aerobic, such as walking, jogging, swimming, cycling and aerobic dancing (Dubnov *et al*, 2003; Phan-Hug *et al*., 2012). Healthy diet and exercise is the most natural, but not always the easiest.   The food pyramid for healthy diet is indicated in Figure 1.2.
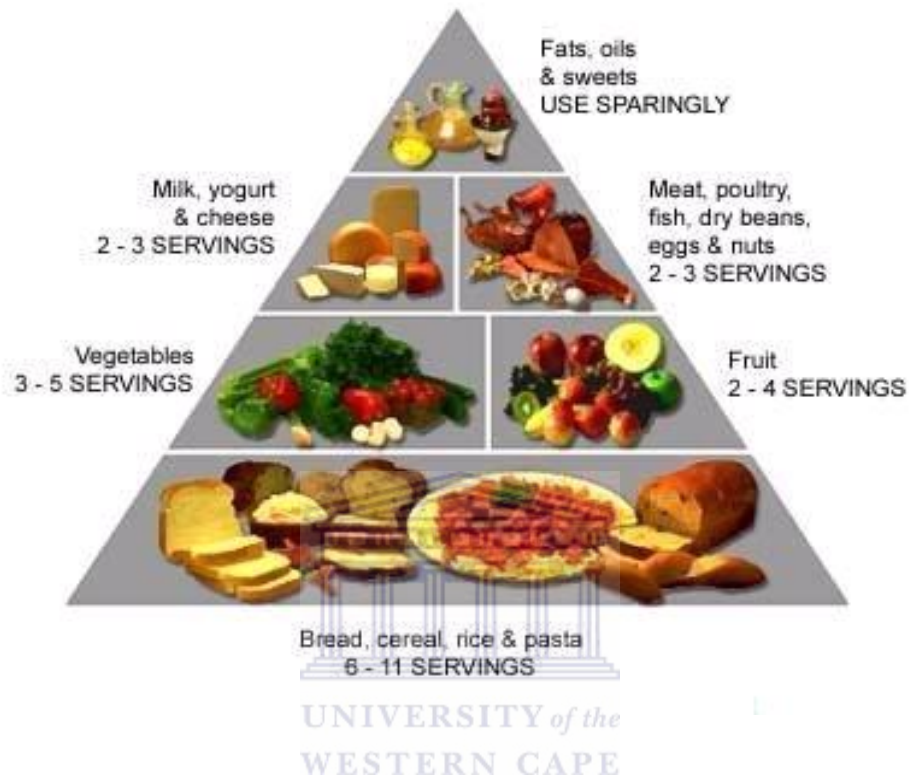
Figure 1.2. The food pyramid, for healthy diet.

The figure represents the food guide pyramid for the recommended intake for each food group (http://sharnyandjulius.com/healthy-food-pyramid-is-making-you-fat/).

1.5.2. Pharmacological treatment

When lifestyle interventions do not induce sufficient weight loss, it may be necessary to add a pharmacologic agent to the treatment regimen. However, it has been recommended that pharmacotherapy should not be initiated without concomitant lifestyle modifications. Anti-obesity medications as listed in Table 1.3, should be used as part of a comprehensive weight loss program that includes diet and physical activity for obese patients, and for those with a BMI >27 kg/m^2 (Claphan *et al*., 2001). Several anti-obesity drugs have been marketed with mechanisms of action targeting various physiological processes including calorie absorption, appetite control, and metabolism (Bray and Greenway, 2007; Arkinson, 1997). Thus far, all have been associated with side-effects spanning from insomnia and depression to potentially lethal cardiotoxicity (Elangbam, 2009). As a result, many of these drugs have been withdrawn (dexfen-fluramine, sibutramine, rimonabant) or restricted in their applications.

However, to date, the number of drugs approved for the treatment of obesity is very limited. Currently, there are virtually no truly effective anti-obesity drugs approved by Unites States Food and Drug Administration (FDA). Orlistat is a lipase inhibitor that has been demonstrated to reduce fat absorption in humans by an impressive 30 % (Bray and Greenway, 2007). Unfortunately, there are gastrointestinal side effects associated with Orlistat and weight loss of 5 % is only achieved by 15 – 30 % of patients. Phentermine functions by suppressing appetite, although 8 – 10 % weight loss has been observed with its use, it is ineffective for a period longer than three months (Sirin and Kolonin, 2012). Due to their side effects, both Orlistat and

Phentermine can only be used by a limited number of patients. Several other drugs against obesity and obesity- associated conditions are now being tested as individual agents or as dual-target treatments, such as Qnexa, the combination Phentermine and Topiramate (Sirin and Kolonin, 2012).

A list of current key drug candidates, which changes intermittently, is shown in **Table 1.3,** (Hossen *et al*., 2012; Sirin and Kolonin, 2012). Because of the problems associated with anti-obesity drugs, there is a need to develop better strategy which will be used in the treatment of obesity.

Table 1.3. A summary of current pharmacological approaches to obesity treatment.

(Sirin and Kolonin, 2012)

Drug	Other names (manufacturer)	FDA status	Indication
Orlistat	Alli (GlaxoSmithKline) Xenical (Roche)	Approved 2007 Approved 1999	Obesity
Phentermine	Suprenza (Alpex Pharma)	Approved 2011	Obesity
Dexfenfluramine	Redux (Wyeth-Ayerst)	Approved 1996 Withdrawn 1997	Obesity
Fenfluramine	Pondimin (Wyeth-Ayerst)	Approved 1973 Withdrawn 1997	Obesity
Rimonabant	Zimulti (Sanofi Aventis)	Rejected 2007	Obesity
Sibutramine	Meridia (Abbott)	Approved 1997 Withdrawn 2010	Obesity
Pramlintide	Symlin (Amylin pharmaceuticals)	Approved 2005	Diabetes
Metformin	Glucophage (Bristol-Myers Squibb)	Approved 1995	Diabetes
Pioglitazone (TZD)	Actos (Takeda Pharmaceuticals)	Approved 1999	Diabetes
Rosiglitazone (TZD)	Avandia (SB Pharmco)	Approved 1999	Diabetes
Phentermine/Topiramate (combination)	Qnexa (Vivus)	Pending	Obesity
Adipotide	(Ablaris Therapeutics)	Investigational new drug (IND)	Obesity

1.5.3. Phenolics and gallic acid

Plants are a well-known source of molecules with pharmacologic activity. A huge number of secondary metabolites of plant origin are now being investigated in pre-clinical and clinical settings, in the treatment of diseases and also as potential anti-tumour drugs (Pellegrina *et al*., 2005). Phenolics such as hydroxybenzoic acid and hydroxycinnamic acids are widespread in the vegetal kingdom and most of these molecules have anti-inflammatory and antioxidant properties (Tapiero *et al*., 2002; Pellegrina *et al*., 2005; Hsu and Yen, 2006). Other phenolics, such as gallic acid (GA), show selective cytotoxicity against a variety of tumour cells. These compounds may serve as anti-tumour drugs or as the molecular basis for the synthesis of new drugs by targeted chemical modifications (Pellegrina *et al*., 2005; Ho *et al*., 2010).

The GA a 3,4,5-trihydroxybenzoic acid, is a type of phenolic acid and a naturally abundant compound found in gallnuts, tea leaves, oak bark, and other plants. It has a chemical formula of $C_6 H_2 (OH)_3 COOH$ as indicated in Figure 1.3. GA is reported to have antioxidant, anti-mutagenic and anti-carcinogenic activity (Pellegrina *et al*., 2005; Hsu and Yen, 2006; You *et al*., 2010) and is expected to reduce the risk of disease and brings health benefits through daily intake. Epidemiological evidence has shown that its dietary intake play a role in the prevention of several chronic diseases such as cancer, cardiovascular diseases (CVD) and diabetes (Hsu *et al*., 2006). A number of studies have demonstrated that antioxidants may modulate obesity in mice or rats fed high fat-diets (HFD) (Han *et al*., 2003; Hsu *et al*., 2006). Some *in vitro* studies indicated that GA has the highest inhibition of 3T3-L1 pre-adipocyte population growth among other phenolic acids tested (Hsu *et al*., 2006). Therefore,

the research on phenolic acids is of major interest due to their important biological

and pharmacological properties.
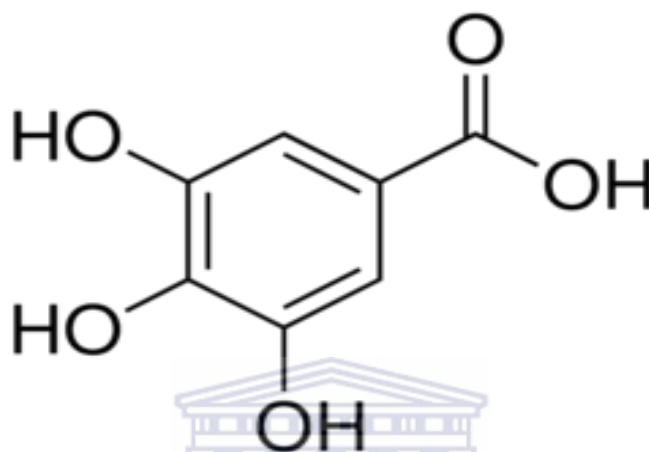
Figure 1.3. Representation for the structure of gallic acids

1.5.4. Bariatric surgery

Surgical approaches to weight loss, such as bariatric surgery to inactivate parts of gastrointestinal tract have shown to be effective as a long-term weight loss intervention in morbidly obese patients (BMI $\geq$ 40kg/m^2 (Kissler and Settmacher, 2013). Bariatric surgery can be defined as surgery that modifies the gastrointestinal tract with the purpose of decreasing calorie absorption and therefore decreasing body weight (Buchwald *et al*., 2004; Kissler and Settmacher, 2013).

It encompasses a range of surgical procedures that classified as either restrictive or malabsorptive. The restrictive procedure includes laparoscopic gastric banding (LAGB) and laparoscopic sleeve gastrectomy (LSG), both designed to decrease the quantity of food intake by reducing the available gastric volume. Malabsorptive bariatric procedures, which include Roux-en-Y gastric bypass (RYGB) and biliopancreatic diversion or duodenal switch (BPD-DS), are designed to decrease absorption of nutrients ingested. Restriction of calories or diet therapy reduces overall weight in the short term, however, unless coupled with a weight management strategy or program, are relatively ineffective at producing long-term weight loss (Buchwald *et al*., 2004; Gill *et al*., 2011).

1.6. Adipose tissue

Adipose tissue (AT) is an innervated loose connective tissue, classically defined as a tissue mass that stores excess energy and provides insulation and padding to the body (Kershaw and Flier, 2004). It is composed of number of different cell types held together by matrix of collagen fibres. This includes mature fat cells (adipocytes) surrounded by a stromal vascular cell fraction containing preadipocytes, endothelial cells, pericytes, fibroblasts, macrophages, monocytes and mesenchymal stem cells (Kershaw and Flier, 2004).

The growth of AT involves both cellular hypertrophy and hyperplasia. Hypertrophy (increase in cell size) is due to excess triglyceride accumulation in the adipocyte and hyperplasia (increase in cell number) results from the recruitment of new adipocytes from precursor cells (preadipocytes) in AT. Hypertrophy usually preceeds hyperplasia. Expansion of adipose tissue can be supported by both neovascularization (for adipocyte hyperplasia) and dilation and remodeling of existing capillaries (for adipocyte hypertrophy). The development of hyperplastic adipose tissue is associated with the most severe forms of obesity and has the poorest prognosis for treatment. Proliferation of adipocytes is influenced by circulating factors, neuronal inputs, and autocrine/paracrine factors secreted by cells within the AT (Dizdar and Alyamak, 2004).

The AT secretes various pro-angiogenic substances and growth factors (Trayhurn and Beattie, 2001; Balwierz *et al.*, 2008). It has been reported that human adipose tissue contains a population of non-characterized cells that are able to undergo adipogenic,

osteogenic, chondrogenic or miogenic differentiation *in vitro.* Such cells, called stromal-vascular fraction (SVF) cells, can be used for repair of tendons and bone as well as skeletal muscle (Balwierz *et al*., 2008). Wosnitza and co-workers have shown, that adipose tissue also contains a population of CD31- as well as CD31+ cells, and both cell populations could be differentiated into adipocytes as well as endothelial cells; this could indicate a potential of trans differentiating endothelial cells to adipocytes (Wosnitza *et al*., 2007).

The AT plays a crucial role in the regulation of whole-body fatty acid homeostasis (Galic *et al*., 2009). The functions of adipose tissue can be classified into three aspects. The first function is related to lipid metabolism including triglycerides (TGs) storage and fatty acids (FA) release. Second, it catabolizes TGs in order to release glycerol and FAs that participate in glucose metabolism in liver and other tissues. Finally, adipocytes secrete adipokines, which include hormones, cytokines and other proteins with specific biological functions (Morrison *et al*., 2000; Galic *et al*., 2009). For these reasons, adipose tissue has an important influence on physiological processes such as development and growth of the adipocyte and energy homeostasis. In addition, adipocytes and adipose tissue are actively involved in metabolic processes such as angiogenesis, adipogenesis, extracellular matrix dissolution and reformation, steroid metabolism, immune response and hemostasis (Bays *et al*., 2008).

There are two main types of AT depending on the cell structure, location, colour, vascularization and function: brown adipose tissue and white adipose tissue.

1.6.1. Brown adipose tissue (BAT)

The BAT also known as "brown fat" are specialized thermogenic adipose tissue used for thermoregulation and cold defence of small mammals (Kershaw and Flier, 2004). It is mainly responsible for energy metabolism, and its function requires efficient blood perfusion to supply nutrients and oxygen and to export heat. BAT contains multilocular adipocytes. It has a large number of mitochondria and is specialized in heat production and energy expenditure. Research interest in brown fat has risen greatly upon the discovery that in certain animal models increased BAT thermogenesis can be a means of dissipating excess energy and thus preventing obesity (Cypess, 1999). The structure of BAT is shown in figure 1.4.
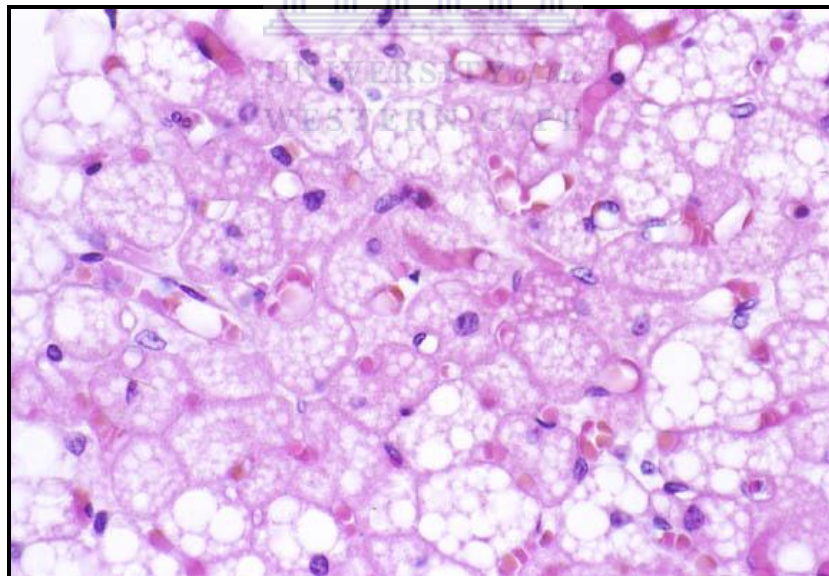
Figure 1.4. The structure of the brown adipose tissue.

(http://www.pathologyoutlines.com/topic/softtissueadiposebrownfat.html)

1.6.2. White adipose tissue (WAT)

The WAT is the primary site of energy storage in a lipid droplet of the adipocytes in the form of triglycerides (TGs). Its main role is to store TGs during energy consumption and to release fatty acid (FA) when energy expenditure exceeds energy intake (Dizdar and Alyamac, 2004). It has recently been defined as an active endocrine organ that secretes a number of signalling peptides or molecules, collectively known as adipokines (Galic *et al*., 2009).

Adipokines includes factors such as leptin, adiponectin, resistin, tumor necrosis factor α (TNFα), interleukin-6 (IL-6), macrophage migration inhibitory factor and chemokine (Vazquez-Vela *et al*, 2008). Most of these factors have important roles in energy homeostasis, insulin sensitivity, immune function, inflammation, and even in tumor progression in the local oncogenic microenvironments. Adipokines have important autocrine and paracrine roles in regulating adipocyte differentiation and metabolism (Goralski *et al*., 2007; (Christiaens and Lijnen, 2010). A well-defined vascular system is present in adipose tissue, with every adipocyte surrounded by one or more capillaries as shown in Figure 1.5.
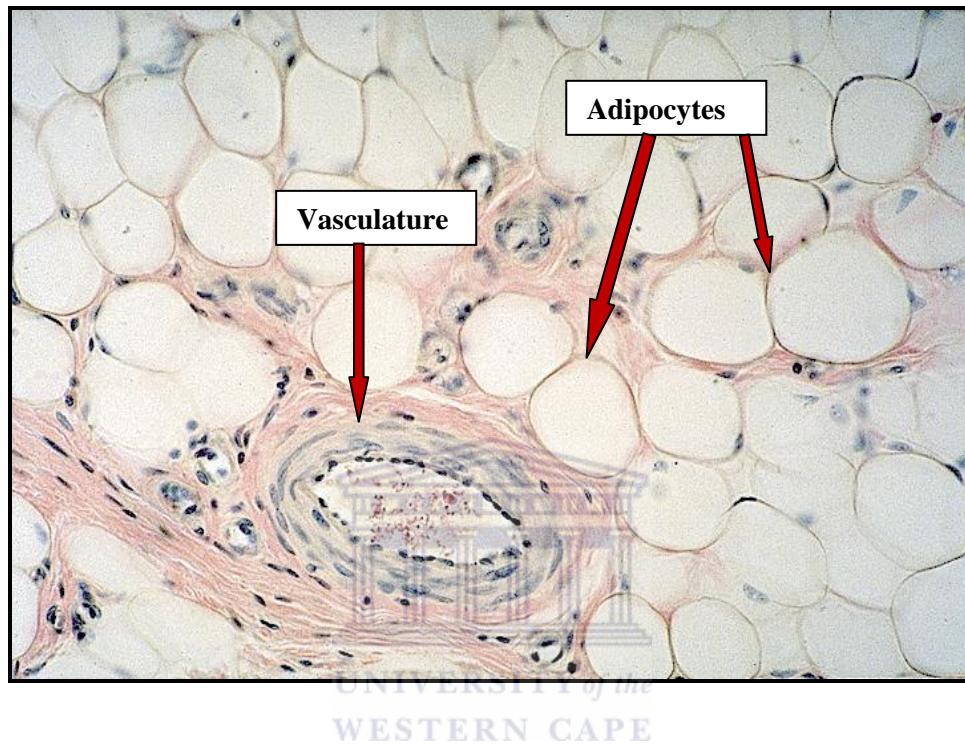
Figure 1.5. The structure of the white adipose tissue.

The figure represents the structure of WAT with different cells type including adipocyte, indicated by

the arrow and the vasculature which is the blood vessels supplying the cells with oxygen and nutrients

(http://stevegallik.org/sites/histologyolm.stevegallik.org/htmlpages/HOLM_Chapter04_Page01.html.)

1.6.3. The WAT as an endocrine organ

Obesity is strongly associated with changes in the physiological function of adipose tissue, leading to insulin resistance, chronic inflammation, and altered secretion of adipokines (van Kruijsdijk *et al*., 2009).WAT is a complex and metabolically active organ, with a relevant important role in regulating whole-body metabolism. WAT is the largest energy storage organ, having an important lipid storing capacity in periods when energy input exceeds energy expenditure and with a lipolytic function (release of NEFA) during energy deprivation. In addition to its primary role as a fuel reservoir, white adipose tissue has been confirmed as a major endocrine organ, since the tissue synthesizes and secretes an array of sex steroids, and bioactive peptides termed "adipokines" (Scherer, 2006; Prieto-Hontoria *et al*., 2011).

Adipokines participate in various metabolic processes including regulation of appetite, fat distribution, energy expenditure, inflammation, insulin sensitivity and insulin secretion. Via autocrine, paracrine and/or endocrine secretion, adipokines contribute to the modulation of adipogenesis, adipocyte metabolism and have systemic effects on appetite control, regulation of energy expenditure and activity, influence insulin sensitivity and energy metabolism in insulin sensitive tissues, such as liver, muscle and fat as well as insulin secretion in pancreatic beta cells (Trayhurm et al., 2006; Blüher, 2009; Blüher, 2013). The adipokine secretion pattern reflects adipose tissue function and seems to be important for determining the individual risk to develop metabolic and cardiovascular co-morbidities of obesity. With the development of adipose tissue inflammation and dysfunction, secretion of adipose tissue derived factors is significantly altered toward a diabetogenic, proinflammatory,

and atherogenic adipokine pattern (Blüher, 2013). Major adipokines secreted from

WAT are shown in Figure 1.6.
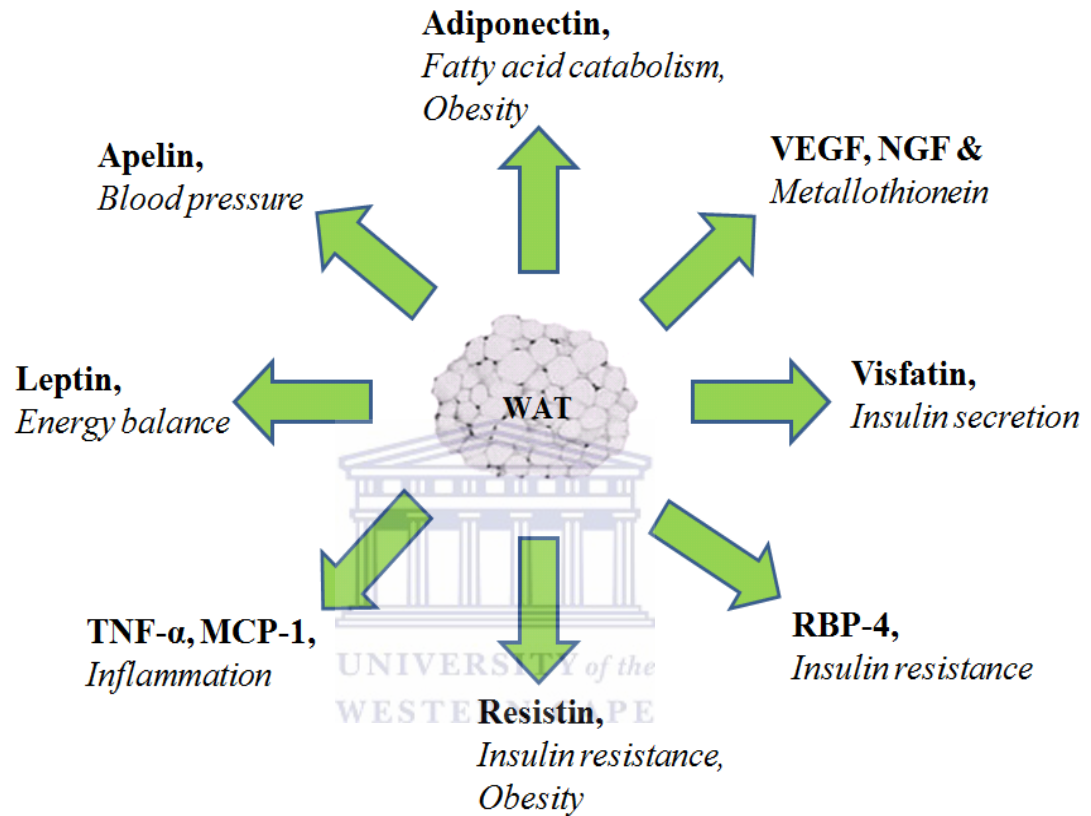
Figure 1.6. Major adipokines secreted from white adipose tissue and their roles.

1.6.4. Role of WAT in obesity

The biological foundation of obesity is the overgrowth of WAT. Adipose tissue is a complex organ with major functions in metabolic and physiological processes (Daquinag *et al*., 2011). The main role of WAT is to store energy in form of lipids, while its other beneficial functions include thermal insulation aiding in the maintenance of body temperature, in addition to endocrine and immune system regulation. The main component of WAT is adipocytes; these are differentiated cells that accumulate lipid droplets. Weight gain occurs when the calorie expenditure is less than its intake, resulting in increased storage of lipids and an expansion of WAT by both hyperplasia (increase of cell number) and hypertrophy (enlargement of cells).

Besides playing a major role in storage of energy, WAT is also an active endocrine organ secreting soluble molecules (adipokines) into the surrounding tissue and vasculature, which has systemic metabolic consequences. For this reason, any change in WAT has systemic effects and is often associated with serious health issues. WAT is composed of stromal mesenchymal progenitors known as adipose stem cells (ASC), endothelial vascular cells and infiltrating leukocytes. This heterogeneous and dynamic pool of cells secretes a plethora of proinflammatory signals that contribute to a state of chronic inflammation in obesity. In fact, adipose tissue dysfunction plays a crucial role in the different obesity linked diseases including inflammation, insulin resistance and cancer (Prieto-Hontoria *et al*., 2011). Inflammation, being a strong platform for development of many diseases could be a major reason why obesity is accompanied by a range of disorders (Sirin and Kolonin, 2012).

1.7. The Adipose tissue and targeting molecules

Protein targeting is the mechanism by which a cell transports proteins to the appropriate positions in the cell or outside the cell. Targeting can be in the inner space of an organelle, any of several interior membranes, the cell's outer membrane, or its exterior via secretion, based on information contained in the protein itself (Wang *et al*, 2008). The peptides may be attached to various therapeutic agents for targeted delivery. Attachment of therapeutic agents to targeting peptides results in selective delivery of the agent to a desired organ, tissue or cell type. Arap *et al* showed that, targeted delivery of chemotherapeutic agents and proapoptotic peptides to receptors located in tumor vasculature resulted in a marked increase in therapeutic efficacy and a decrease in systemic toxicity in tumor bearing animal models (Arap *et al*., 1998a, 1998b).
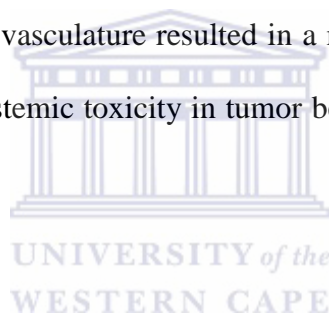
Adipose-targeting peptides are peptide targeting the adipose tissue. These peptides may be used in methods for weight control, inducing weight loss and treating lipodystrophy syndrome. They can also be accomplished using other binding moieties selectively targeted to adipose receptors, such as a prohibitin receptor protein complex (Kolonin *et al*., 2004). These peptides could be used to control obesity and related conditions and would also be of potential use to treat HIV related adipose malformations such as lipodystrophia and/or hyperlipidemia (Zhang *et al*., 1999).

1.7.1. Prohibitin

Prohibitin (PHB) is a human gene, which has been described in animals, fungi, plants and unicellular eukaryotes as growth-suppressive protein that has multiple functions in the nucleus and the mitochondria. PHB is divided in two classes, termed Type-I (PHB1) and Type-II (PHB2) prohibitins, based on their similarity to yeast. Each organism has at least one copy of each type of PHB gene. PHB1 has a molecular mass of 30-32 kDa, whereas the closely related protein known as prohibitone or prohibitin 2 (PHB2), has a mass of 37 kDa (Kasashima *et al*., 2006). The prohibitins (PHB1 and PHB2) together can form a high molecular weight complex. These complexes have been identified in both the mitochondria and the plasma membrane (Mishra *et al*., 2005).

Reports indicate that PHB is localized to the plasma membrane in certain cell types, and was suggested that it might function as a surface-binding site, (Sharma and Qadri, 2004; Kolonin *et al*., 2004). Furthermore, these reports provide proof of principle that membrane-associated PHB can be targeted to modulate disease states (Sharma and Qadri, 2004; Kolonin *et al*., 2004). In summary, Sharma and Qadri, identified PHB as a component of the cell-surface-associated molecular complex in Caco-2 (human intestinal epithelium) cells, which binds to Vi (capsular polysaccharide of *Salmonella typhi*), the causative agent of typhoid fever in humans. The interaction of Vi with the PHB complex on Caco-2 cells resulted in the attenuation of IL-8 production by a process that appeared to involve the mitogen-activated protein (MAP) kinase pathway. These findings suggest that surface-bound PHB complexes might be important targets for modulation by small molecules of the inflammatory response

(Sharma and Qadri, 2004). PHB is also a highly conserved multi-functional protein, which is mainly localized in the inner mitochondrial membrane (Mishra *et al*., 2005) and has been implicated in regulating mitochondrial function in yeast (Kasashima *et al*., 2006). It has roles in transcription regulation, suppression of oncogenesis and metabolism. It has also been detected in serum from normal and cancer patients and known to be present on cell membranes and in lipid droplets released from adipocytes (Kolonin *et al*., 2004).

PHB has potential roles as a tumour suppressor, an anti-proliferative protein, a regulator of cell-cycle progression, and it might also function as a cell-surface receptor (Mishra *et al*., 2005). Cell-associated PHB in the gastrointestinal tract has been implicated in protection against infection and inflammation and the induction of apoptosis in other tissues (Mishra *et al*., 2005). The diverse array of functions of PHB, together with the emerging evidence that its function can be modulated specifically in certain tissues, suggest that targeting PHB would be a useful therapeutic approach for the treatment of variety of diseases including inflammation, obesity and cancer (Kolonin *et al*, 2004; Schleicher *et al*., 2008).

1.8. Adipogenesis

Adipogenesis is the process by which undifferentiated precursor cells differentiate into fat cells. It involves production and formation of fat. Its main role is to store energy in the form of fat. The nuclear hormone receptor PPARg is the central regulator of adipogenesis and plays a dominant role in fat tissue development (Vazquez-Vela *et al*., 2008).

1.9. Lipogenesis

Lipogenesis is the synthesis of esterified fatty acids (FAs), which form triglycerides (TGs) from carbohydrates or other energy sources acquired in the diet. In rats, lipogenesis occurs in liver and WAT, whereas in humans lipogenesis contributes mildly to the fat balance (Vazquez-Vela *et al*., 2008). It occurs predominantly in liver and to a lesser extent in adipose tissue, even with high-carbohydrate diets. In rodents, nutritional status and small changes in insulin levels are factors that influence lipogenesis rate (Vazquez-Vela *et al*., 2008). Lipid synthesis is augmented during postprandial state and after carbohydrate consumption and is inhibited under fasting conditions. Lipid accumulation in adipose tissue depends on circulating FA uptake (Vazquez-Vela *et al*., 2008).
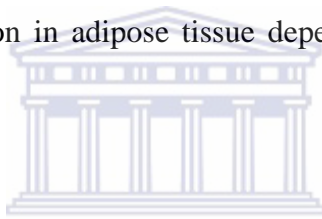
FAs are provided by the enzymatic hydrolysis of TG contained in the chylomicrons by the lipoprotein lipase. After FAs enter the adipocyte, reesterification is necessary for lipid storage in TG form. Several enzymes involved in adipose tissue lipogenesis are induced by insulin. These are fatty acid synthase (FAS), acetyl CoA carboxylase (ACC) and malic enzyme (ME). Newly synthesized FAs are used as substrates in TG synthesis (Sul and Wang, 1998). Insulin-mediated stimulation of lipogenesis in response to nutritional status is the result of an increase in the enzyme activities involved in FA biosynthesis, as well as an increase in the gene expression of these enzymes (Vazquez-Vela *et al*., 2008).

1.10. Non-esterified fatty acids (NEFA)

The NEFA are the fraction of plasma fatty acids. The NEFA impairs insulin-stimulated glucose uptake and glycogen synthase activity in skeletal muscle. Circulating NEFA stimulate β-cell insulin secretion which eventually contribute in the development of insulin resistance in both skeletal muscle and liver, prominent abnormalities in obese individuals (Mohamed-Ali *et al*., 1998).There is a widespread acceptance in the literature that plasma NEFA also called free fatty acids (FFA), can mediate many adverse metabolic effects, mostly insulin resistance. Elevated NEFA concentrations in obesity are thought to arise from an increased adipose tissue mass. It is also argued that the process of fatty acid mobilization from adipose tissue, normally suppressed by insulin, itself becomes insulin resistant, thus lipolysis is further increased, potentially leading to a vicious cycle (Karpe *et al*., 2011).
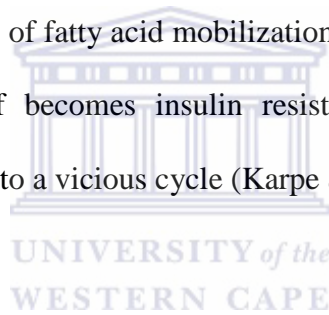
1.11. Angiogenesis

Angiogenesis also known as neovascularization is a multistep process of new blood vessel formation from pre-existing vasculature. It is crucial for all tissue growth, expansion and repair (Cao, 2010). Angiogenesis usually takes 2 forms: sprouting and unsprouting. Sprouting angiogenesis is the development of new blood vessels through proteolytic degradation of the extracellular matrix, migration/proliferation of endothelial cells (ECs), new organization of the luminal membrane, and maturation of endothelial cells to functional capillaries (Pandya *et al*., 2006). New vessels can arise from postcapillary venules (angiogenesis) or from precapillary arterioles (arteriogenesis). Nonsprouting angiogenesis occurs by intussuception, which means

the splitting of primary vessels by transcapillary pillars. Most normal angiogenesis occurs in the embryo. In adults, occurs during the ovarian cycle, pregnancy, and during physiologic repair processes such as wound healing or endometrial regrowth. In normal circumstances, angiogenesis is a highly ordered process that is under tight regulation by both angiogenesis-inducing factors and angiogenesis-inhibiting factors. These factors include soluble growth factors secreted from cells, such as vascular endothelial growth factor (VEGF), angiopoietins, fibroblast growth factor (FGF), platelet-derived growth factor (PDGF), transforming growth factor (TGF), and membrane- bound molecules, such as integrins, cadherins, and ephrins (Liu and Deisseroth, 2006; Pandya *et al*., 2006).

1.11.1. Process of angiogenesis

During angiogenesis, the diseased or tumor cells produce and release angiogenic growth factors (proteins) that diffuse into the nearby tissues. The angiogenic growth factors bind to specific receptors located on the endothelial cells (EC) of nearby preexisting blood vessels. Once growth factors bind to their receptors, the endothelial cells become activated. Signals are sent from the cell's surface to the nucleus. The endothelial cell's machinery begins to produce new molecules including enzymes. Enzymes will then dissolve tiny holes in the sheath-like covering (basement membrane) surrounding all existing blood vessels. The endothelial cells will begins to divide or proliferate, and migrate out through the dissolved holes of the existing vessel towards the diseased tissue (tumor). Specialized molecules called adhesion molecules, or integrins serve as grappling hooks to help pull the sprouting new blood vessel sprout forward. Additional enzymes (matrix metalloproteinases, or MMP) are

produced to dissolve the tissue in front of the sprouting vessel tip in order to accommodate it. As the vessel extends, the tissue is remolded around the vessel. Sprouting endothelial cells roll up to form a blood vessel tube. Individual blood vessel tubes connect to form blood vessel loops that can circulate blood. Finally, newly formed blood vessel tubes are stabilized by specialized muscle cells (smooth muscle cells, pericytes) that provide structural support. Blood flow then begins (Pandya *et al*., 2006).

Table1.4. Selected stimulatory and inhibitory regulators of angiogenesis.

(Pandya *et al*., 2006).

Stimulators	Inhibitors
VEGF	Angiostatin
Angiopoietin-1	Anti-angiogenic anti-thrombin
β-Estradiol	Canstatin
IL-8	Fibronectin fragment
Leptin	Heparinases
MCP-1	IFN-α,β,χ
TNF-α	Prolactin 16 kDa fragment
Angiogenin	TSP-1
MMPs	IL4, IL12, IL18
FGF	Endostatin (collagen XIII fragment)

*Abbreviations***: VEGF-vascular endothelial growth factor; IL8-interleukin 8; MCP-1-macrophage chemoattractant protein; MMPs-matrix metalloproteases, TSP-** Thrombospondin **and TNF-tumor necrosis factor**

Table 1.5. Selected anti-angiogenic agents and their mechanism of action.

(Brakenhielm *et al*., 2004; Clarke and Sharma, 2006).

Inhibitors	Mechanism of action
Angiostatin	Inhibit cell proliferation
	Induce apoptosis of endothelial cells
	Inhibit binding activity of VEGF and bFGF
αVβ3	Induce apoptosis of endothelial cells
Vasostatin	Inhibit cell proliferation of endothelial cells
Interferon –alfa	Inhibit endothelial cells migration
Bevacizumab	Monoclonal antibody against or which bind to VEGF
	Delay tumor growth
	Prevent VEGF from binding to its receptoe
Prolactin 16 kDa fragment	Inhibit VEGF and Bfgf
Thalidomine	Reduction of TNF alpha, bFGF and VEGF
TNP 470	Reduce neovasculation in the adipose tissue
	Inhibit endothelial cells growth
Endostatin (collagen XIII fragment)	Inhibit cell migration, cell proliferation and survival of endothelial cells
Platelet factor 4	Inhibit binding of VEGF and bFGF

1.11.2. Regulation of adipose tissue-related angiogenesis

Both WAT and BAT produce and secrete many different types of proangiogenic factors such as vascular endothelial growth factor (VEGF)-A and hepatocyte growth factor (HGF), which are two key angiogenic factors specifically produced by adipocytes. Other adipose tissue-derived factors with proangiogenic effects include VEGF-B, VEGF-C, placental growth factor (PlGF), fibroblast growth factor (FGF)-2, leptin, platelet-derived growth factor (PDGF), tumor necrosis factor (TNF), tissue factor (TF), plasminogen activators and cathepsins. Adipose tissue also produces endogenous antiangiogenic factors, such as adiponectin, thrombospondin (TSP)-1, TSP-2, ADAM and ADAMTS family members. Thus, the regulation of angiogenesis in adipose tissue may depend on the local balance between proangiogenic and antiangiogenic factors (Christaens and Lijnen, 2010).

1.11.3. Angiogenesis and obesity
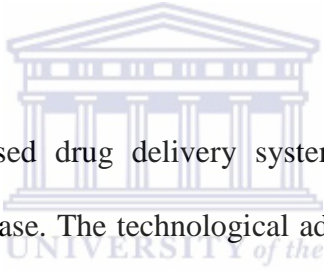
Emerging evidence shows that adipose depot development and tissue growth is coupled to angiogenesis. In preclinical models, delivery of antiangiogenic agents effectively prevents development of obesity in genetic and high fat-diet-fed obese mice. These angiogenesis inhibitors do not cause obvious adverse effects in animals and anti-obesity effect is reversible (Pandya *et al*., 2006). Adipose tissue and blood vessels intimately interact with each other throughout the life hood. In addition to supplying nutrients and oxygen to the adipocyte, blood vessels also provide growth and survival factors to co-opt the growth and regression of adipose depots throughout the adulthood. It has recently been reported that a fraction of adipocyte stem cells reside within the vascular cell population, suggesting that angiogenic vessels may

provide precursors for adipose tissue expansion. Angiogenic vessels are not only required for adipose tissue growth but may also actively participate in regulation of adipose metabolism and energy expenditure. For example, in the metabolically active brown adipose tissue the vascular density is considerably higher than those in white adipose tissues (Pandya *et al*., 2006).

1.12. Nanotechnology

The term nanotechnology is derived from the Greek word *nano*, meaning dwarf, which applies the principles of engineering, electronics, physical and material science, and manufacturing at a molecular or submicron level (Sahoo *et al*., 2007). Nanotechnology can be described as a branch of engineering that involves research and technology development. It involves working with small particles at atomic, molecular and macromolecular scale. It generally deals with structures of the size 100 nanometers or smaller, and involves developing materials or devices within that size (Paull, 2008).

Recently, nanotechnology-based drug delivery systems have shown considerable potential for treatment of disease. The technological advantages of NPs used as drug delivery systems are high stability, high carrier capacity, feasibility of incorporation of both hydrophilic and hydrophobic agents, ease of chemical synthesis, less toxicity, and the feasibility of variable routes of administration (Park, 2007). Various NPs functionalized with different biomolecules have been successfully used in many therapeutic and research applications due to their versatility, ease of chemical synthesis, less toxicity and unique properties (McNeil, 2005). Figure 1.7 shows medical application of nanotechnology.
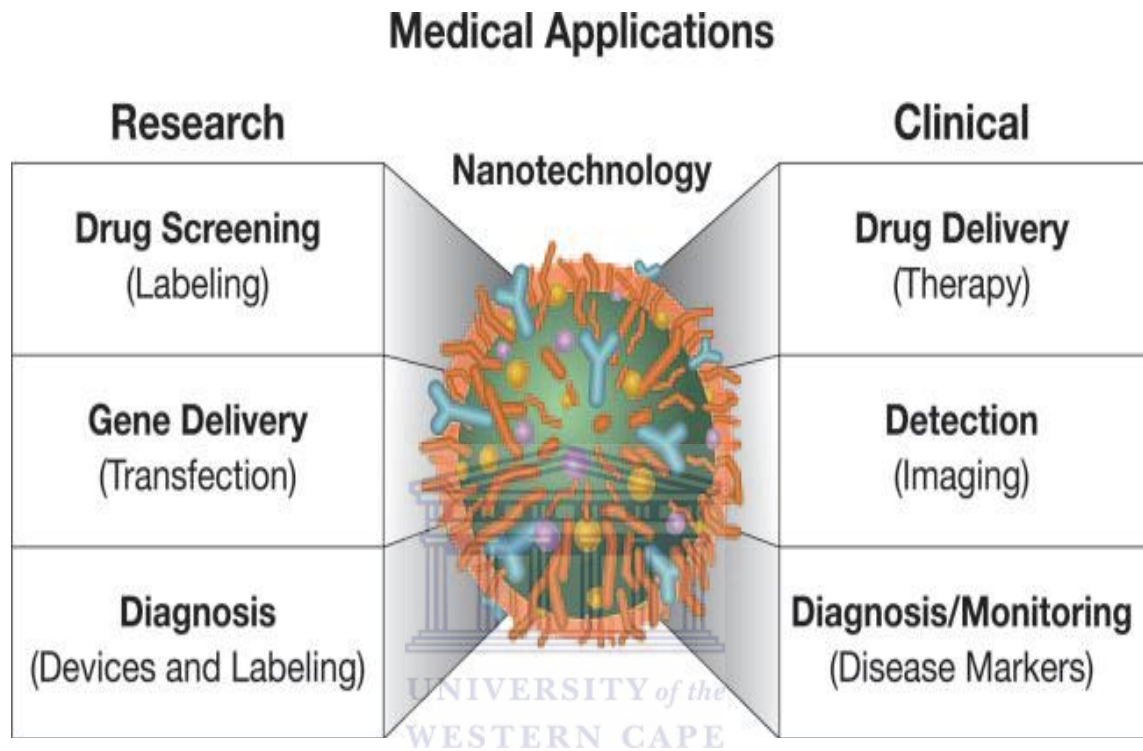
Figure 1.7. Medical application of nanotechnology.

 The figure represent application of nanotechnology in both research and clinical (Reprinted with

permission from Journal of Leucocyte in Biology, Copyright, 2005 (McNeil, 2005)

1.12.1. The use of nanoparticles in nanotechnology

NPs are submicron-sized colloidal particles with a therapeutic agent of interest that are encapsulated within the polymeric matrix or conjugated onto the surface (Misra *et al*., 2010). The sizes range from 10-1000 nm in diameter. NPs offer a great possibility for biomedical application, not only to deliver pharmaceutics, but also to be used as novel diagnostic and therapeutic approaches (Jain, 2005; Abdelhalim and Moussa, 2013). Many types of NPs can be used as imaging and drug-delivery systems and these can be formulated from diverse materials with unique architectures to serve as a possible drug-delivery vehicle to treat a particular disease (Parveen *et al*., 2012). These includes: carbon nanotubes, dendrimers, nanoshells, nanorods, liposomes, magnetic NPs, quantum dots (QDs) and gold NPs (GNPs) (Kim, 2007; Hossen *et al*., 2010; Qiu *et al*., 2010); Papasani *et al.*, 2012; Parveen *et al*., 2012).

Concern has been expressed about the introduction of metallic NPs into the human body for therapeutic purposes and possible toxic effects. The small size of particles, particularly those below 20 nm, makes them versatile therapeutic tools for drug delivery. Their biological effects may vary according to size, chemical composition, surface structure, solubility, shape, and aggregation (Goodman *et al*., 2004; Connor *et al*., 2005). QDs may release potentially toxic cadmium and zinc ions into cells. However, because of their protective coating made of zinc-selenide (ZnS), the QDs have minimal toxicity on cells (Cai and Chen, 2008). Studies using 2-nm core GNPs have shown that cationic particles are moderately toxic, whereas anionic particles are quite nontoxic (Goodman *et al*., 2004; Connor *et al*., 2005). So therefore, this study will focus on the use of GNPs and QDs as drug delivery and imaging agents.

1.13. Gold nanoparticless (GNPs)

The gold nanoparticless (GNPs) also known as nanogold or colloidal gold are colloidal suspension of sub-micrometre-sized particles of gold in a fluid (Ghosh *et al*., 2008). The GNPs have been synthesized by an array of methods which mainly are based on the reduction of chloroauric acid in the presence of a stabilizing agent (Tiwari *et al*. 2011). The most commonly used method, the citrate synthesis method, involves reduction of chloroauric acid using trisodium citrate resulting in the formation of GNPs (Liang *et al*., 2007; Turkevich *et al*., 1951; Tiwari *et al*., 2011). The liquid is usually either an intense red colour (for particles less than 100 nm), or a dirty yellowish colour (for larger particles). The size of GNPs is determined mainly by the salt concentration, temperature and rate of addition of reactants resulting in size range of 10–25 nm (Ghosh *et al*., 2008). However, the size range from 1–100 nm or more can also be achieved by varying the salt concentration and temperature (Tiwari *et al.,* 2011).

The GNPs are non-toxic, inert, stable, sub-micrometer sized particles (mostly used as gene and drug delivery agent), (Ghosh *et al*., and 2008). Among other nanocarriers, GNPs are emerging as a lead candidate in the field of nanotechnology because they can be easily tailored to a desired size from 0.8 to 200 nm, their ease of preparation, they can be easily modified to impart various functionalities and good biocompatibility and can be readily conjugated to proteins and other molecular species without altering the biological activity of the conjugated species (Abdelhalim and Mady, 2011; Wang *et al*., 2008).

Additionally, GNPs have unique optical properties such as distinctive bands in the visible region, due to surface plasmon oscillation of free electrons (Wang *et al*., 2008). They can be used as targeted molecules, drug carriers and as an image contrast agent (McNeil, 2005 and Ghosh *et al*., 2008). GNPs are capable of delivering large biomolecules. Tunable size and functionality make them a useful scaffold for efficient recognition and delivery of biomolecules (Ghosh, 2008; Abdelhalim and Moussa, 2013).

1.13.1. Application of GNPs

GNPs show unique optical properties as indicated in section 1.9.1.1; this property allows the use of NPs for many applications, Figure 1.8 (Niidome *et al*., 2006; Chanda *et al*., 2008; Jiao *et al*., 2011). GNPs have the potential application in field such as electronics, optoelectronics and biosensors. Most application of GNPs as sensors are based on detecting the shift in surface plasmon resonance (SPR) peaks due to either change in the local dielectric constant of the NPs to adsorbed bio-molecules or due to biomolecules induced agglomeration of NPs (Ghosh *et al*., 2008). They have a wide range of applications in areas such as catalysis, medical diagnostics and biological imaging, Figure 1.8, (Ghosh *et al*., 2008; Parimal *et al*., 2010)).

Drug delivery

Cancer therapy

GNPs

Targeting

Diagnostic sensor

Gene therapy

Imaging
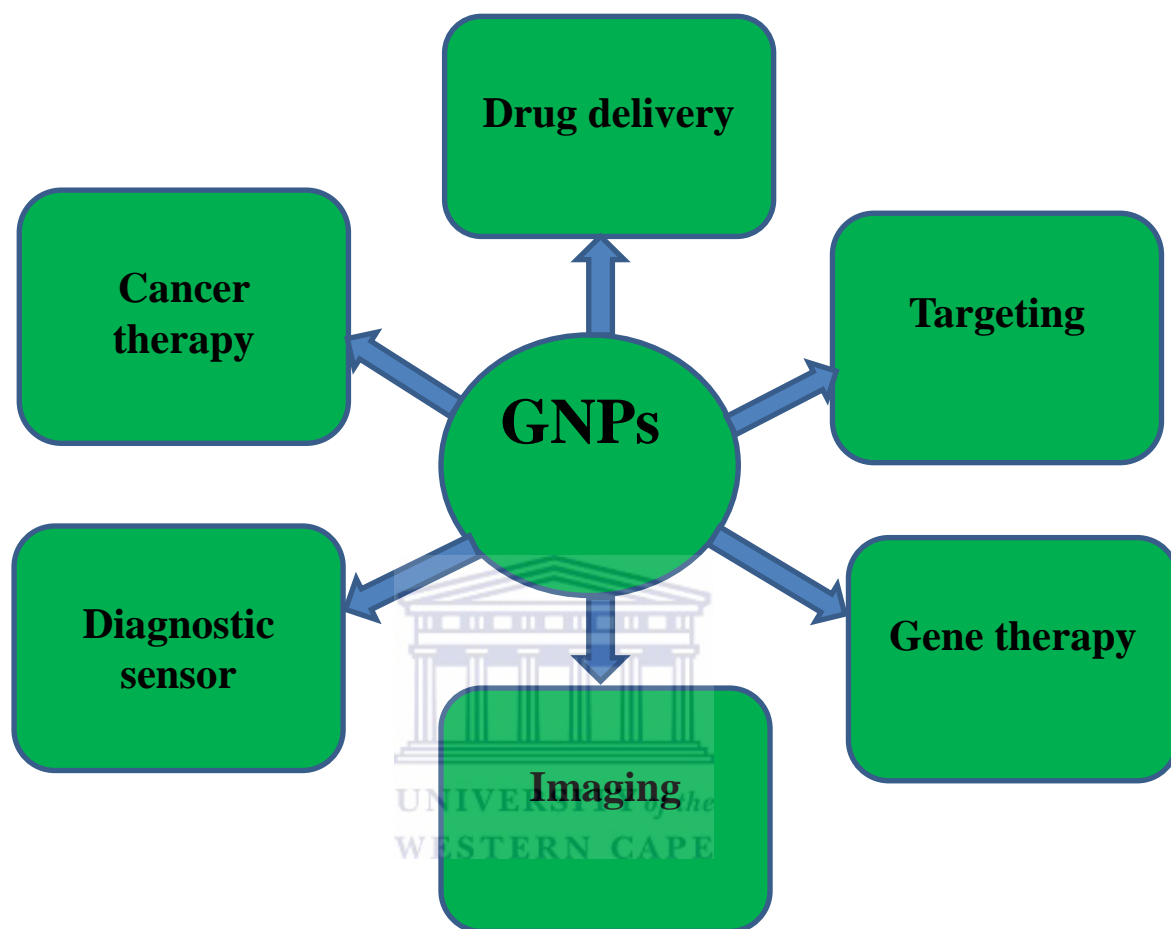
Figure 1.8. Schematic representation for the applications of GNPs

GNPs have a high surface reactivity and biocompatible properties and have gained

considerable attention in recent years for the potential applications in nanomedicine

due to their interesting size dependent chemical, electronic and optical properties (Poportzer *et al.*, 2008). They are also used for *in vivo* molecular imaging and therapeutic applications, including cancer detection and therapy (Poportzer *et al.*, 2008). Studies have been conducted on NPs functionalized with fluorophores, peptides, cell adhesion molecules, aptamers or other biomolecules to target specific tissues and thereby holding promise to be used for imaging of tumors, drug delivery and detection of apoptosis (Sun *et al.*, 2008; Chanda *et al.*, 2010). For GNPs to be effective as a pharmaceutical, it is essential to have a firm understanding of their biodistribution/accumulation in living systems (Chanda *et al.*, 2010). The biodistribution of drug carriers is often affected by the route of administration (Arvizo *et al.*, 2010). NPs used as drug carriers tend to have a longer retention time, generally in the local lymph node, compared to the free drug when administered subcutaneously, intramuscularly, or topically. However, the biodistribution of the NPs largely depends on its surface charge and hydrodynamic radius (Arvizo *et al.*, 2010).

1.13.2. Biodistribution of GNPs

It was shown in the literature that the size and surface-capping of GNPs play an important role in the biodistribution of GNPs in mice (Cho *et al.*, 2009; Morais, 2011). Studies done by Sonavane *et al.*, (2008) also showed that naked gold can accumulate in the liver and spleen. The size-dependent organ distributions of GNPs have been investigated, and the results showed that small GNPs of 5–15 nm had wider organ distribution than that of large GNPs of 50–100 nm, and liver and spleen were the dominant targeted organs (De jong *et al.*, 2008 and Cho *et al.*, 2009; Papasani *et al.*, 2012). Meanwhile, it has been found that GNPs with a long blood circulation time

can accumulate in the liver and spleen, and have obvious effects on gene expression (Balogh *et al*., 2007; Kim *et al*., 2009)

Efficient delivery of GNPs into a living system requires overcoming natural biological barriers such as the cell membrane and the reticuloendothelial system (RES) (Niidome *et al*., 2006). For specific tumor targeting, GNPs face additional challenges from receptor specificity and intratumor barriers. Potential approach for optimizing GNPs delivery is particle size or acquisition of surface modification. For example, large GNPs are quickly opsonized by blood and eliminated by the RES in mammalian cells (Woodle *et al*., 1994; Raynal *et al*., 2004; Roger and Basu 2005; Paciotti *et al*., 2006).

To bypass RES, antibiofouling agents such as thiol-derivatized poly-ethylene glycol (PEG-SH) have been grafted onto GNPs surface as secondary coating. It has been observed that this secondary coating could delay RES clearance to liver from 0.5 hours to 72 hours in a mice model, an approximately 150-fold improvement compared with the unmodified CTAB-capped GNPs (Niidome *et al*., 2006). Several investigators have grafted different delivery platforms onto GNPs surface to attempt cellular selectivity, internalization, and localization within heterogeneous population of cancer cells in solid tumors (Chen *et al*., 2008). Organs of the RES can efficiently accumulate nanoparicles via opsonization, that is, NPs could bind to antibody in the plasma and are subsequently recognized by the phagocyte-rich RES (Balasubramanian *et al*., 2010; Zhang *et al*., 2012)

Opsonization is the process by which a foreign organism or particle becomes covered with opsonin proteins, thereby making it more visible to phagocytic cells. Phagocytosis is a cellular process involving the engulfing or removal of foreign materials from the bloodstream (OwensIII and Peppas, 2006). Together, these two processes form the main clearance mechanism for the removal of undesirable components larger than the renal threshold limit from the blood. In the case of polymeric NPs, which cannot normally be destroyed by the phagocytes, sequestration in the mononuclear phagocytic system (MPS) organs typically occurs. If the polymeric NPs is non-biodegradable, then accumulation of particles in these organs, most commonly the liver and spleen, occur leading to toxicity and other negative side effects (OwensIII and Peppas, 2006; Gaumet *et al*., 2008).

1.13.3. Surface coating of GNPs

Studies have shown that factors such as size, shape, surface coating and charge, affects physicochemical properties of GNPs, with the size being a major determinants for biodistribution (De Jong *et al*., 2008; Ghosh *et al*., 2008). Functionalization through the addition of ligands on the surface of the GNPs is of great interest, as capping can grant some slyness capacity to remain undetected by the RES, thus prolonging their half-life in the bloodstream. In addition, coating can also be employed as a targeting strategy to guide the nanoparticle to a desired organ. These capping agents can be varied in nature including polymers like polyethylene glycol (PEG) and peptides. Peptides as surface capping agents of GNPs are advantageous as they can increase stability, biocompatibility and solubility in aqueous solution. Studies on PEG-coated GNPs biodistribution have shown that NPs exhibit longer

blood circulation times both in mice and in rat. Nevertheless, liver and spleen remained the preferential sites of the accumulation of the PEG-GNPs (Morais *et al.*, 2011).

Longer circulation of NPs, with minimum uptake by the cells of RES is desirable in terms of better targetability of the NPs. The major obstacle to active targeting of colloidal particles in the body system has been the ability of the cells of the RES to rapidly remove intravenously applied particulates from the systemic circulation. The usual strategy taken to avoid the uptake of NPs is by coating the particle surface with hydrophilic polymers, like PEG derivatives such as poloxamers and poloxamines. It has been demonstrated that the RES evasion and long circulation by the particles are possible if the NPs are of ultra-low size (usually <100 nm diameter) and have surface hydrophilicity (Lasagna-Reeves *et al.*, 2010, Zhang *et al.*, 2012. According to Sonavane *et al.*, 2008, smaller GNPs sizes, such as 15 and 50 nm revealed higher amount of gold in the blood after 24 h of intravenous administration while GNPs of higher particle sizes including 100 and 200 nm showed problem of settling in distilled water. Hence, it is necessary to stabilize the GNPs with biodegradable or biocompatible stabilizer.

1.13.4. Cytotoxicity of GNPs

The toxicity of NPs is thought to depend on the size, surface area, composition, and shape of the nanomaterial (Abdelhalim and Mady, 2011). The NPs size also plays a role in how the body responds, distributes, and eliminates materials. Therefore, for applications of GNPs in therapy and drug delivery, it is necessary to know

bioaccumulation and systemic toxicity associated with the NPs (Kamat, 2002; Abdelhalim and Mady, 2011).

The cytotoxicity of GNPs in human cells has been studied (Lu *et al*., 2012). Results have shown that GNPs are nontoxic up to 250 mM, while ionic gold shows obvious cytotoxicity at 25 mM (Connor *et al*., 2005). The toxicity of GNPs *in vivo* is determined by many parameters including dose, route of exposure or administration, metabolism, excretion, and immune response. The toxicologic profiles of nanomaterials might also be determined by nanomaterial chemical composition, size, shape, aggregation, and surface coating (Connor *et al*., 2005). GNPs are stable and non-toxic, so they do not degrade during the transport and are safe to normal tissue (Lu *et al*., 2012).

1.14. Targeted drug delivery

Drug delivery is the method of administering a pharmaceutical compound to achieve a therapeutic effect in humans or animals. Drug delivery technologies can either modify drug release profile, absorption, distribution and/or elimination for the benefit of improving drug efficacy and safety. Current efforts in the area of drug delivery include the development of targeted delivery in which the drug is only active in the target area of the body (e.g., cancer), and sustained release formulations in which the drug is released over a period of time in a controlled manner (Ravi Kumar, 2008; Farokhzad and langer, 2009).

Targeted drug delivery can be defined as the process of releasing or delivering a bioactive agent at a specific rate and at a specific site (Papasani *et al*., 2012). The goal

of a targeted drug delivery system is to prolong, localize, target and have a protected drug interaction with the diseased tissue. This improves efficacy, while reducing side effects (Manish and Vimukta, 2011; Papasani *et al*., 2012). Most conventional anticancer agents do not differentiate between cancerous and normal cells, leading to systemic toxicity and adverse effects (Parveen and Sahoo, 2008).

One of the better strategies is to engineer NPs that are able to target to tumor cells or tumor environment after systemic delivery. This is achieved by conjugating NPs with a molecule or biomarker that binds to receptors found on tumor cells (Brannon-Peppas, 2004). Functional NPs are prepared by covalently linking them to biological molecules such as peptides, proteins, nucleic acids, or small-molecule ligands (Calle *et al*., 2003; Flegal *et al*., 2007). The NPs technology holds great promise in simultaneously diagnosing disease, providing targeted drug delivery with minimal toxicity, and monitoring treatment (Parveen and Sahoo, 2008). The NPs-based drug-delivery systems provide an advantage over free drugs, improving delivery efficiency, solubility, *in vivo* stability and biodistribution. **Figure 1.9** shows drug targeted NPs to disease cell.
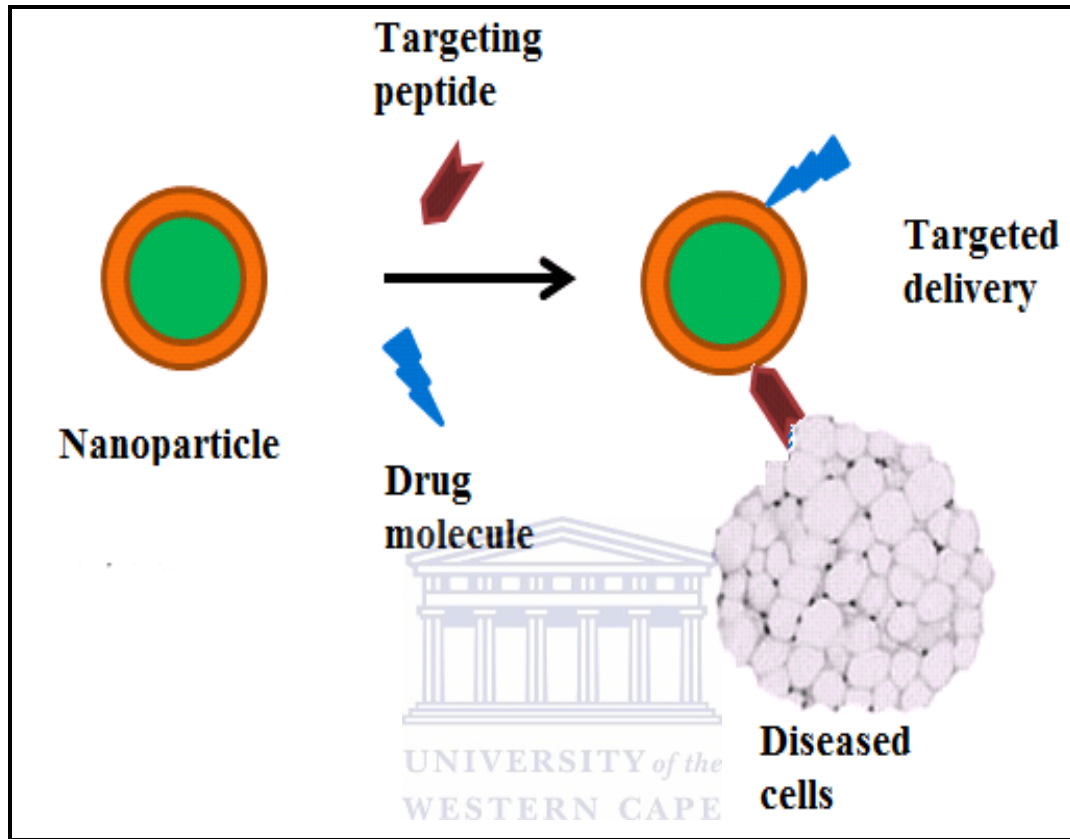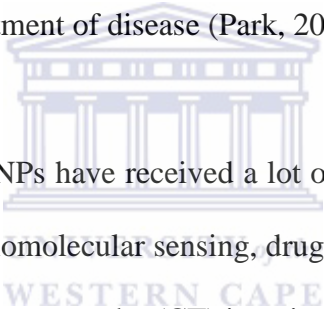
Figure 1.9. Mechanism on peptide targeted NPs, showing targeted delivery to disease cells.

1.14.1. GNPs as targeted drug delivery agent

The GNPs are currently being investigated for their potential uses in targeted cancer detection and treatment. They can be engineered to target specific tissues or cancer cells for use in molecular imaging, making it possible to see diseased cells that are undetectable by conventional imaging methods (Akerman *et al*., 2002; Koo *et al*., 2005; Jiao *et al.*,2011) The small size and configuration of NPs also allow them to pass through biological membranes into cells, where they can act as targeted drug delivery systems for malignant cells while sparing healthy neighboring cells, (Kamat, 2002, Fent *et al*., 2009). Nanoparticle-based drug delivery systems have shown considerable potential for treatment of disease (Park, 2007).

Over the past few decades, GNPs have received a lot of attention in a broad range of biomedical fields, including biomolecular sensing, drug delivery, photothermal cancer therapy, and X-ray computed tomography (CT) imaging. Particularly in drug delivery, GNPs have emerged as an attractive candidate for the creation of efficient nucleic acid delivery systems, mostly due to their excellent biocompatibility, versatility in synthesis, high surface-area-to-volume ratio, and facile surface functionalization through intracellularly displaceable gold-thiol linkages (Manish and Vimukta, 2011; Papasani *et al*., 2012). Furthermore, GNPs functionalized with bio-recognizable ligands have been developed for specific cell-targeting and delivery applications (Kong *et al*, 2011). GNPs have been proposed for diverse biomedical applications due to their unique surface, electronic, and optical properties. Because of the strong and size-tunable surface plasmon resonance, fluorescence, and easy-surface

functionalization, GNPs have been widely used in biosensors, cancer cell imaging, photothermal therapy, and drug delivery (Ghosh *et al*., 2008).

1.15. Quantum dots (QDs)

QDs are nanometer sized fluorescent semiconductors that are increasingly used as labeling and imaging tools in medical research (Xiao and Barker, 2004; Garon *et al*., 2007; Savla *et al*., 2011). They range from 2-10 nanometers in diameter and can glow or fluoresce when stimulated by a light source such as laser (Garon *et al*., 2007). They are near-spherical semiconductor nanocrystals composed of a Cadmium selenide (CdSe), Cadmium sulphide (CdS) or Cadmium Telluride (CdTe) core together with a Zinc sulphide (ZnS) shell and have recently attracted major interest as novel fluorophores (Byers and Hitchman, 2011).

They can be specifically attached to biological materials such as cells, proteins and nucleic acids making them powerful agents (Byers and Hitchman, 2011). QDs can be designed to emit light at any wavelength from the infrared to visible to ultraviolet. Larger QDs emit red light, whereas smaller crystals emit light at the blue end of the spectrum. These nanometer-sized particles are able to display any chosen colour in the entire ultraviolet-visible spectrum through a simple change in their size or composition as indicated in **Figure 1.10** (Zrazhevskiy and Gao, 2009).

QDs have physical properties, such as high quantum yield and resistance to photo bleaching, that make them attractive molecular probes for tracking hematologic cells (Garon *et al*., 2007). They are photostable and size tunable, with narrow, symmetric

emission spectra and broad continuous excitation. They allow excitation of multiple QDs with a single wavelength. In addition, QDs are inorganic and so these are very stable, and their inert surface coating makes them less toxic than organic dyes (Jamieson *et al*., 2007). QDs fluorescence is so bright that it is possible to detect a cell carrying a single crystal. These properties make QDs very attractive luminescent labels for biological applications (Chalmers *et al*., 2007).

More importantly, their strong and stable photo luminescent properties make them promising candidates for use in bio-imaging applications, they can emit different colors, based on pre-determined biological tags/signals. This means that scientists can attach quantum dots to a given protein or receptor to observe normal or abnormal cell functions (Pathak *et al*., 2007). Unlike conventional organic dyes, QDs are highly photostable (Wickline *et al*., 2003; Jamieson *et al*., 2007). This allows them to track cell processes for longer periods of time and to shed more light on molecular interactions.
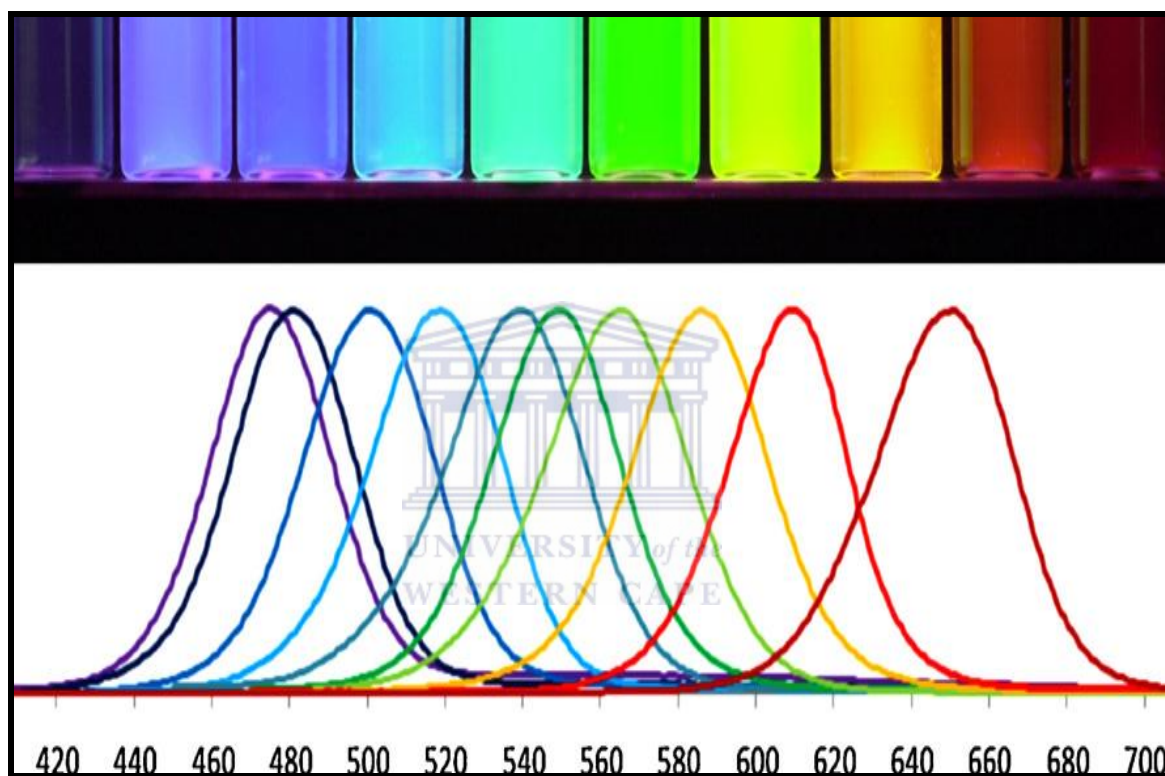
Figure 1.10. Different sizes, colour and emission spectra of QDs

(Reprinted with permission from Nano today, Copyright, 2009,Zrazhevskiy and Gao, 2009)

53

1.15.1. Optical properties of QDs

The QDs are inorganic fluorescent semiconductor NPs. The quantum confinement effects give rise to unique optical and electronic properties in QDs, giving them numerous advantages over current fluorophores, such as organic dyes, fluorescent proteins and lanthanide chelates. The classic and most commonly used QDs consist of CdSe core and a shell layer made of ZnS or CdS (Zrazhevskiy and Gao, 2009). Fluorescence properties of QDs are determined by the core materials and the shell layer (Yezhelyer *et al*., 2001). For biological imaging applications, QDs can be made water soluble by exchanging with bifunctional ligands or coating with amphiphilic polymers that contain both a hydrophobic segment or side chain (mostly hydrocarbons) and a hydrophilic group (Yezhelyer *et al*., 2001; Rosenthal *et al*., 2011).
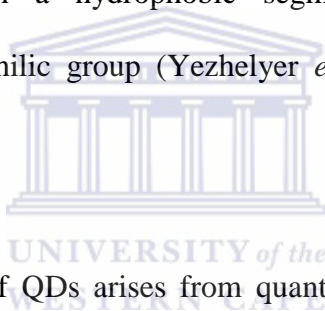
The novel optical property of QDs arises from quantum confinement effect of the semiconductor materials. This refers to the size and composition dependence of the semiconductor band gap energy (Garon *et al*., 2007). Photostability of QDs is a critical feature in most fluorescence applications, and is an area in which QDs have singular advantage. Unlike organic fluorophores which bleach after only a few minutes on exposure to light, QDs are extremely stable and can undergo repeated cycles of excitation and fluorescence for hours with a high level of brightness and photobleaching threshold (Jamieson *et al*., 2007). QDs have been shown to be more photostable than a number of organic dyes. QDs also have a long fluorescent lifetime after excitation, which may be taken advantage of in time-gated imaging. The fast fluorescence emission of organic dyes upon excitation coincides closely with short-

lived autofluorescence background from many naturally occurring species, reducing the signal-to-noise ratio. Conversely, QDs emit light with a decay time in the order of a few tens of nanoseconds (30–100 ns) at room temperature, which is slower than the autofluorescence background decay, but fast enough to maintain a high photon turnover rate (Walling *et al*., 2009).

1.15.2. Toxicity of QDs

One of the major issues that hinder the application of QDs to human subjects is the concern about their safety. Cadmium and selenium are potential hazard for neurological and genitourinary toxicity (Jamieson *et al*., 2007). Cytotoxicity of QDs has been observed in a large number of *in vitro* studies affecting cell growth and viability (Wickline *et al*., 2003). The extent of cytotoxicity has been found to be dependent upon a number of factors including size, dose, and surface chemistry of QDs. A number of mechanisms have been proposed to be responsible for QDs cytotoxicity. These include desorption of free Cd (QDs core degradation) free radical formation, and interaction of QDs with intracellular components (Wickline *et al*., 2003; Jamieson *et al*., 2007).

1.15.3. Application of QDs

The QDs have been used for labelling, imaging, detection, and quantification of bacteria (Savla *et al*, 2011). Beside *in vivo* and cellular imaging, QDs can be used for a wide range of other applications (Rosenthal *et al*., 2011), relevant to the life sciences, such as fixed tissue analysis, spectral encoding of microparticles, and as quantitative analysis of ions (Larson *et al.,* 2003; Yezhelyev *et al*., 2007). Figure 1.11 shows multifunctionality of QDs.

Multi-QD labeling of the diseased site (by coating QDs with targeting molecules of different emission wavelengths) can provide more information on the state and evolution of the disease (Jiang *et al*., 2004). Several groups report homing of QDs to biological targets *in vivo*. Targets have included tumours, vasculature in several different tissue targets (Lim *et al*., 2003) and also a number of targets in necropsy and tissue sections after *in vivo* injection of QDs. One group used antibody-conjugated, PEG-encapsulated QDs to target a prostate-specific membrane antigen, a cell surface marker for prostate epithelium, which is also expressed in the neovasculature of a large number of nonprostatic primary carcinomas (Weissleder, 2001; Pathak *et al*., 2007)   Another group report the synthesis of a tumour-specific chimera phage incorporating a streptavidin- binding site to which QDs may be attached, which is able to specifically target and fluorescence tumour (Chen *et al*., 2004).
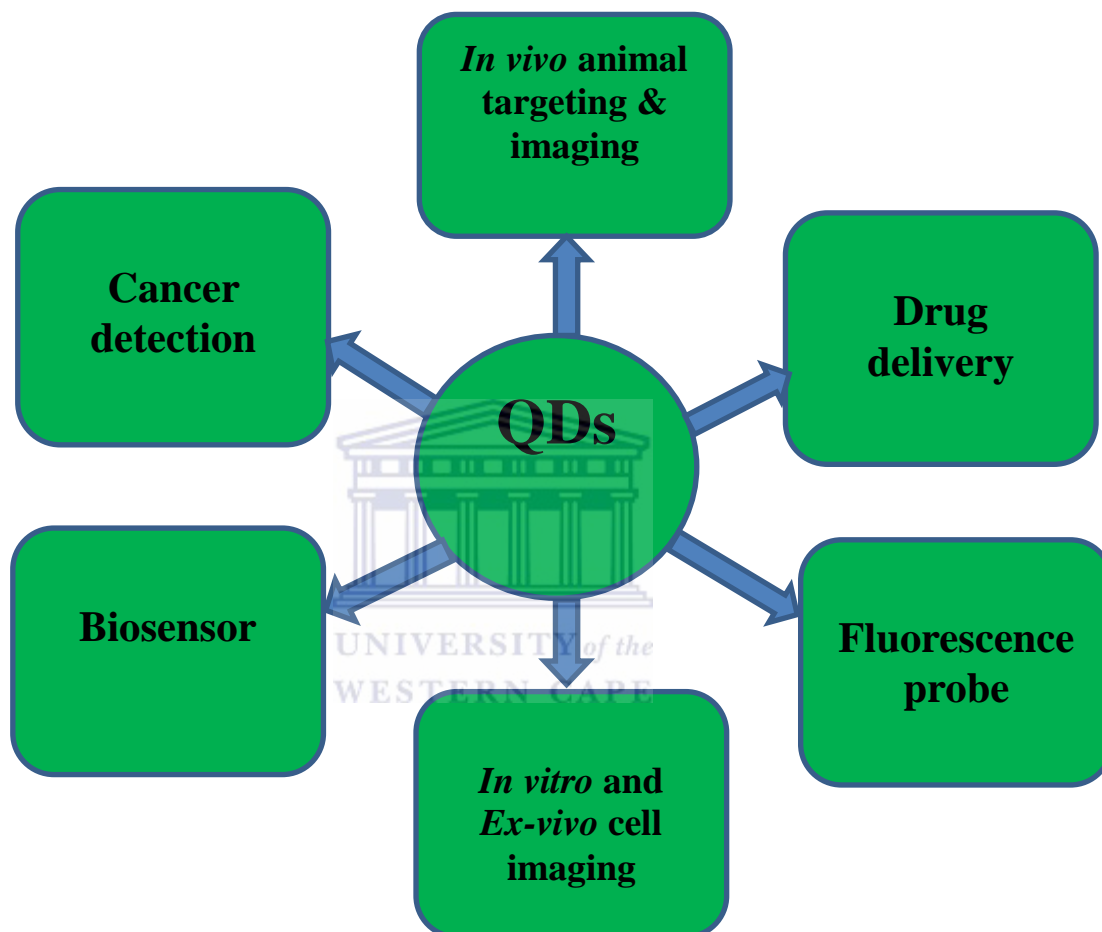
Figure 1.11. Schematic representation for the application of QDs

1.15.4. Biofunctionalization of QDs

To make QDs more useful for molecular imaging and other biological applications, QDs need to be conjugated to biological molecules without disturbing the biological function of these molecules. Biomolecules including peptides, proteins and oligonucleotides have been successfully linked to QDs. Several successful approaches have been used to link biological molecules to QDs (Alivisatos *et al.*, 2005). These includes non-specific adsorption, electrostatic interaction, mercapto (-SH) exchange, and covalent linkage (Xing and Rao, 2008). The biological molecules containing thiol groups can be conjugated to the QDs surface through mercapto exchange process. Unfortunately, since the bond between Zn and thiol is not very strong and is dynamic. Biomolecules attached to QDs in this way can readily dissociate from the nanoparticle surface, causing QDs to precipitate from the solution. It has also been reported that simple small molecules, such as oligonucleotides and various serum albumins are readily adsorbed to the surface of water soluble QDs. This adsorption is nonspecific and depends on ionic strength, pH, temperature, and the surface charge of the molecule (Hanaki *et al.*, 2003; Mahtab *et al.*, 2000).

Mattoussi and coworkers presented a method of conjugating proteins to QDs surfaces, using electrostatic interactions. The protein of interest was engineered with a positively charged domain (poly histidine), which in turn interacted electrostatically with the negatively charged surface of dihydrolipoic acid (DHLA)-capped QDs. The protein-QDs conjugates prepared in this way were stable and the fluorescence quantum yield was even higher than that from the non-conjugated QDs (Mattousi *et al.*, 2000 and Xing *et al.*, 2008). A more stable linkage is obtained by covalently

linking biomolecules to the functional groups on the QD surfaces using cross-linker molecules (Xing *et al*., 2007). This method is the most commonly used approach for making biofunctionized QDs for *in vitro* cell labelling and *in vivo* imaging purposes.

Most water solubilization methods result in QDs covered with carboxylic acid, amino or thiol groups. Under these situations, it is easy to link QDs to biological molecules which also have these functional groups. For example, the cross-linker 1-ethyl-3-(3-dimethylaminopropyl) carbodiimide (EDC) is commonly used to link NH_2 and COOH groups, whereas 4-(N-maleimidomethyl)- cyclohexanecarboxylic acid N-hydroxysuccinimideester (SMCC) can be used to cross-link -SH and -NH2 groups. Using these methods, there have been numerous reports of conjugating QDs with various biological molecules, including biotin oligonucleotides peptides and proteins including avidin/streptavidin albumin adaptor proteins (e.g. protein A, protein G) and antibodies (Pinaud *et al*., 2004; Xing *et al*., 2007; Yang *et al*., 2010; Chirra *et al*., 2011).

For biological applications, QDs must be linked to biomolecules without altering the biological activity of the conjugated form. A number of successful conjugation methods have been developed, including covalent and non-covalent attachment methodologies. Specific conjugation methodologies include direct adsorption on the quantum dot surface, the use of inert polymer coatings, or biotin-streptavidin linkages (Bruchez *et al*., 1998; Walling *et al*., 2009; Chirra *et al*., 2011). Another common conjugation scheme employs the biotin-streptavidin linkage, which requires coupling of the quantum dot to streptavidin. Quantum dot-streptavidin conjugates are useful because a wide range of proteins and other biomolecules can be biotinylated. These

conjugates have applications in staining and labelling, live tracking and drug screening (Bruchez *et al*., 1998; Jaiswal *et al*., 2003; Walling *et al*., 2009; Chirra *et al*., 2011).

1.16. Molecular imaging

Molecular imaging is an emerging field that integrates molecular biology with *in vivo* imaging in order to gain information regarding biological processes and to identify diseases based on molecular markers. It is a new approach for detecting diseases much earlier, visualizing biological processes at the cellular and molecular level in living organisms, and detecting changes in biochemistry. Currently, positron emission tomography and single photon emission tomography are the main molecular imaging modalities in clinical use (Ghosh *et al*., 2008).

However, they provide only functional information regarding molecular processes and metabolites, which is indirect and nonspecific to distinct cells or diseases. Various types of targeted nanoprobes have been developed for optical and molecular imaging such as super paramagnetic NPs; quantum dots and GNPs as cancer optical imaging probes (Ghosh *et al*., 2008). Molecular imaging improves diagnostic accuracy and sensitivity, by providing an *in vivo* analogue of immunocytochemistry or *in situ* hybridization. It seeks to enhance the conspicuity of microscopic pathologies by targeting the molecular components or processes that represent mechanisms of disease (Wickline *et al*., 2003; Barteneva and Vorobjev, 2010).

1.16.1. *In vivo* imaging of QDs

Semiconductor QDs are emerging as a new class of fluorescent labels for biology and medicine and has become a topic of great research interest in both chemists and biologists. The broad absorption and narrow emission characteristics of the QDs make it possible to perform multicolor imaging with a single excitation source. The high fluorescence quantum yield of the QDs, their resistance to photo bleaching and their unique physical, chemical and optical properties make them good candidates for fluorescent tagging for *in vivo* molecular and cellular imaging (Gao *et al*., 2005; Kirchner *et al*., 2005; Li and Wu, 2010). The surface of QDs can be engineered or modified to improve QDs solubility, sensitivity, specificity and visualization in target tissue (Misra *et al*., 2010). Because visible QDs are more synthetically advanced, most animal imaging studies implementing QDs have used CdSe/ZnS QDs that emit visible light and a few recent studies started the use of near-infra red dots. Although still far from its mature stage, these studies have demonstrated the great performance and promise of QDs as fluorescent imaging agent in living animals (Kim *et al*., 2004 and Cai *et al*., 2006).

QDs have utility for a number of live cell imaging and detection applications, which can be done externally, but could also require the internalization of quantum dots by cells. Internalization of quantum dots for targeting and imaging applications has been achieved using a number of different strategies, including modifications to surface coatings for passive uptake and the use of specific molecules for mediated delivery (Zhu *et al*., 2008; Walling *et al*, 2009; Jaiswal *et al*., 2003). These altered surface coatings have been developed to increase the versatility and labelling efficiency of

quantum dots for live cells, both prokaryotes and eukaryotes (Walling *et al*., 2009). The various surface coatings enhance aqueous solubility, and provide varying functional groups for conjugation to antibodies, peptides, and other biomolecules, and reduced nonspecific binding to the cell surface (Bruchez *et al*., 1998). Other improvements to cellular imaging involve variations to the core composition for decreased cytotoxicity and increased biocompatibility (Walling *et al*., 2009). The ability to internalize quantum dot conjugates, along with the increased multiplexing capabilities, offers a major advancement in time- and cost-effectiveness over single-color experiments. Ultimately, these advantages will contribute to the detection of various cell proteins or other components of heterogeneous tumor or tissue samples (Xing and Rao, 2008).

1.17. The *in vivo* imaging techniques

The *in vivo* imaging system is an optical imaging technique which looks deep into the tissues of living test subjects. Applications for *in vivo* imaging include studying biological signaling networks and pathways, gene expression, angiogenesis, and apoptosis. In order to take a picture of a tissue a centimetre or more into the animal, and accurately visualize the processes inside, it is necessary to use near-infrared light. The tools and technologies associated with the near-infrared window vary from standard fluorescence imaging tools. A number of CCD camera systems optimized for near-infrared imaging are now available (Shaffer, 2009).

 An *in vivo* imager generally consists of a box for the animal, a near-infrared-capable CCD imaging system, and a computer interface. The animal box is designed to keep the animal comfortable and, typically, anaesthetized. Ports are included for

connecting supplies of anaesthetic gas, oxygen, and heat. Normally, optical imaging systems can only look at the surface of an object. However, in the near-infrared window of the spectrum, living tissues become "transparent" and the light source will penetrate the tissue and pick up fluorescence from near-infrared dye molecules Shaffer, 2009).

1.17.1. The IVIS Luminar XR (Xenogen imaging system)

The Xenogen IVIS imaging system is an advanced single-view 3D optical imaging system, design to improve quantitative outcomes of *in vivo* imaging. It is a sensitive imaging system that is easy to use for both fluorescent and bioluminescent imaging *in vivo.* IVIS uses a large CCD camera, cooled to -90°C which gives the camera a very high sensitivity for deep image sources. The Xenogen IVIS® Lumina XR from Caliper Life Sciences is an affordable, highly sensitive imaging system that offers users the flexibility to image fluorescent and/or bioluminescent reporters both *in vivo* and *in vitro*.

It relies on Xenogen's novel patented optical imaging technologies to facilitate non-invasive longitudinal monitoring of disease progression, cell trafficking and gene expression patterns in living animals. This user-friendly system includes a light-tight imaging chamber with complete computer automation, and the Living Image® software package for image acquisition and analysis. The system includes premium animal handling features such as a heated sample shelf, gas anesthesia connections and manifold, and an optional full gas anesthesia system. The imager can accommodate the maximum of five rats which can be imaged simultaneously. For the advanced fluorescence imaging, IVIS imaging system has the capability to use either

trans-illumination or epi-illumination to elluminate *in vivo* fluorescence source. The instrument is equipped with 10 narrow band excitation filters and 18 narrow band emission filter that assists in significantly reducing autofluorescence by the spectral scanning of filter and the use of spectral unmixing algorithms (Shaffer, 2009). The IVIS Lumina XR as indicated in Figure1.12.

Figure 1.12. The IVIS Luminar XR, imaging system

1.18. Application of nanotechnology in obesity

Vascular targeting can be done both *in vitro* and *in vivo*. For the interest, the *in vivo* phage display method is a method for studying interactions between receptors expressed preferentially in an organ or tissue of interest and their corresponding ligands (Kolonin *et al*., 2004). Kolonin and his coworkers screened the phage display library in the discovery of the synthetic peptide motifs (sequence CKGGRAKDC), which was then named adipose homing peptide (AHP). The AHP was found to be a vascular targeting peptide that homes to the white fat vasculature in obese leptin-deficient (*Lep $^{ob/ob}$*) mice. This peptide motif was found to associates with prohibitin, a (PHB) multifunctional membrane protein and establish PHB as a vascular marker of adipose tissue. Kolonin further showed that by targeting the proapoptotic peptide to PHB in the adipose vasculature caused ablation of white fat (Kolonin *et al*., 2004).
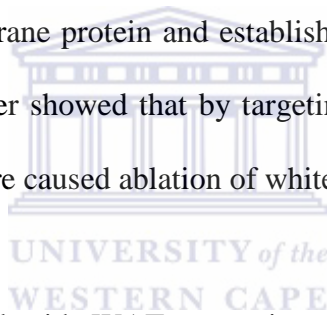
Because obesity is connected with WAT expansion, targeting the WAT will be a better approach for obesity treatment. Furthermore, obesity management is associated with side effects; therefore, a need still exists, to develop a better strategy which will be used in the treatment of obesity, nanotechnology can be considered as a new field of science that involves research and technology development to modify obesity treatment.

Various nanoparticle functionalized with different biomolecules have been used due to their versatility, ease of chemical synthesis and less toxicity, because of this advantages and its safety it can therefore, hold effective role. Developing nanotechnology based approach, combined with the synthetic peptide motifs,

CKGGRAKDC, together with an anti-obesity drug will be a better way to target WAT vasculature. This will limit the problem of untargeted delivery which results in side effects and toxicity. Target-specific drug therapy and methods for early diagnosis of pathologies are the priority research areas in which nanotechnology would play a vital part (Misra *et al*., 2010).

1.19. Problem statement

Nanotechnology has been used in cancer research for drug delivery, cell detection and imaging (Atlanta, 2005; Lira *et al*., 2012). Recent studies suggest that physical characteristics of GNPs and QDs continue to be refined to further their utility. Synthetic methods, including conjugation and aqueous solubilisation steps, are critical in maximizing their properties for broader use. To the best of our knowledge the use of AHP functionalized QDs and GNPs as imaging and drug delivery agents in targeting the WAT vasculature of Wistar rats for obesity reversal has not been investigated before. Therefore this study will focus on the development of nanotechnology-based drug delivery using AHP functionalized GNPs, and imaging using AHP functionalized QDs in targeting the WAT vasculature of lean and obese male Wistar rats.

1.20. Aim and objectives of the study

Aim of the study is to develop nanotechnology-based drug delivery and imaging system to the WAT vasculature of the male Wistar rats.

Objectives:

- To use biocompatible GNPs and QD625 functionalized with AHP to specifically target the WAT vasculature.

- To test the use of AHP-GNPs and AHP-QDs as delivery and imaging agents to the WAT vasculature of obesity induced Wistar rats model, both *in vitro* and *in vivo*.

- To isolate endothelial cells from the stromal vascular fraction of rats WAT, for *ex vivo* studies.

- To functionalize AHP-GNPs with an anti-obesity drug (GA); (AHP-GNPs-GA) and test for cytotoxicity and apoptotic effects *in vitro*.
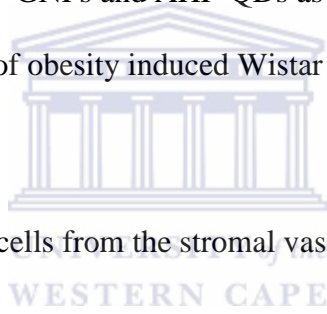
1.21. Hypothesis

The AHP-functionalized GNPs and QDs will specifically target the WAT vasculature; while a drug-loaded AHP functionalized GNPs (AHP-GA-GNPs) target and deliver the drug inside the cells.

UNIVERSITY *of the*

WESTERN CAPE

CHAPTER 2

2. Materials and Methods

2.1. Materials: General Chemicals and Suppliers

All chemicals used in the study and their suppliers are listed in Table 2.1

Table 2.1. General chemicals and suppliers

Chemical	Supplier
0.4 % Trypan Blue Solution	Invitrogen
1X PBS, pH 7.2	Invitrogen
2.5 % Trypsin	Gibco
6x orange DNA loading dye	Fermentas
AHD- FITC	Anaspec
Alexa-flour Anti-rabbit 647 IgG (H+L)	Invitrogen
Anti-Prohibitin antibodies	Biolegend
Biotin -AHP (AHP, CKGGRAKDC)	Anaspec
BSA	Seravac
Cell culture media and reagents	Roche/ Lonza Diagnostics
Cell proliferation Reagent WST-1	Roche
Collagenase from *Clostridium histolyticum*	Sigma
DAPI(4,6-Diaminidine-2-phenylindoledihydrochloride)	Sigma

Dimethyl sulphoxide (DMSO)	Sigma
Dynabeads® CD31 Endothelial cells	Invitrogen
Ethanol 99.9 %	Kimix
Fluoroshield	Sigma
Foetal bovine serum (FBS)	Lonza
Gallic acid	Sigma-Aldrich
Gold NPs, streptavidin conjugate	Mintek
Hydrochloric acid (HCl)	Merck
Mitotracker	Invitrogen
Nitric acid (HNO$_3$)	Merck
Paraformaldehyde	Sigma-Aldrich
Penicillin-Streptomycin	Lonza
Quantum dots, streptavidin conjugate 625nm	Invitrogen
Agarose	Lonza

Table 2.2. Biochemical assay, kits and supplier

Glucose (GO) assay kit	Sigma
Mercodia ultrasensitive Rat insulin ELISA kit	Mercodia developing diagnostic
NEFA C kit	Wako

Table 2.3. Stock solutions and buffers.

Stock solution /Buffer	Composition
4 % Paraformaldehyde	4 g Paraformaldehyde in 100 mL PBS
10X PBS:	80 g NaCl, 2 g KCl, 14.24 g $Na_2HPO_4.2H_2O$, 2 g KH_2PO_4 in dH_2O
10x TBE	0.9 M Tris, 0.89 M boric acid, 25 mM EDTA, pH 8.3
Aqua regia	3:1 (V/V) HCl: HNO_3
Collagenase buffer	40 ml PBS, 1 % BSA and 2 mg/ml Collagenase filter sterilized

Table 2. 4. Tissue culture media

Media	Components
Complete DMEM	DMEM, 10 % FBS and 1 % penicillin-streptomycin
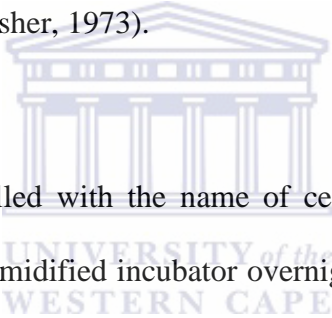
Table 2.5. Cell lines, species, source and media used.

Cell line	Species	Source	Media
Caco-2	Human Epithelial	Colorectal adenocarcinoma	Complete DMEM
MCF-7	Human	Breast carcinoma	Complete DMEM
CHO	Chinese Hamster	Ovary	Complete HamsF12
KMST-6	Human	Normal fetal fibroblast	Complete DMEM

2.2. Methodology

2.2.1. General tissue culture procedures
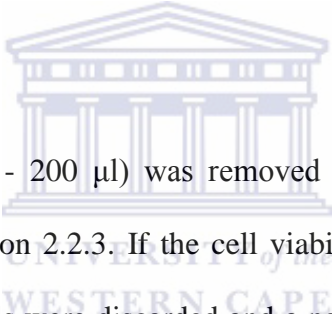
Vials of frozen cells were stored within a -150 ^{o} C freezer. The cells were thawed at 37° C water bath by submerging the lower half of the vial in the water to thaw only until a small amount of ice remained in the vial. The vial was thereafter placed in a laminar flow cabinet. Using a paper towel moistened with 70 % alcohol, the outside of the vial was wiped and the lid was loosened. The cells were transferred into tissue culture flasks containing pre-warmed appropriate culture medium supplemented with 10 % FBS and 1 % streptomycin - penicillin (Absher, 1973).

The flasks were properly labelled with the name of cell line and date of culture and incubated at 37°C, 5 % CO2 humidified incubator overnight. The following day the cells were inspected using inverted light microscope. Media was changed and cells were incubated for a further 24 hrs. When the cells reached confluency, they were washed once with 1X PBS and trypsinized with 0.125 % trypsin. Upon addition of trypsin, the cells were incubated for 5 to 10 minutes at 37°C. The cells were examined under light inverted microscope to monitor the detachment and floating of the cells. If they were not detached, the flask was gently tapped on the side until the cells were completely detached. Trypsin was inhibited by addition of complete media. The cells were centrifuged at 300 rpm for 3 minutes and resuspended in trypsin free complete media.

2.2.2. Cryo-preservation of cell lines

Cells were maintained in an incubator at 37 $^{\circ}$C in 5 % CO_2. They were monitored using an inverted microscope to assess the degree of cell density. Once the cells reached the required confluency and that they were free from bacterial or fungal contamination, they were washed with PBS and trypsinized as above. Trypsinization was stopped by the addition of 1ml complete medium. Cells were recovered by aspiration and transferred into a centrifuge tube. The tube was centrifuged for 3 minutes at 300 rpm in a bench top centrifuge. The supernatant was discarded and cell pellet was re-suspended in a solution of 90 % FBS and 10 % DMSO.

A small aliquot of cells (100 - 200 μl) was removed and a cell viability count was performed as indicated in section 2.2.3. If the cell viability was in excess of 90 % the cells were frozen, if not the cells were discarded and a new culture was grown. This was done so as to achieve a good recovery after freezing. Cryo-vials were labelled with date of freezing, name of cell line, media in which the cell line was grown and the name of the person freezing the cells. The cells were then aliquoted into 1ml aliquots in the labelled cryo-vials at a concentration of $2.4x10^6$ cells per ml and were frozen at -150° C. Before freezing, another aliquot of 50 - 100 μl was removed from the tube and cultured as a quality control to assess if the vials being frozen were free from contamination. The cells for quality control were grown for 24 - 48 hrs. If the cells were found to be contaminated, the vials were withdrawn from the freezer and discarded.

2.2.3. Cell count

Under sterile conditions, 20-50 µl of the cell suspension was removed and mixed with an equal volume of Trypan Blue in a 0.6 ml Eppendorf tube and mixed by gentle pipetting. The countess chamber slides were properly filled with 10 µl of the sample without overfilling or under filling. The cells were then counted using the Countess® Automated Cell Counter (Invitrogen).

2.3. *In vitro* Binding studies

The 10^6 cells/mL of Caco-2 cells, MCF-7, CHO and KMST-6 were cultured on cover slips in a 6 well plate for 24 hrs. The coverslips were removed and incubated at 25 ˚C with 20 µl of 4 % paraformaldehyde to fix the cells for 10 minutes. The cells where then washed with PBS to remove the paraformaldehyde. The cells were then incubated with the NPs for 1 hr at RT. Thereafter, the cells were washed three times with 1x PBS. The coverslip were placed upside down on a slide containing the mounting media (fluoroshield). The slides were viewed under the fluorescent microscope using DAPI, FITC and DsRed filters. The results were analyzed using Axio vision software.

2.4. Cytotoxicity and Cell viability studies

2.4.1. Cell viability using WST-1 assay

The cell viability test was determined using WST-1 according to reported protocols (Ngamwongsatit *et al*., 2008 and Yin *et al*., 2013) with some minor modification. In brief, the 2×10^5 cells/mL of Caco-2 cells were cultured in a 96 well plate for 24 hrs. The cells were then treated with different concentration of the NPs in complete media and then incubated for 24 hrs. Thereafter, the old media were removed and replaced with fresh media. The 10 µl of WST-1 was added to each well and incubated for 2 hrs at 37 $^{\circ}$C. The Abs was measured by a POLAR star microplate reader at 430 nm with a reference wavelength at 620 nm. All experiments were done in triplicate and the relative cell viability was expressed as a percentage relative to the untreated control cells. The results were analyzed using a formula indicated below:

% viability = OD treated- OD blank / OD control - OD blank X 100
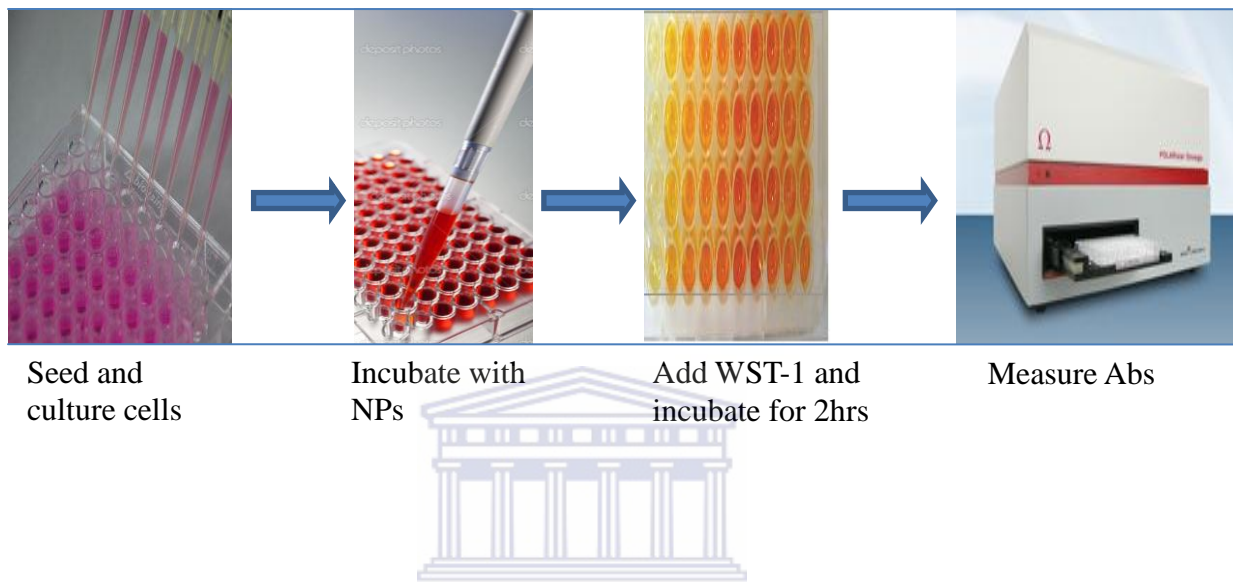
Figure 2. 1. Schematic procedure representing WST-1 cell viability assay

2.5. Quantification of cellular uptake of NPs

The cellular uptake was determined following the methods described by Kumar *et al*., 2012; Reuveni *et al*., 2011) with some minor modification. Briefly, the 5×10^5 cells/mL of Caco-2 cells were cultured in a 12 well plate for 24 hrs. The cells were then treated with different concentration of the NPs and further incubated for 24 hrs. Thereafter, the cells were trypsinized with 1X trypsin and cell pellet were washed twice with PBS to remove any unbound NPs. The pellets was resuspended in 2 ml of aqua regia (HCl: HNO_3 (3:1) and were digested at $90^{\circ}C$ oven for 2 hrs, the digested sample were diluted with 2 % HNO_3 to a final volume of 10 ml. The samples were analyzed using Inductive Coupled Plasma Optical Emission Spectroscopy (ICP-OES) by Ms Ilsie Wells at the Department of Chemistry, University of the Western Cape (UWC). The amount of NPs was calculated based on the concentration of cadmium (Cd) or gold (Au) found in the sample, thus using Cd and Au as standards. The results were expressed as percentage treated dose, using the formula below:

For Gold (Au) quantitation

% Au = Concentration of Au detected / Concentration of Initial amount of Au x 1000

For Cadmium (Cd) quantitation

% Cd = Concentration of Cd detected / Concentration of Initial amount of Cd x 1000

2.6. Agarose gel electrophoresis

Gels were prepared by boiling the appropriate mass of agarose in 1x TBE, cooled to 50°C and left to solidify at room temperature. Then fifteen (15) µl of the sample was mixed with 3 µl volumes of 6x DNA loading buffer and loaded into the gel. The 1x TBE was used in the electrophoresis of the gel. The gels were run at 115V for 20 minutes at room temperature. Gels were viewed and photographed using UVP imaging system. This was done to confirm the functionalization of the NPs.

2.7. Nanotechnology

2.7.1. Synthesis, functionalization and characterization of Gold NPs (GNPs)

Streptavidin conjugate GNPs 520nm were synthesized and functionalized by the Advanced Material Division (Mintek, South Africa). They were functionalized with a biotinylated (Biotin-Tyr-Cys-Lys-Gly-Arg-Ala-Lys-Asp-Cys-OH), Adipose Homing Peptide (AHP, Anaspec) and polyethylene glycol (PEG). Both functionalized (AHP-GNPs) and unfunctionalized GNPs (GNPs) were characterized using UV-VIS spectroscopy, Transmission Electron Microscopy (TEM) and agarose gel electrophoresis.

2.7.2. Functionalization and characterization of Quantum dots (QDs)

Streptavidin conjugate QDs emitting at 625nm were purchased from Invitrogen. QDs were functionalized with biotinylated AHP (Biotin-Tyr-Cys-Lys-Gly-Arg-Ala-Lys-Asp-Cys-OH, Anaspec). Briefly, 5 µl of 1µM streptavidin QDs was mixed with 4 µl of 25 µM biotin AHP, and 1X PBS (pH 7.4) was added to make a final volume of 100 µl. Both functionalized (AHP-QDs) and unfunctionalized QDs (QD625) were characterized using agarose gel electrophoresis and HORIBA Nanolog FL3-22 Triax. This was done following the procedure described by Yang *et al*., 2010, with some minor modification.

2.7.3. Synthesis, functionalization and characterization of AHP-GA-GNPs

The Gallic acid (GA) was used as a drug in this study. It was prepared by dissolving the appropriate amount in grams in PBS, pH 7.4. The GA was filter sterilized using 0.22 μm filters and was kept at 4°C until use. In this study, GA was conjugated to AHP functionalized GNPs through (1-Ethyl-3-(3-dimethylaminopropyl)carbodiimide (EDC) chemistry, to form a peptide-targeted, drug-loaded GNPs (AHP-GA-GNPs).

The AHP-GA-GNPs were synthesized and functionalized by the Advanced Material Division (Mintek-South Africa) according to the procedure represented in Figure 2.2. The functionalized AHP-GA-GNPs were characterized using UV-vis spectroscopy and transmission electron microscopy (TEM).
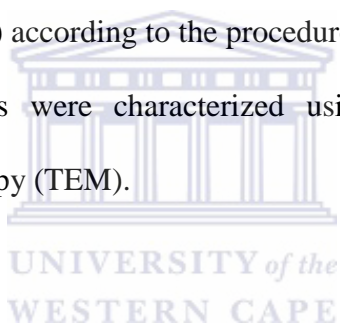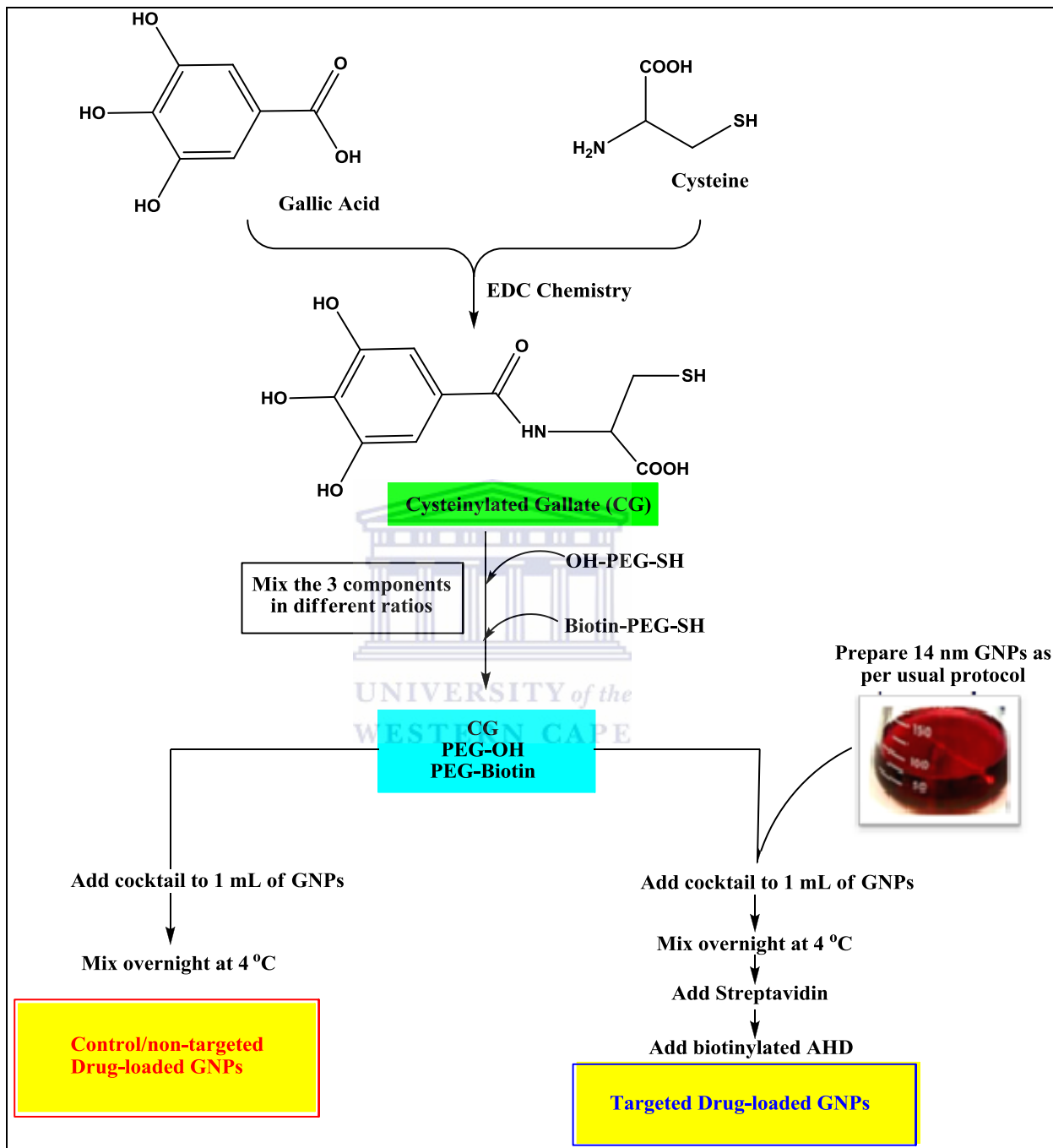
Figure 2.2. Schematic representation of the synthesis of AHP-GA-GNPs.

2.8. Quantitative Cellular uptake of GNPs, QDs and GA

The cellular uptake experiment was determined following the methods described by (Kumar *et al*., 2012 and Reuveni *et al*., 2011) with some modification. Briefly, the 5×10^5 of Caco-2 cells were cultured in a 12 well plate for 24 hrs. The cells were then treated with QDs, AHP-QDs, GNPs, AHP-GNPs, GA or AHP-GA-GNPs for 24 hrs. The cellular uptake was determined using ICP-OES or ICP-MS, as described in Section 2.5.

2.9. Cell viability test on GA, GNPs, QDs and AHP

The cell viability test was determined using WST-1 following the methods described by Ngamwongsatit *et al*., 2008, Maurya *et al*., 2011, and Yin *et al*., 2013, with some modification. In brief, the 2×10^5 of Caco-2 cells were cultured in a 96 well plate for 24 hrs. The cells were then treated with different concentration of either QDs; AHP-QDs, (0, 6.25, 12.5,25 nM), GNPs; AHP-GNPs (0, 1, 2, 4), GA (0, 12.5, 25, 50 nM), AHP-GNPs-GA (0, 1, 2, 4 nM) or AHP (0, 6.25, 12.5, 25 nM) for either 24 or 48 hrs. The cell viability was determined using WST-1 as described in Section 2.41.

2.10. Determination of apoptosis by APOP*ercentage* ^{TM}

Apoptosis assays involve detection and measurement of apoptosis in mammalian, anchorage-dependent cells during *in vitro* culture. The assay was done according to Meyer *et al*., (2008) protocol, with some minor modification. The assay uses a dye that is selectively imported by cells that are undergoing apoptosis. Necrotic cells cannot retain the dye and therefore are not stained. To determine the apoptotic effect of GA, the Caco-2 cells ($1x10^6$ cell/mL) were seeded in a 12 well plate for 24 hrs. The cells were then treated with 25 nm, GA, 2nm AHP-GA-GNPs and Cisplatin 10 µM (positive control) for 24 hrs. The negative control cells remain untreated for 24 hrs. The cells were examined under microscope for morphological changes. They were then trypsinized and washed twice with PBS, and thereafter, resuspended in PBS. The 200 µl APOP*ercentage*^{TM} dye in complete media (1:60 dilutions) was added to the tubes and cells were incubated for 30 minutes at 37°C humidified CO_2 incubator. The 500 µl of PBS was then added and spun for 5 minutes at 300 rpm. The cells were washed twice with PBS and resuspended in 400 µl PBS. The cells were then acquired and analyzed on FACScan ^{TM} (Becton Dickson) instrument. Acquisition was done by setting forward scatter (FSC) and side scatter (SSC) on a scale dot plot.

The APOP*ercentage*^{TM} (FL-3 channel) was measured against relative cell numbers. Negative control cells were used to set cells in the negative quadrant before all sample were acquired. Acquisition was done in Log mode. A minimum of 10,000 cells per sample were acquired and analyzed using CELL Quest PRO software (BD Biosciences),

by setting the non-stained (untreated) cells population in the first quadrant (10^1) of the forward side scatter histogram dot plot and cells which appeared after 10^1 and in the second (10^2) or third (10^3) quadrant were regarded as APOP*ercentage*^{TM} positive (apoptotic/necrotic).

2.11. Determination of Caspase 3 activity

Caspase 3 activation plays a major role in the execution of apoptosis. To determine whether GA-loaded GNPs activate Caspase 3 in Caco-2 cells, the cells (2.5×10^4 cell/mL) were seeded in a 24-well culture plate and were incubated at 37 $^\circ$C in a humidified 5% CO_2 incubator for 24 hrs. The assay was done following the work done by Budihardjo and colliques (1999) with some modification. The cells were then treated with GA (25 nM), AHP-GA-GNPs (2 nM) and Cisplatin (10 µM) (positive control) for 24hrs at 37 $^\circ$C incubator. The negative control cells were untreated for 24 hrs. The cells were examined for morphological changes using an inverted light microscope. Cells were trypsinized as described in section 2.2.1. The pellet was washed twice with 500 µl cold PBS and resuspended in 0.5 ml Cytofix/Cytoperm^{TM}, and then incubated on ice for 20 minutes. The cells were then spun in a bench top centrifuge at 300xg for 2 minutes. The Cytofix/Cytoperm^{TM} was then aspired and discarded. The pellets were washed twice with 0.5ml Perm/Wash^{TM} buffer. Total number of samples was determined, and the amount of Perm/Wash^{TM} buffer and anti-active Caspase-3 Antibody were calculated so that each sample received 100 µl Perm/Wash^{TM} buffer and 20 µl anti-active Caspase 3 Antibody.

The cells were then incubated for 30 minutes at RT in the dark. At the end of the incubation period, the cells were washed twice with 1.0 ml Perm/Wash™ buffer. The supernatant was discarded and the pellets were resuspended in 0.5ml Perm/Wash™ buffer. The cells were acquired and analyzed on FASCcan™ FACScan™ (Becton Dickson) instrument. Cell fluorescence was measured using dot plot, (by setting the forward scatter (FSC) and side scatter (SSC) to differentiate cell populations and cell debris. Active Caspase 3 FITC was measured against relative cell numbers. Negative control cells were used to set the cells in the negative quadrant before all samples were acquired. A minimum of 10,000 cells per sample were acquired and analyzed using CELL Quest PRO software (BD Biosciences).

2.12. *Ex vivo* binding and cellular uptake studies

2.12.1. Isolation of Endothelial cells (ECs) from WAT using Dynabeads®

2.12.2. Digestion of WAT by collagenase method

The 5 g of white adipose tissue (WAT) isolated from Epidydimal and Inguinal (subcutaneous) fat depots of the male Wistar rats, fed a high fat (HF) diet or chow control diet were weighed and rinsed in PBS. The tissues were minced in PBS using a sharp sterile scissor. The 1 % BSA and 1mg/ml collagenase prepared in PBS, was added to the minced tissue in a 200 ml conical flask and incubated at 37°C water bath until completely digested. Tubes were checked every 10 minutes. The homogenates were filtered through 200 µm nylon filters to remove any large pieces of undigested tissue and were then kept at room temperature for 3-5 minutes to allow visible separation. The upper layer

(supernatant) which contained the adipocyte was discarded and the bottom layer (the microvascular fraction) was then filtered using 20 μm nylon filters. The filtrate was used for the isolation of the endothelial cells using Dynabeads® method.

Dynabeads® CD31 are uniform, superparamagnetic polystyrene beads (4.5 μm diameter) coated with a mouse IgG1 monoclonal antibody specific for the CD31 cell surface antigen PECAM-1 (platelet endothelial cell adhesion molecule-1). The Dynabeads® were prepared by resuspending a vial of 25 μL with an equal amount of the buffer in a 2ml Eppendorf tubes. The tubes were placed in a magnet (DynaMag™-2 Magnet, Invitrogen) for one minute and the supernatant was discarded. The tubes were then removed from the magnet and were again mixed with equal amount of buffer as the initial volume of the Dynabeads. The dynabeads were then ready to be used, in the isolation of the ECs. The ECs was prepared by adding an appropriate amount of the Dynabeads® to a single suspension of the microvascular fraction. The tubes were then incubated for 20 minute at $4°C$ with gently titling and rotation. The tubes were thereafter placed in a magnet for 2 minutes. The supernatant was discarded and the beads bound endothelial cells were washed 3 times with PBS (equal amount with the initial dynabeads). The beads bound endothelial cells were counted using the Countess® Automated Cell Counter (Invitrogen) and then used for cellular uptake experiment.

2.12.3. Treatment of primary ECs with AHP functionalized QDs

For the binding of AHP- QDs to primary cells, the isolated microvascular ECs from the inguinal and epididymal WAT of both lean and obese rats were incubated with 50 and 25 nM concentration of AHP-functionalized and unfunctionalized QDs for 1hr at 37°C. The cells were spun at 300 rpm for 3 minutes and the cell pellets were washed twice with 1X PBS and processed for ICP-OES as described in section 2.5.

2.13. Caco-2 cells

The Caco-2 cells are a continuous line of heterogeneous human epithelial colorectal adenocarcinoma cells. Although derived from a colon (large intestine) carcinoma, when cultured under specific conditions the cells become differentiated and polarized such that their phenotype, morphologically and functionally, resembles the enterocytes lining the small intestine. The Caco-2 cell line was used as an *in vitro* model in this study. The choice of the cell line was based on presence of PHB which is expressed on the surface of this cell line (Sharma and Qadri, 2004).

Caco-2 cells were grown in Dulbecco's modified Eagle's medium (DMEM) as described by Klein *et al*, 2009, supplemented with 10 % foetal bovine serum (FBS), 2 mM glutamine and antibiotics (2 % penicillin and streptomycin) under standard cell culture conditions (humidified incubator maintained at 37°C and 5 % carbon dioxide). Growing

cells were observed daily under a Nikon inverted light microscope to monitor confluency and contaminations.

## 2.14. Indirect cellular binding of AHP using competitive displacement

Caco-2 cells were used as *in vitro* model as described in section 2.9. The binding and internalization of AHP was determined at $4°C$ and $37°C$, by flow cytometry (FACS) and fluorescence microscopy.

2.14.1. Flow cytometer

Cells were seeded in a 24 well plates for 24hrs. They were then incubated with different concentrations of FITC-labelled AHP (AHP-FITC, 0-2 mM) at $4°C$ and $37°C$ for 1 hr. The cells were trypsinized for 5 minutes at $37°C$ and centrifuged at 300 rpm for 5 minutes and the pellets were resuspended in 500 µl PBS, and the cells were analysed using FACScan[TM] (Becton Dickson) flow cytometer. A minimum of 10,000 cells per sample were acquired and analysed using CELL Quest PRO software (BD Bioscience).

2.14.2. Fluorescence microscopy

Cells were seeded on a cover slip in a 6 well plate. They were incubated with different concentrations of FITC-labelled AHP (AHP-FITC, 0 - 2 mM) at 4°C and 37°C for 1 hr. The cells were thereafter, fixed with 4 % paraformaldehyde for 15 minutes at both 4°C and 37°C. The cells were then washed twice with 1X PBS. The cover slip were removed, and placed upside down on a slide containing mounting media (flouroshield). The slides were viewed under fluorescence microscopy, using DAPI and FITC filters and results analysed under Axio vision software. The specific binding was also examined by competitive binding with AHP-GNPs at 4°C and 37°C. In brief, the cells were incubated with 1mM AHP-FITC and 3nM AHP-GNPs at 4°C and 37°C for 1 hr. The cells were then prepared for flow cytometry and fluorescence microscopy as described above.
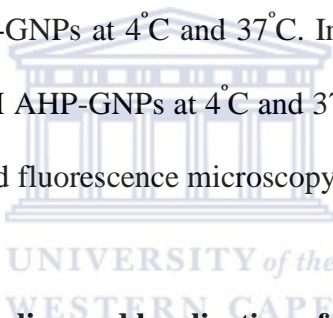
2.15. Immunofluorescence labeling and localization of prohibitin

The 10^{6} cells/mL were cultured on a cover slip in a 6 well plate for 24 hrs at 37°C. The cells were incubated with 1mM AHP-FITC for 24 hrs. They were washed twice with 1X PBS and fixed with cold methanol (methanol in Triton^{R} X-100) for 5 minutes at 4°C. The cells were then washed twice with PBS and incubated with PBS/BSA (0.5 % BSA in PBS) at room temperature (RT) and incubated for 30 minutes. They were then incubated with primary antibody; purified anti-prohibitin (1:10 dilution, diluted in PBS/BSA) for 1 hr and thereafter washed twice with PBS and incubated with secondary antibody; donkey anti-rabbit-IgG-FITC, diluted as the primary antibody. The cells were washed twice with

PBS and the cover slips were transferred to the slide containing mounting media, and slides viewed under fluorescence microscopy using Texas Red filter.

2.16. MitoTracker$^®$ staining

To label mitochondria, MCF-7 cells were simply incubated with MitoTracker$^®$ Red. The 10^6 cells/mL were grown on coverslips in a 6 well plate for 24 hrs at 37 $^°$C. The media was removed and cells were washed with PBS and trypsinized for 5 minutes at 37$^°$C. They were then spun for 3 minutes at 300 rpm and washed twice with PBS. The cells were then stained with pre-warmed MitoTracker$^®$ Red prepared in media and incubated at 37$^°$C for 30 minutes. They were then washed twice with PBS and fixed with 4 % paraformaldehyde at 37$^°$C for 15 minutes, and were again washed with PBS. The cells were thereafter, incubated with 0.1 % Triton^R X-100 in PBS for 10 minutes to permebialize the cells. The cells were rinsed with PBS and the coverslips were transferred to a slide containing mounting media and placed upside down. The slides were viewed under fluorescence microscopy and results analysed using Axio-vision software.

2.17. *In vivo* studies

2.17.1. Animals and Ethics approval

Twenty (20), 3 weeks male Wistar rats weighing 40-50 g were obtained from Medical Research Council (MRC) animal facility. All procedures involving animals were approved by the MRC Ethics Committee for Research on Animals (ECRA), ethics number: **03/10**. The study was also recommended for approval to the University of the Western Cape (UWC) Senate's Research and International Relations Committee (RIRC) by UWC's Faculty of Natural Sciences RIRC, reference number: **SCR IRC 2012/06/17**. All rats were housed under a controlled temperature (22-25 $^{\circ}$C), humidity (45-55 %), ventilation (15-20 cycle/hour) and a 12 hour photo-period. They were body weight matched and assigned to different groups. Four rats were housed per cage from the beginning of the study and throughout the obesity induction phase. The cages were provided with bedding material and a black perspex nest box. The cages were changed weekly. Fresh food (HF patties and Chow) and water were provided *ad libitum* daily.

2.18.2. Grouping of animals and induction of obesity

The 20 male Wistar rats were divided into two groups: one group was the rats fed on standard chow (n= 4) and other was rats fed on high fat diet (n= 16) as indicated in section 2.13.3, to induce obesity. The rats were monitored daily and their body weights were measured twice per week.

2.18.3. Preparation of Lard high fat (HF) Diet

The lard high fat diet was prepared using lard, sugar and chow as indicated in **Table 2.6**. The lard was melted and sugar and chow were weighed. All the ingredients were mixed in a bowl with the addition of warm water. They were rolled on a tray and cut into cubes using a sharp knife or pizza cutter and was kept at $4^{°}$C until set. The diet was then divided into plastic bags and stored at -20$^{°}$C until use.

Table 2. 6. Ingredients for Lard HF diet preparation

Ingredients	Amount (g)	Percentage (%)
Chow	1800	72
Lard	600	24
Sugar	100	4
Water	**1 liter**	

2.19. Treatment of rats
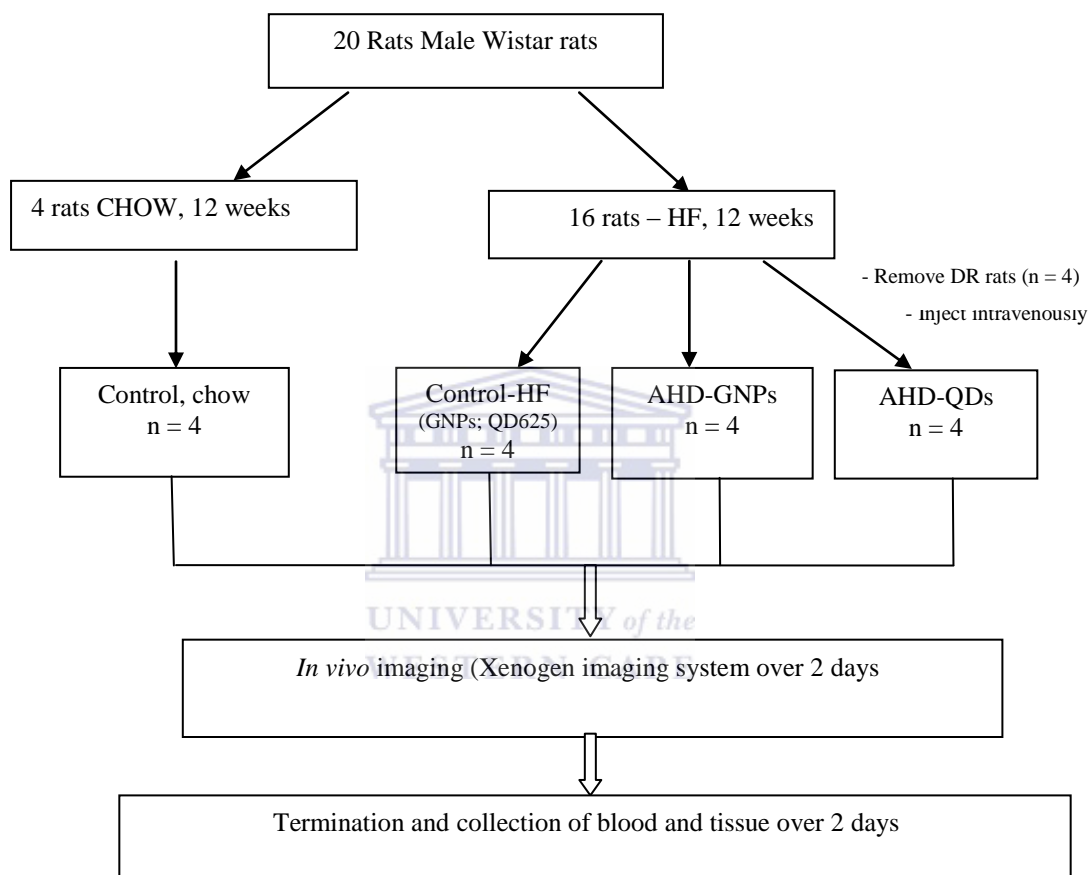
## 2.19.1. General experimental design

Figure 2.3. Schematic diagram representing experimental design used for the *in vivo* studies

2.19.2. Experimental procedure: Treatment of animal with nanoparticles

Twenty male Wistar rats were used in the study. Four rats were fed CHOW (n = 4), and sixteen rats were fed a high fat diet (HF) diet (n = 16) for 12 weeks *ad libitum*. The body weights were measured twice per week. After 16 weeks on HF diet, diet resistance (DR) rats were removed from the study, and the 12 rats divided into three groups (n = 4 per group). Imaging and termination by exsanguinations were performed over two days, 8 rats per day. On the day, eight rats (2 at a time) were anesthetized by nasal inhalation of halothane (initiation at 5 %, and maintenance at 1 % in oxygen at 1L/min flow rate). Rats were injected intravenously through the tail vein with 200 µl of PBS (CHOW and HF control groups), 200 µl of AHP functionalized GNPs (AHP-GNPs group), or unfunctionalized GNPs dissolved in PBS and 200 µl of AHP functionalized QDs (AHP-QDs group) or unfunctionalized QDs (QD625) dissolved in PBS and kept for 24 hrs.
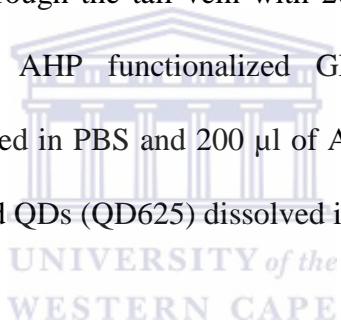
2.19.3. Termination of animals

After 24 hrs, rats were terminated via exsanguination under anaesthesia with an ip injection with sodium pentobarbital, 30 mg/kg body weight. Bloods were collected through hepatic vein and tissues (adipose tissues, liver, kidney, lungs, spleen, stomach, brain, heart, pancreas, testes, and adrenals) were dissected, weighed and imaged using IVIS® Lumina XR (Caliper Life Sciences) as shown in **Figure 2.4**. The adipose tissue and organs were snap-frozen in liquid nitrogen to be used for analysis of any effects inflicted by the therapy using molecular and cellular techniques. The tissues and organs were stored at -80°C until analysis. The blood was stored in the refrigerator at 4°C.

The serum samples were prepared followed the methods described by Yen and Hsu, (2007), with some minor modification. The 10ml blood samples were collected from both lean and obese rats through hepatic vein. The bloods were centrifuge at 12000 rpm for 10 minutes, the resulting supernatant, designated serum, was carefully removed using a micropipette and was transferred to 2 ml tubes. The serum was then stored at -80°C fridge for later use.

2.20. Tissue biodistribution of gold and ccadmium

The tissue and organs were processed according to the work done by Sonavane *et al*., 2008 with some modifications. The tissues and organs were cut into small pieces (1g each), homogenized and completely lysed in 2ml of aqua regia in a screw cap glass bottles. The homogenate was digested in a 70°C oven for 24 - 48 hrs. They were then redissolved in 2ml of 2 % HCl and sonicated for 2 - 5 minute or until resuspended. The resultant samples were diluted in 2 % HNO_3 and analyzed by ICP-OES. Cadmium (Cd) and gold (Au) were used as standards to quantify the concentration of QDs and GNPs in the tissue samples.

Figure 2.4. The *Ex vivo* tissue imaging using IVIS® Lumina XR (Xenogen imaging system)

2.21. Biochemical assays

## 2.21.1. Insulin, non-esterified fatty acid (NEFA) and glucose measurements

The Glucose oxidase assay, NEFA C and Rats Insulin Elisa kits were used to measure the serum concentration of glucose, free fatty acid and insulin. Serum samples were obtained from lean and obese Wistar rats, treated with GNPs, AHP-GNPs, GDs, AHP-QDs and PBS.

2.21.2. Quantitative determination of Insulin concentration

The concentration of insulin was measured using Mercodia Ultrasensitive Rat Insulin Elisa kit, (Mercodia developing diagnostics, 2010). Samples were measured in triplicate. The 25 µl of the serum samples, calibrators and 100 µl of the enzyme conjugate were added and mixed in a 96 well plate. The plate was incubated at room temperature (25°C) for 2 hrs with shaking. The plate was thereafter washed 6 times, with 300 µl wash buffer using an automatic plate washer. The 200 µl substrate TMB was then added to each well and incubated for 15 minutes at 25°C. The 50 µl of stop solution was added to each well to stop the reaction. The plate was shaken for 15 sec and the optical density or Abs was taken at 450 nm using a POLAR STAR plate reader. The concentration of insulin in µg/L was determined from the standard curve generated from calibrators.

2.21.3. Quantitative determination of NEFA concentration

The Wako NEFA C test kit was used to measure the concentration of free fatty acid from serum samples. The samples were measured in triplicate, according to the manufacturer protocol, (Wako). The 20 µl of the serum sample, standard, reagent blank and 500 µl of colour reagent A were mixed in a 0.6 eppendorf tube, and incubated at $37^{\circ}C$ for 10 minutes. The 1000 µl of the colour reagent B was added to all tubes and were further incubated for another 10 minutes. The tubes were thereafter mixed and 200 µl of each sample were transferred to a 96 well plate. The NEFA concentration were obtained by measuring Abs of the blue purple colour at 550 nm using Polar star plate reader. The samples were measured in triplicate. The results were determined using the formula below:
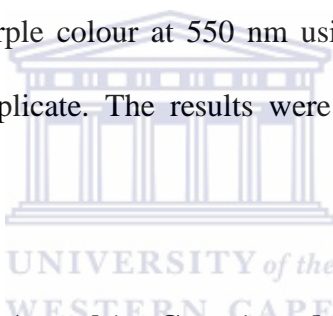
Free fatty acid (mg/dL) = Abs (sample) x Conc (standard) (mg/dL) / Abs (standard)

2.21.4. Quantitative determination of glucose concentration

In this experiment, the glucose concentrations from lean and obese rats were determined using glucose oxidase assay kit, (Sigma Aldrich). Briefly, 50 µl of serum sample, 5 µl standards and 100 µl of assay reagent were added to 96 well plates and were incubated at 37°C for 30 min. Then 100 µl of H_2SO_4 was added to stop the reaction and the plate was further incubated for 5 minute. The glucose concentrations were obtained by measuring the Abs or intensity of the pink color at the wavelength of 540 nm. The samples were measured in triplicates using a POLAR STAR plate reader. The glucose concentration was determined using the formula:

Glucose (mg) = Abs (sample) x (mg glucose in standard)/ Abs (standard)
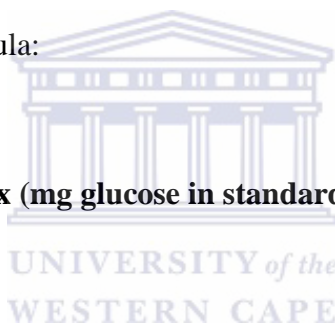
2.22. Statistical Analysis of data

The different parameter were analysed using one way Anova, to assess the different between samples used for *in vitro* experiments. Student's t-test was used to compare the differences between two groups used for *in vivo* experiments. All the analyses were performed using Graph pad prism 5 statistical package. The samples were considered statistically significant when $p < 0.05$

UNIVERSITY *of the*

WESTERN CAPE

CHAPTER 3

3. Results and discussion

3.1. Synthesis, functionalization and characterization of gold NPs (GNPs)

The AHP-functionalized GNPs (AHP-GNPs) were synthesized at Mintek, as described in section 2.7.1. To confirm the functionalization of GNPs, agarose gel electrophoresis (A) and UV-Vis spectroscopy (B) were performed (Figure 3.1) before (GNPs) and after functionalization (AHP-GNPs). The gel electrophoresis (Figure 3.1.A) showed that the functionalized GNPs migrate slower in the gel than unfunctionalized GNPs (GNPs) while UV-Vis spectrum (Figure 3.1.B) showed the functionalized GNPs has a higher absorption peak as compared to unfunctionalized GNPs and Transmission electron microscopy (TEM) analysis (Figure 3.1.C) shows that the functionalized GNPs are spherical in shape and well dispersed.
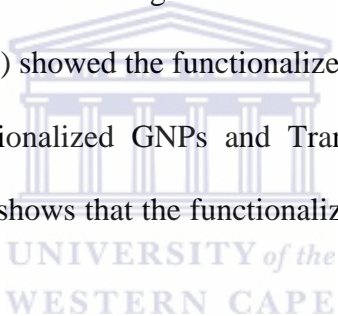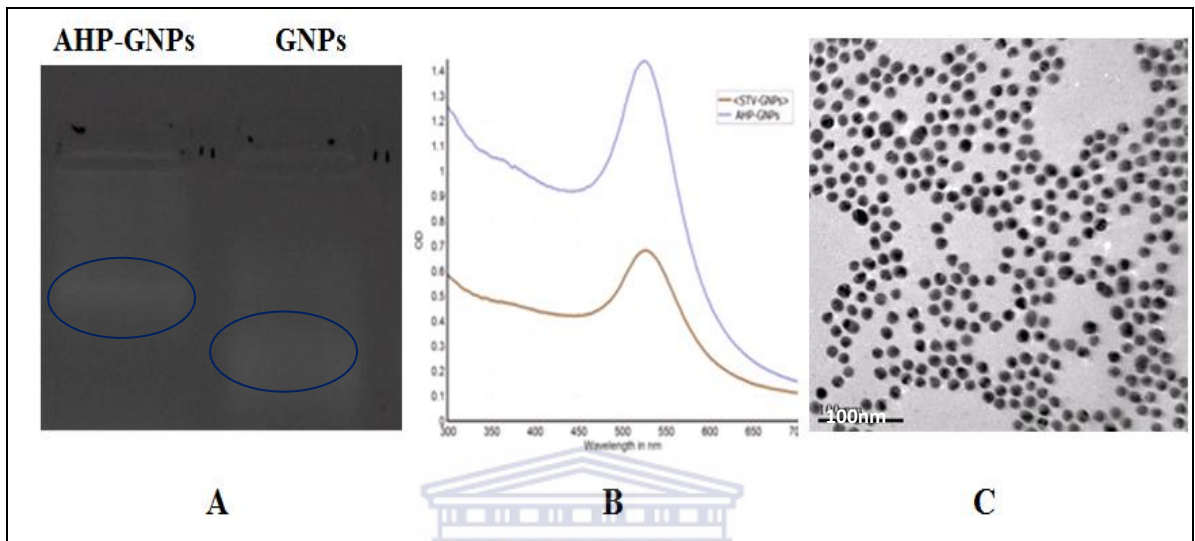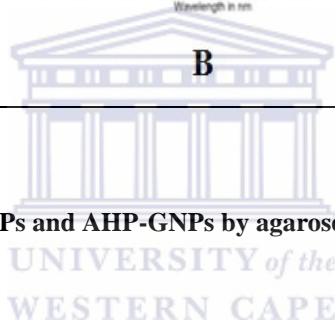
Figure 3. 1. Characterisation of GNPs and AHP-GNPs by agarose gel electrophoresis (A), UV-vis spectroscopy (B) and TEM (C).

3.2. Synthesis, functionalization and characterization of AHP-GA-GNPs

The nanoparticles functionalized with AHP and gallic acid (GA) was also synthesized at Mintek. The nanoparticles were characterized using TEM and UV-Vis spectroscopy. As indicated in **Figure 3.2,** the particles were found to be uniform and spherical in shape as determined by TEM and UV-Vis spectrum indicates the maximum absorption peak of 530 nm.
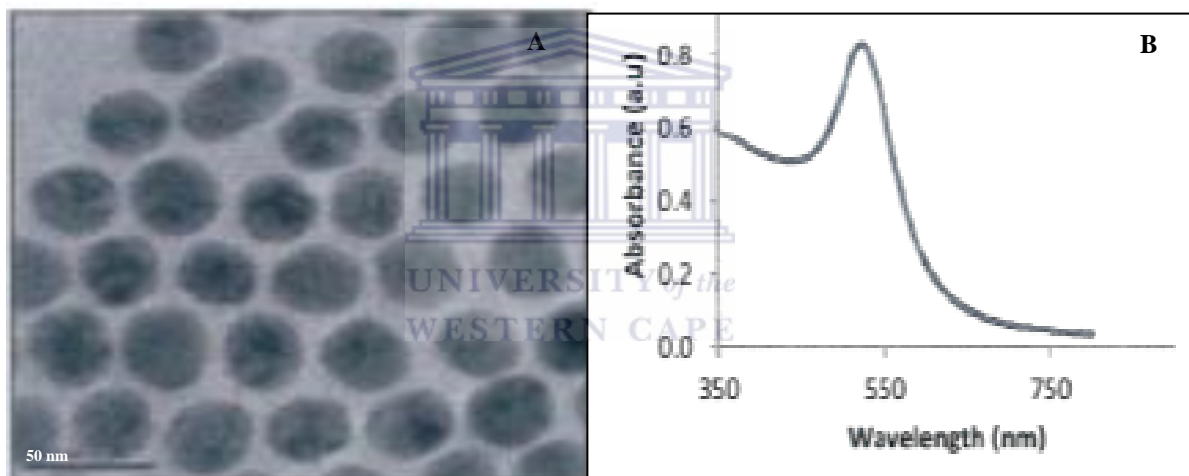

Figure 3. 2. The TEM (A) and UV-VIS spectrum (B) analysis of 14nm AHP-GA-GNPs.

3.3. Functionalization and characterization of Quantum dots (QDs) and AHP-QDs

The QD625 (Invitrogen) were functionalized with AHP as described in section 2.7.2. To confirm the functionalization of QDs with AHP (AHP-QDs), agarose gel electrophoresis was performed. As shown in **Figure 3.3 (B),** AHP functionalized QDs migrate slower in the gel as compared to unfunctionalized QDs. **Figure 3.3 (A)** shows the fluorescence of QD625 and AHP-QDs, under UV (365 nm) light, using UVP imaging system. The HORIBA Nanolog FL3-22 Triax was also used to confirm the photoluminescence of the QDs. The emission wavelength for both QD625 and AHP-QDs was 625 nm as indicated in **Figure 3.4.**
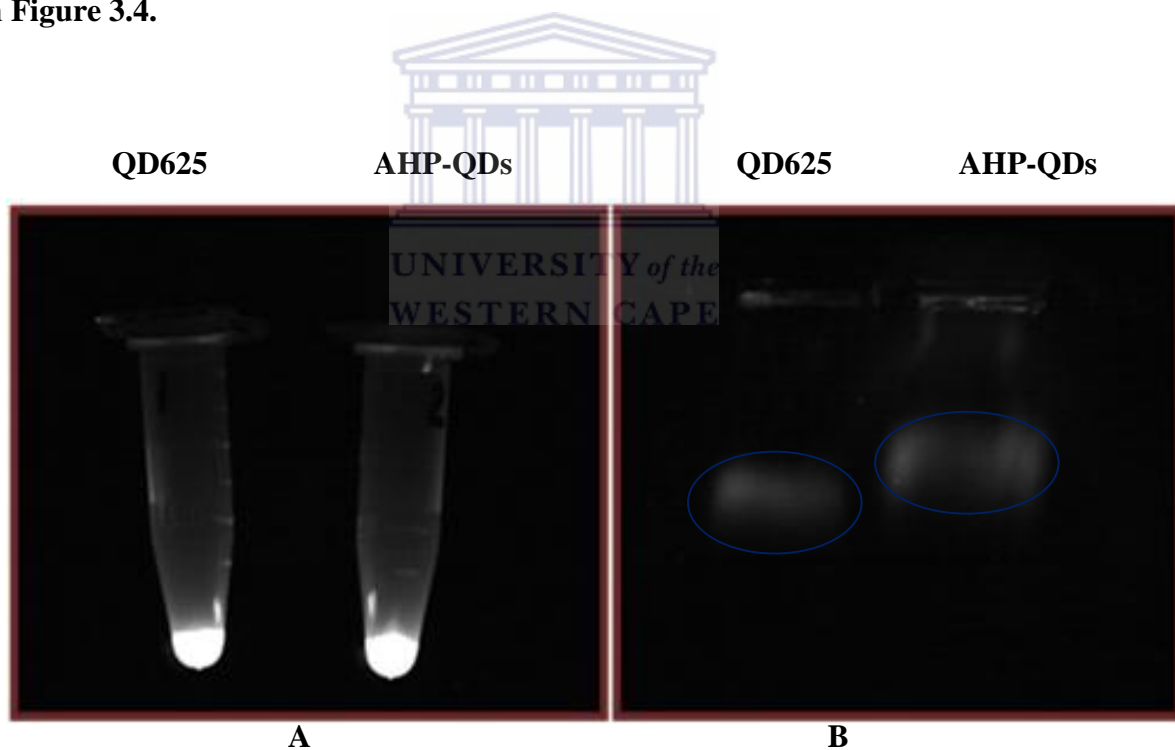

Figure 3.3. Fluorescence images of QD625 and AHP-QDs.

Image **(A),** represent the fluorescence of QD625 and AHP-QDs before gel electrophoresis while image **(B),** show agarose gel electrophoresis of both QD625 and AHP-QDs.
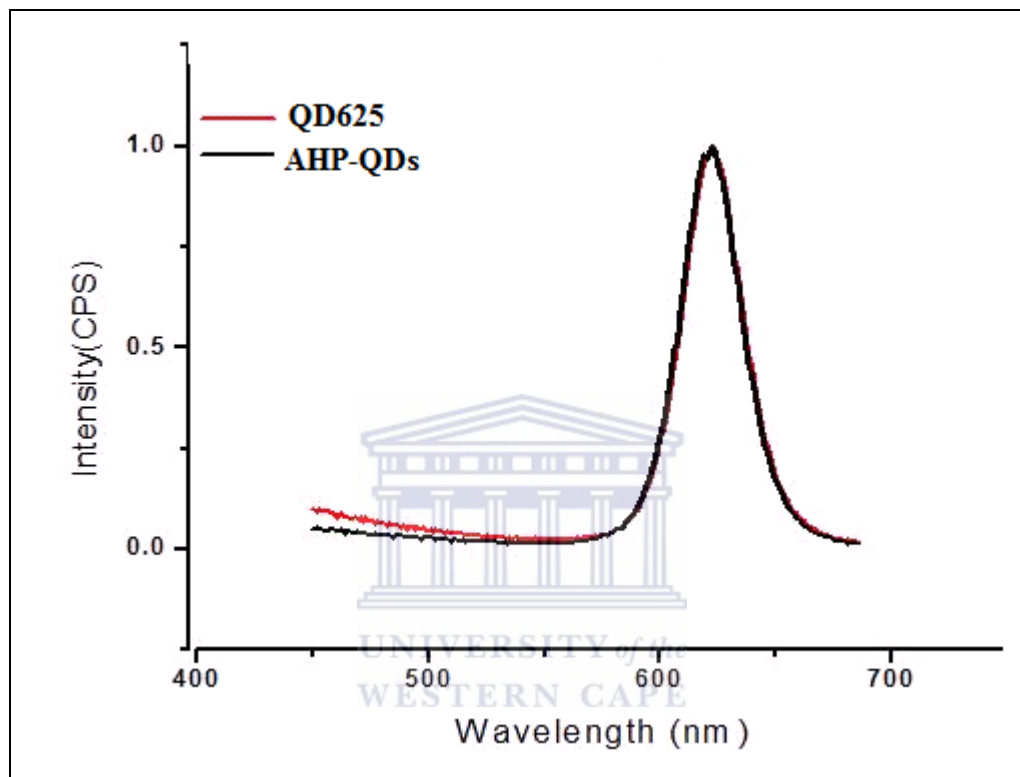
Figure 3.4. Photoluminescence (PL) spectra of QD625 and AHP-QDs.

The spectrum were measured using HORIBA Nanolog FL3-22 Triax

3.2. Immunofluorescence labeling and localization of prohibitin

MCF-7 is a breast cancer cell line that expresses prohibitin (PHB), (Rastogi *et al*., 2006), a multifunctional membrane protein receptor. PHB is expressed on the plasma membrane and the mitochondria. To investigate the localization of PHB in MCF-7 cells, the cells were stained with Anti-PHB-FITC (Figure 3.5.A) and the Mitotracker[R] Red (Figure 3.5.B) and analysed by fluorescence microscopy.
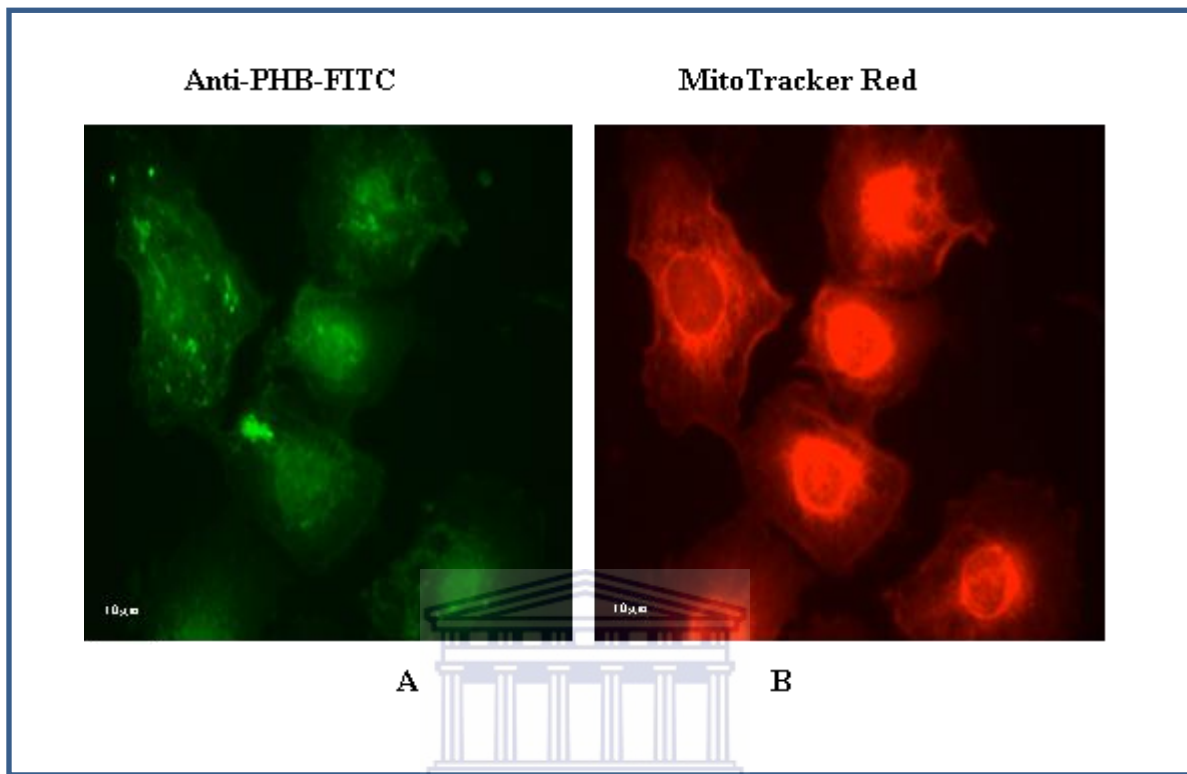
Figure 3. 5. Fluorescence image showing intracellular localization of prohibitin in the mitochondria of MCF-7 cells.

Cells were stained with anti-PHB-FITC (A) and Mitotracker Red (B). Images were taken using fluorescence microscopy at 100 x magnification. The scale bar is 10 μm

To further confirm the presence and expression of PHB on MCF-7, the cells were stained

with Rhodamine conjugated anti-prohibitin antibody (Anti-PHB-Rhodamine) and DAPI.

The Anti-PHB-Rhodamine staining showed the presence of PHB, and that PHB localize

in the nucleus of MCF-7 cells. This is shown in **Figure 3.6,** which shows fluorescence

image of the nucleus under DAPI (A), Rhodamine (B) and the overlay (C), indicating

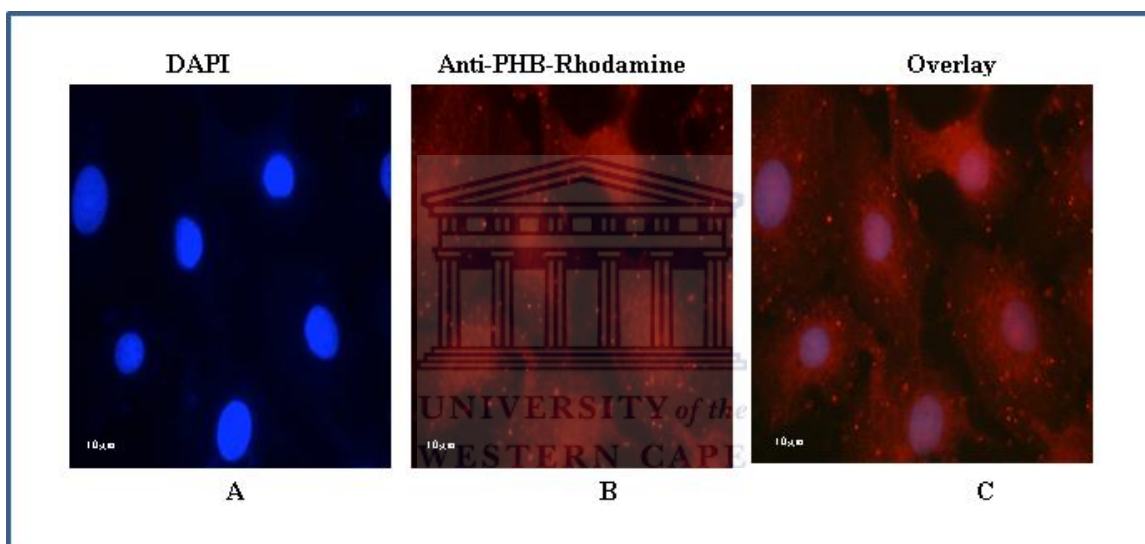Rhodamine staining the nucleus of the cells

Figure 3.6. Fluorescence image showing intracellular localization of prohibitin in the nucleus of MCF-7.

The cells stained with DAPI (A), showing nucleus of the cells, anti-PHB Rhodamine (B), and (C), the

overlay of A and B. Images were taken using fluorescence microscopy at 100 x magnification. The scale

bar is 10 μm.

3.3. Investigating binding and localization of AHP-QDs to PHB expressing cells

3.3.1. Binding to MCF-7

To confirm the binding and localization of AHP-QDs in MCF-7 cells, the cells were incubated with either QD625 or AHP-QDs and were imaged using fluorescence microscopy. It is shown in **Figure 3.7** that the AHP-QDs localized in the nucleus of the MCF-7 cells.
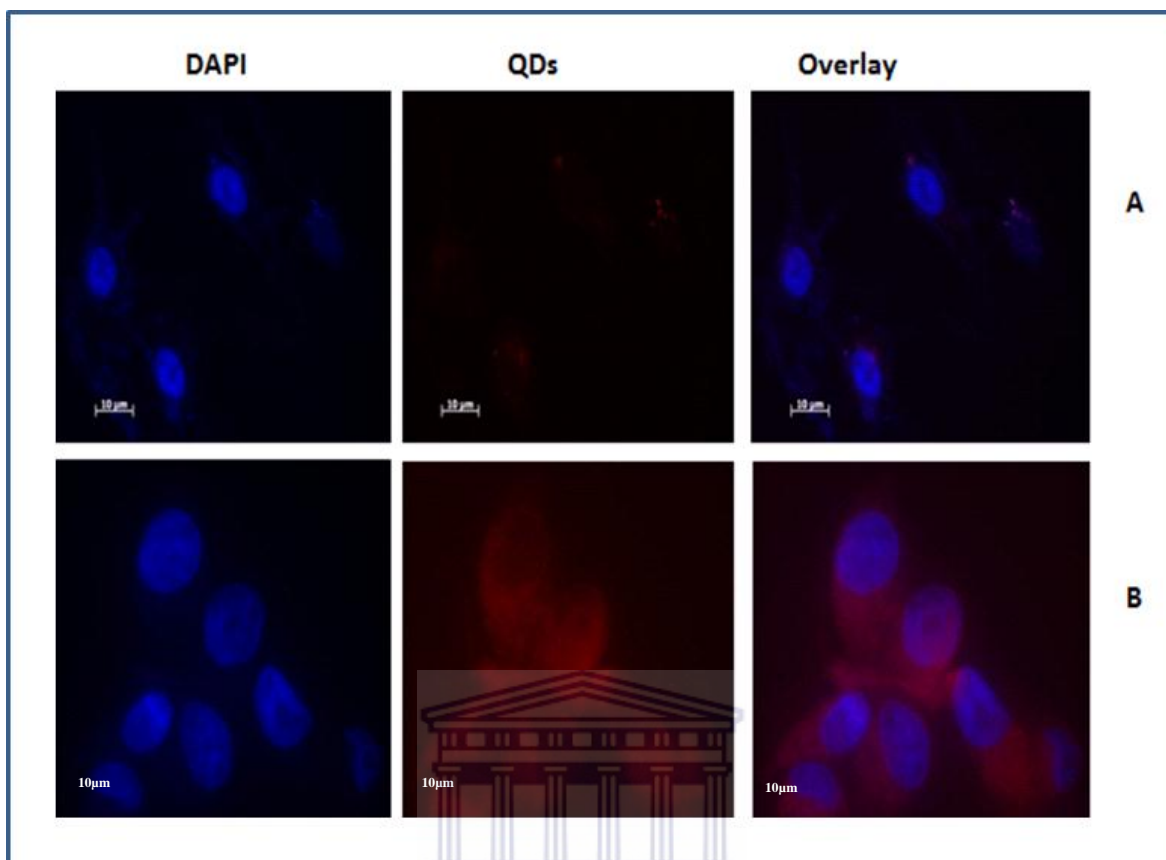
Figure 3. 7. Fluorescence images of MCF-7 cells stained with either QD625 (A) or AHP-QDs (B).

MCF-7 cells were exposed to either QD625 (A) or AHP-QDs (B) for 1 hr. The QD625 fluorescence observed clearly in cells exposed to AHP-QDs (B). Images were taken using fluorescence microscopy at 100x magnification. The scale bar is 10 μm.

3.3.2. Binding to Caco-2 cells

Caco-2 is a colon cancer cell line that was shown to expresses PHB (Sharma and Qadri, 2004). The cells were used to confirm the binding of AHP-QDs to PHB expressing cells. To confirm the binding and localization of AHP-QDs on cells, the Caco-2 was treated with either QD625 or AHP-QDs. The images were taken using fluorescence microscopy. The cells treated with AHP-QDs showed binding to Caco-2 cells, hence red fluorescence while QD625 did not show any fluorescence. This is shown in **Figure 3.8.**
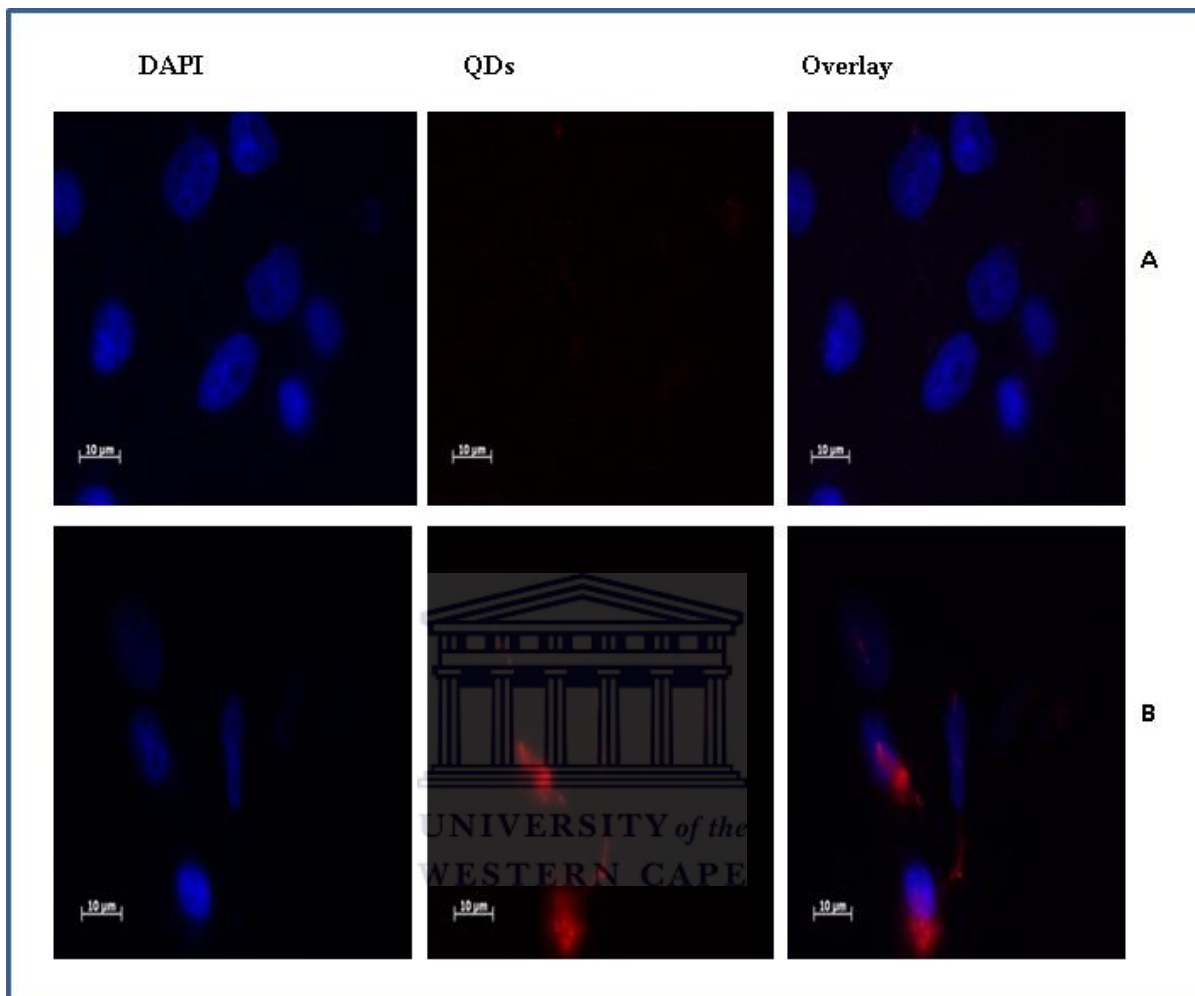
Figure 3. 8. Fluorescence images of Caco-2 cells, treated with AHP-QDs and QD625.

Caco-2 cells were exposed to either QD625 (A) or AHP-QDs (B) for 1 hr. The QD625 fluorescence observed in cells exposed to AHP-QDs (B). Images were taken using fluorescence microscopy at 100x magnification. The scale bar is 10 μm.

3.4. Investigating the Binding of AHP-QDs to non-PHB expressing cells

The binding of AHP-QDs was also investigated using non-PHB expressing cells. These includes: non-cancerous cell lines, CHO (Chinese-Hamster-Ovarian) and KMST-6 (Human-normal fetal fibroblast). These cell lines were used as negative controls. The cells were treated with either QD625 or AHP-QDs. No QDs fluorescence was observed to all the cells treated with either AHP-QDs or QD625 as shown in **Figure 3.9**. This is because the cells don't express PHB, hence no binding, therefore no fluorescence of QDs.
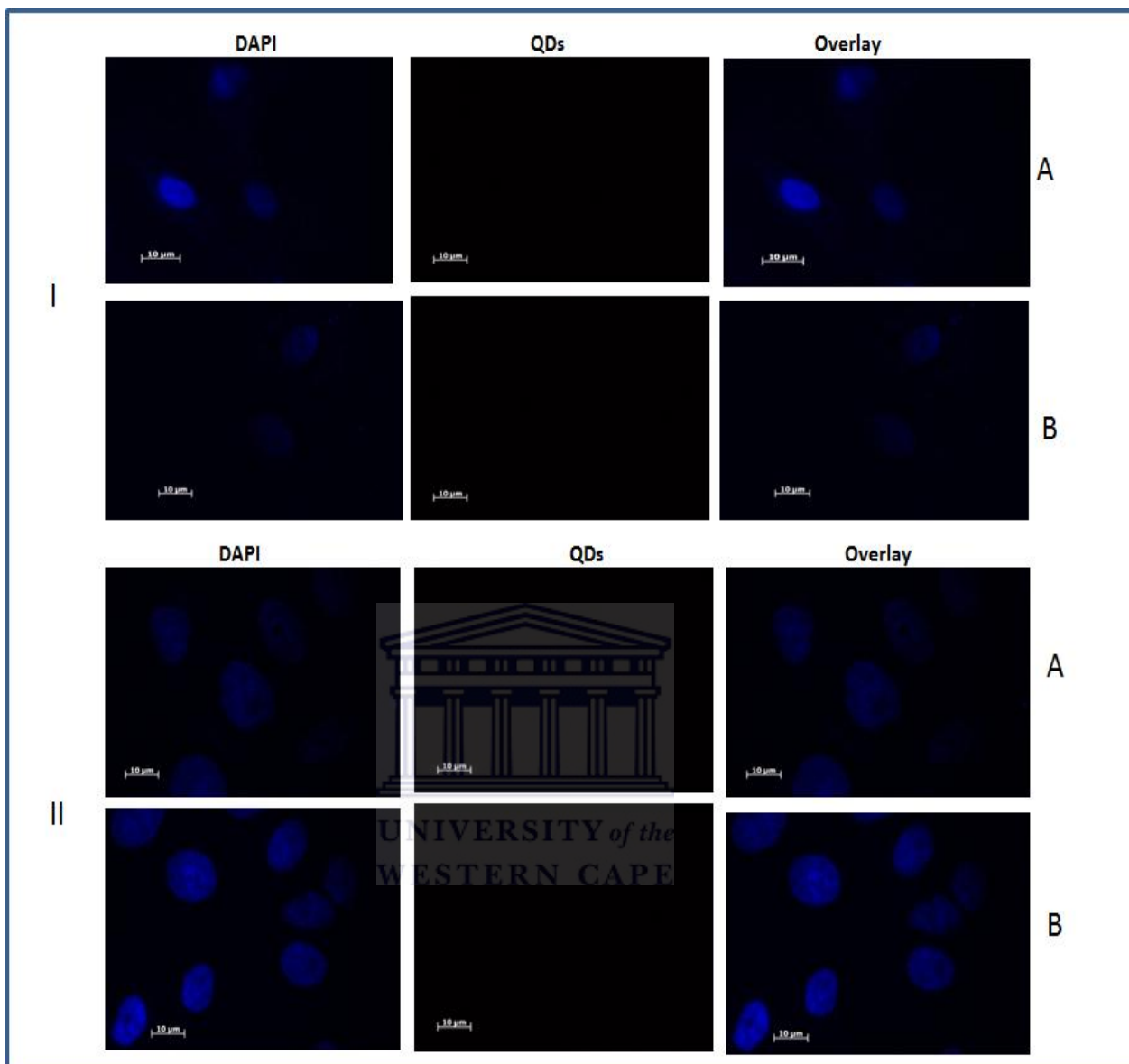
Figure 3. 9. Fluorescence images of CHO and KMST-6 cells treated with AHP-QDs and QD625.

Caco-2 cells were exposed to either QD625 (A) or AHP-QDs (B) for 1 hr. The QD625 fluorescence observed in cells exposed to AHP-QDs (B). (1), represents CHO cells and (11) KMST-6 cells. Images were taken using fluorescence microscopy at 100x magnification. The scale bar is 10 μm.

3.5. Quantitative analysis of AHP binding to Caco-2 cells

To quantitate the binding of AHP to Caco-2 cells (PHB-expressing cells), the cells were incubated with increasing concentrations (0.01-2mM) of AHP-FITC and the fluorescence intensity was measured by flow cytometer. A dose dependent increase in the fluorescence intensity was observed. **Figure 3.10** demonstrating a dose dependent increase in the binding of AHP-FITC to the cells.
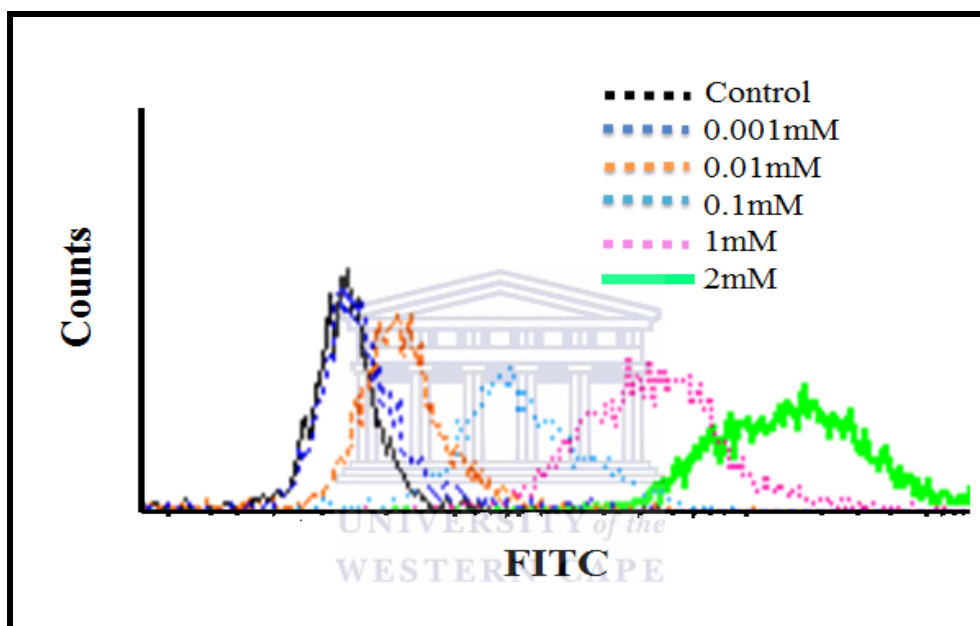
Figure 3. 10. Quantification of cellular binding of AHP-FITC to Caco-2 cells.

Caco-2 cells were exposed to increasing concentration of FITC-labeled AHP (AHP-FITC) for 1 hr at 37°C.
Fluorescence intensity was measured using flow cytometry.

3.5.1. Direct binding of AHP to primary endothelial cells

To examine the specificity of the binding of AHP to primary endothelial cells (ECs), ECs were isolated from the WAT of lean and obese Wistar rats, and incubated with unfunctionalized and AHP functionalized QDs. Binding specificity of AHP-QDs was measured by ICP-OES using cadmium as a standard. The cadmium concentrations in ECs from lean and obese rats were lower for cells exposed to QD625 **(Figure 3.11).** ECs from obese rats also contained higher concentrations of cadmium compared to ECs from lean rats.

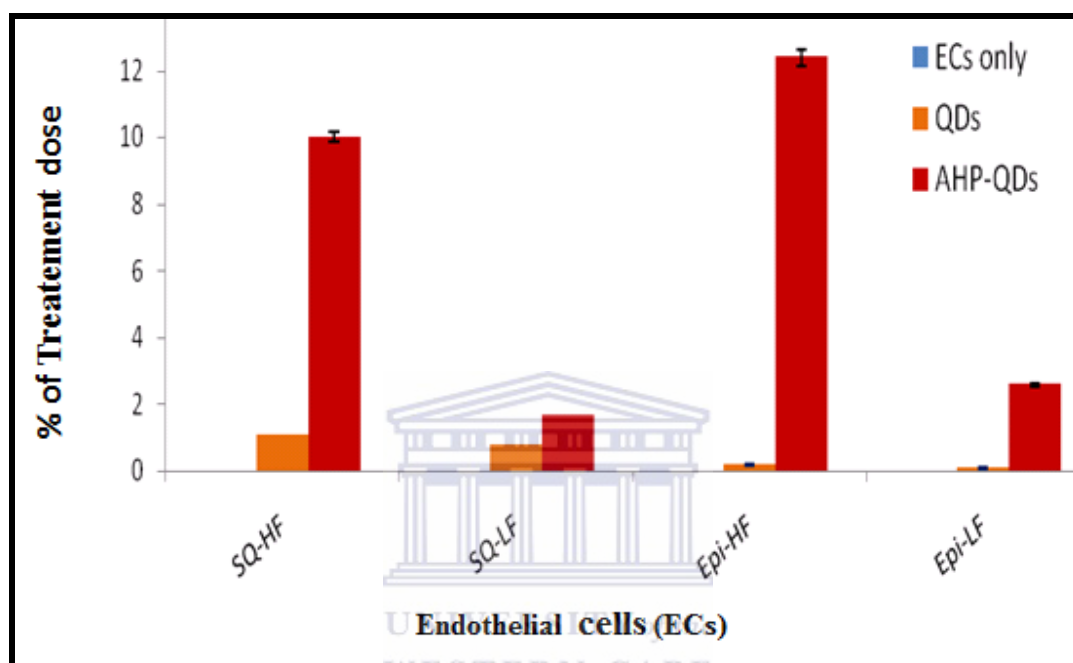**Figure 3. 11. Quantification of AHP-QDs binding to microvascular endothelial cells.**

The ECs from subcutaneous (SQ) and epididymal (Epi) WAT were exposed to either unfunctionalized or AHP-functionalized QDs for 1 hr at 37°C. Bar graph show concentration of cadmium (Cd), as a % of treatment dose present in each sample as determined by ICP-OES analysis.

3.5.2. Indirect binding of AHP

To determine whether the binding of AHP-FITC was specific and temperature dependent, Caco-2 cells were incubated at 4 and $37^{\circ}C$, in the presence or absence of AHP-GNPs which served as a competitor for AHP-FITC. As shown by flow cytometry (**Figure 3.12**). The binding of AHP-FITC to Caco-2 cells was lower at $4^{\circ}C$. Also, incubation of cells with AHP-FITC in the presence of AHP-GNPs prevented the binding of AHP-FITC to Caco-2 cells. These data suggest that the mechanism for the intracellular uptake was mediated by PHB, and also provided an indirect method for the binding of AHP-GNPs to cells.
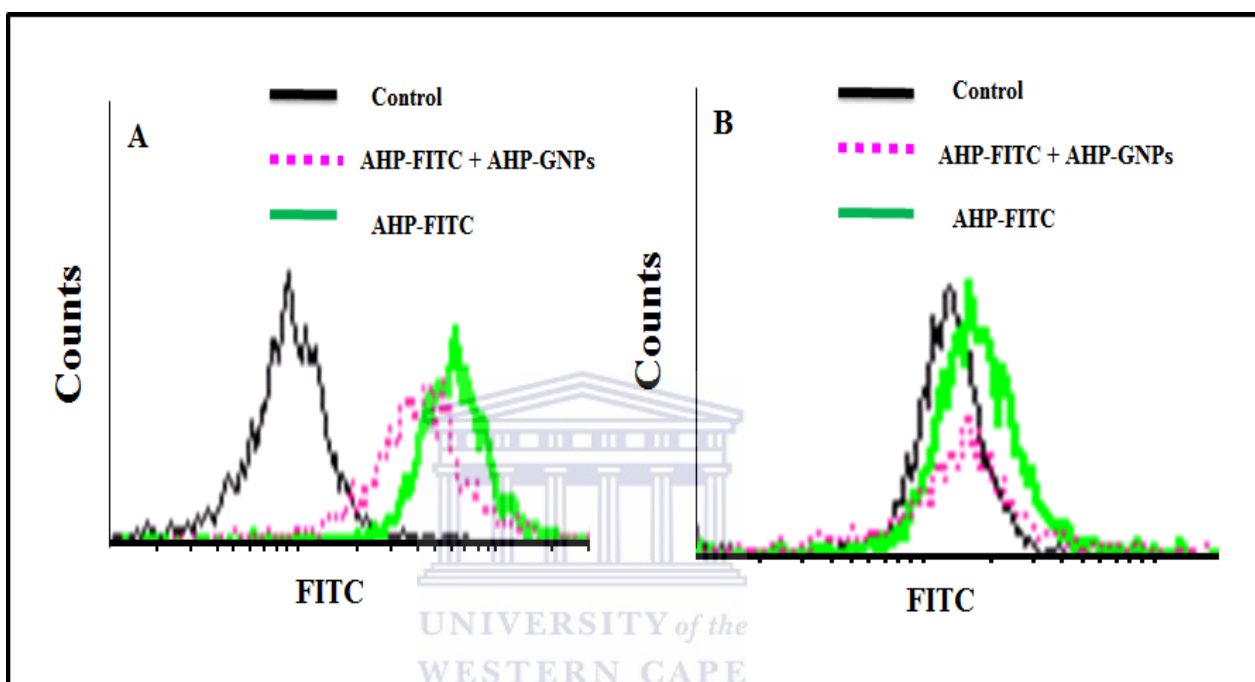
Figure 3.12. Quantification of AHP-FITC binding to Caco-2 cells and the displacement of AHP-GNPs.

The Caco-2 cells were treated with AHP-FITC in the present of AHP-GNPs for 1hr at either 37°C (A) or 4°C (B).

3.6. Intracellular uptake: Quantitative studies

3.6.1. Cellular uptake of AHP-GNPs and AHP-QDs

To assess the cellular uptake, cells were exposed to both unfunctionalized and AHP-functionalized QDs and GNPs to assess the cellular uptake. The cellular uptake was evaluated using ICP-OES. Cadmium and gold were detected in the cells treated with AHP- functionalized QDs and GNPs, No cadmium or gold detected from cells treated with unfunctionalized QDs or GNPs. This is shown in **Figure 3.13.**
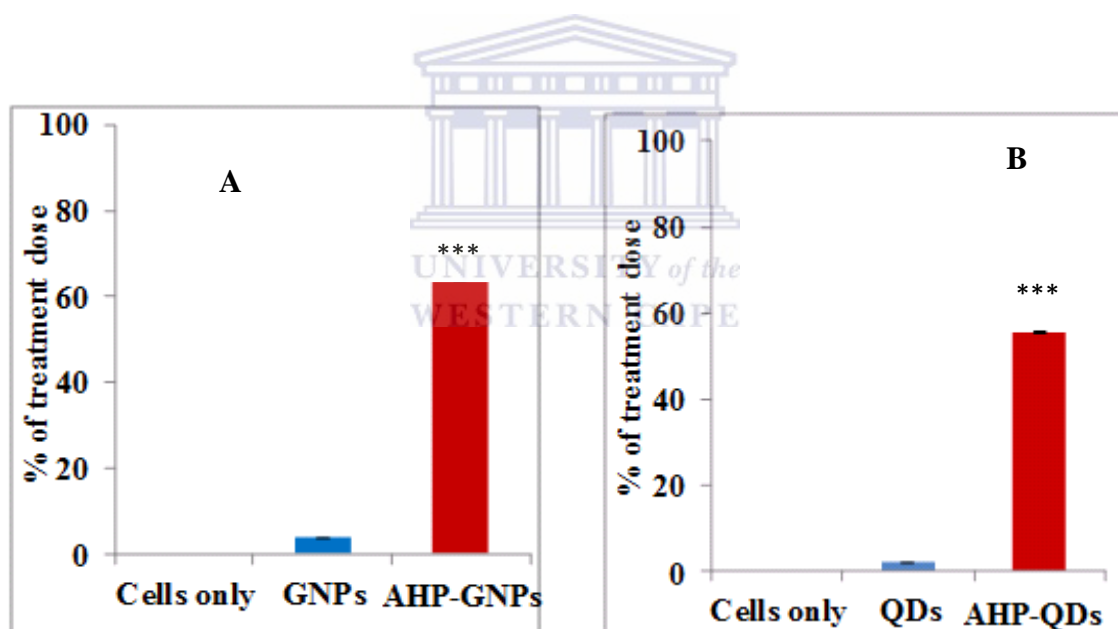
Figure 3. 13. The percentage of treated AHP-GNPs and AHP-QDs as quantified by ICP-OES.

The cells were treated with GNPs, AHP-GNPs or QD625, AHP-QDs. The bar graph indicates cellular uptake of AHP-GNPs (A) and AHP-QDs (B), indicated by % treated dose. Asterisk (***) indicates statistical significance at p<0.0001

3.6.2. Cellular uptake of AHP-GA-GNPs

To assess the cellular uptake, Caco-2 cells were exposed to both unfunctionalized GA-GNPs, and AHP- functionalized GA-GNPs for 24hrs at $37^{\circ}C$ 5 % CO_2 incubator. The cellular uptake were analyzed using both ICP-MS and ICP-OES **(Figure 3.14).** Gold was detected in the cells treated with AHP- functionalized GA- GNPs. No gold was detected from the cells treated with unfunctionalized GA-GNPs. The presence of gold in the cells indicate cellular uptake and binding of the AHP on the cell.
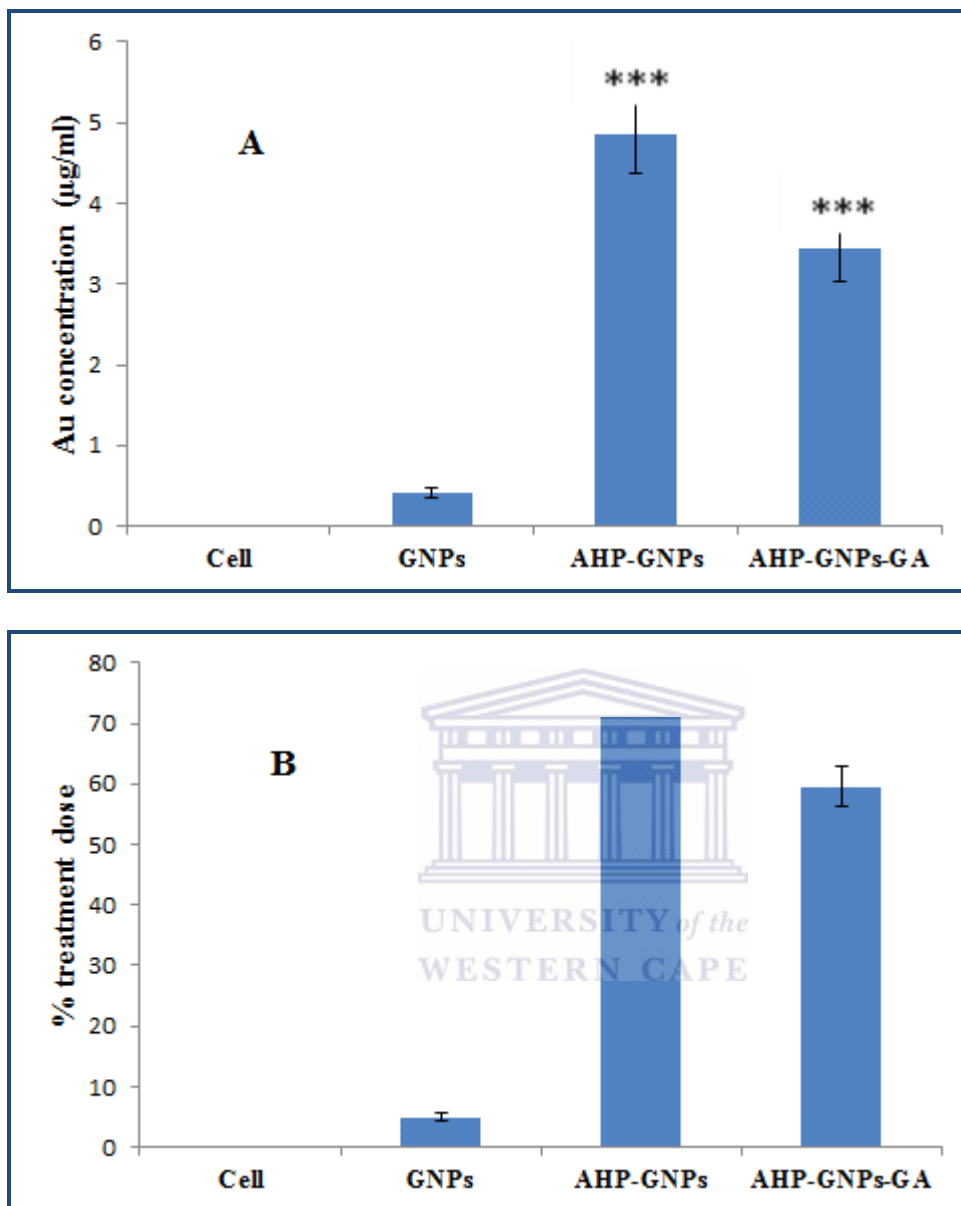
Figure 3.14. Quantification of cellular uptake for AHP-GA-GNPs and AHP-GNPS by ICP-OES.

The cells were exposed to GNPs, AHP-GNPs or AHP-GA-GNPs for 24 hrs. Graph show concentration of gold (Au) present in each sample (A) and as % of treatment dose (B), as determined ICP-OES. Asterisk (***) indicates statistical significance at p<0.0001

3.7. Cell viability studies on Caco-2 cells

3.7.1. Effects of GNPs, AHP and QDs on cell viability

To determine the effects of GNPs and QDs on Caco-2 cells, the cells were treated with GNPs; AHP-GNPs or QD625; AHP-QDs for 24 hrs and cell viability were measured using the WST-1 assay. **Figure 3.15,** shows that, as the concentration of GNPs or AHP-GNPs increases, there were moderate decrease in cellular growth as compared to untreated cells, same trends were observed as the cells treated with QDs or AHP-QDs, **Figure 3.16.**

Figure 3. 15. Graph showing % viability of Caco-2 cells treated with GNPs and AHP-GNPs.

The Caco-2 cells were treated with increase concentration of either GNPs or AHP-GNPs for 24hrs. The cell viability was tested using WST-1 assay. Asterisk (***) indicates statistical significance at $p < 0.0001$
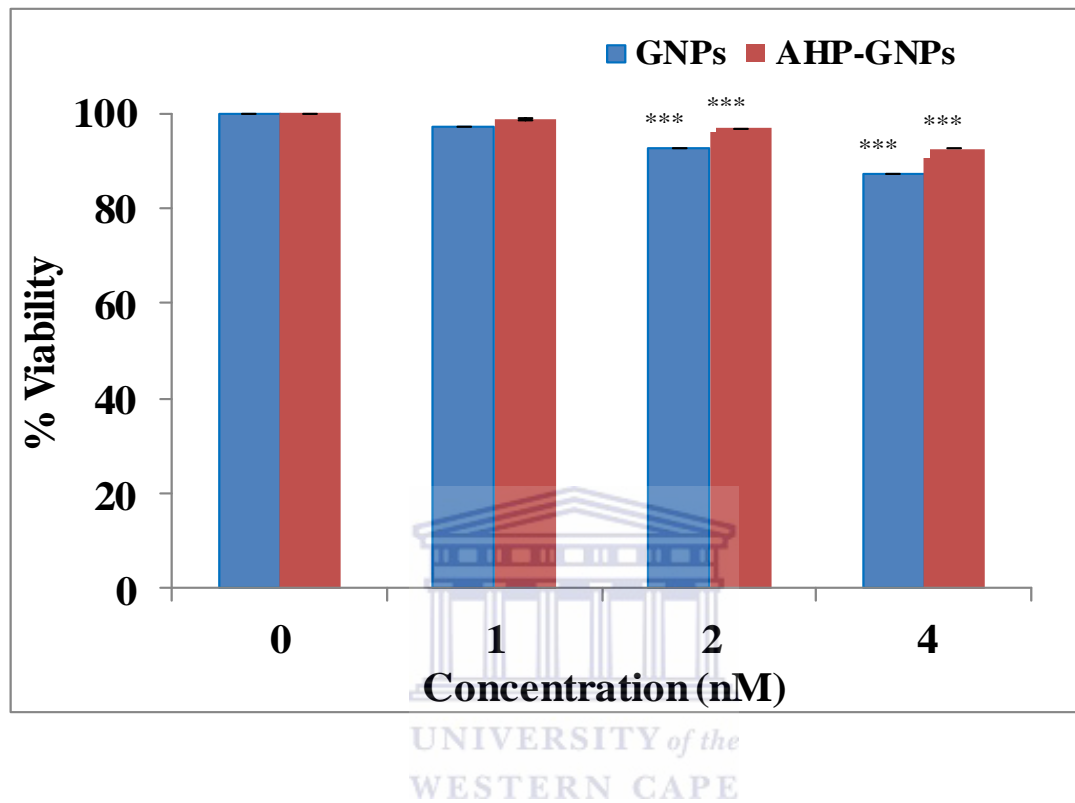
Figure 3.16. Graph showing % viability of Caco-2 cells treated with QD625 and AHP-QDs.

The Caco-2 cells were treated with increase concentration of either QD625 or AHP-QDs for 24hrs. The cell

viability was tested using WST-1 assay. Asterisk (***) indicates statistical significance at $p < 0.0001$

To determine whether the peptide has effects on cellular growth, Caco-2 cells were incubated with increasing concentrations of AHP for 24 hrs. The cell viability was measured using WST-1 assay. **Figure 3.17** shows a moderate decrease in cell viability with increase in AHP concentration
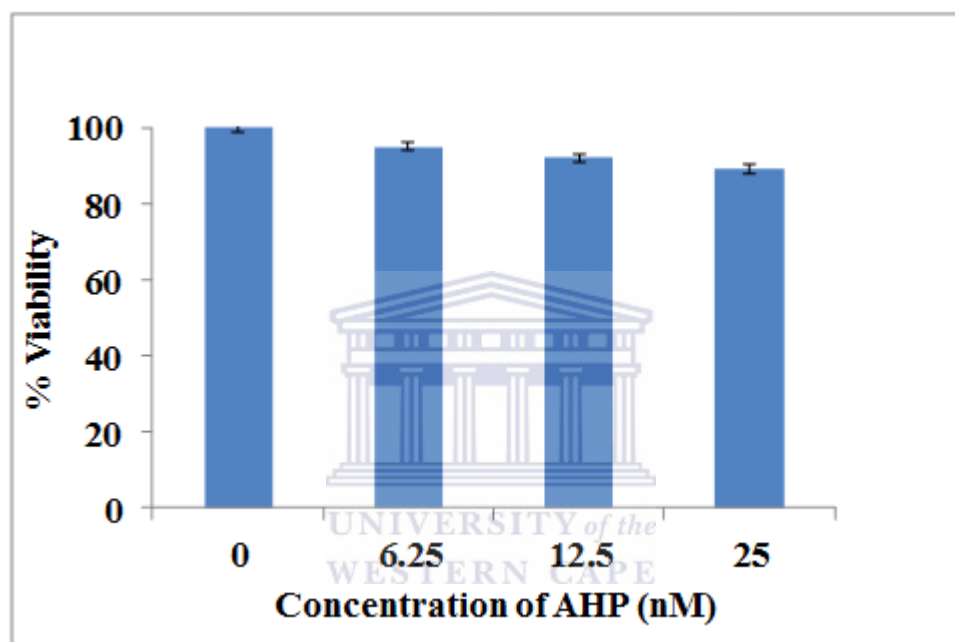
Figure 3. 17. Graph showing % viability of Caco-2 cells treated with AHP, measured for 24 hrs.

The Caco-2 cells were treated with increase concentration of either AHP for 24hrs. The cell viability was tested using WST-1 assay. The sample were not statistical significance at P<0.05.

3.7.2. Cell viability of GA and AHP-GA-GNPs

The cell viability was performed following the methods reported by Maurya *et al*., 2011, with some modification. Briefly, to determine cell viability or cell proliferation of GA on Caco-2 cells, cells were incubated for 24 hrs and WST-1 was used for cell viability. It was observed that, exposure to the increased concentration of GA (0, 12.5, 25, 50 nM) for 24hrs, Caco2 cell growth was inhibited in a dose-dependent manner as compared to control groups at 0 nM. This is indicated in **Figure 3.18.** The same trend was observed as Caco-2 cells treated with the increased concentration of AHP-GNPs-GA (0, 1, 2, 4 nM), as shown in **Figure 3.19.** The Caco-2 cell growth was not inhibited when exposed to the peptide (AHP) alone; this is shown in **Figure 3.20.** The results were performed in triplicate and they were statistically significant where $P<0.05$, as analysed by prism 5 statistics package.
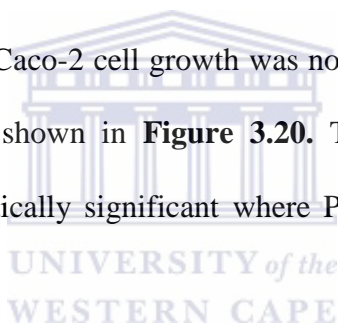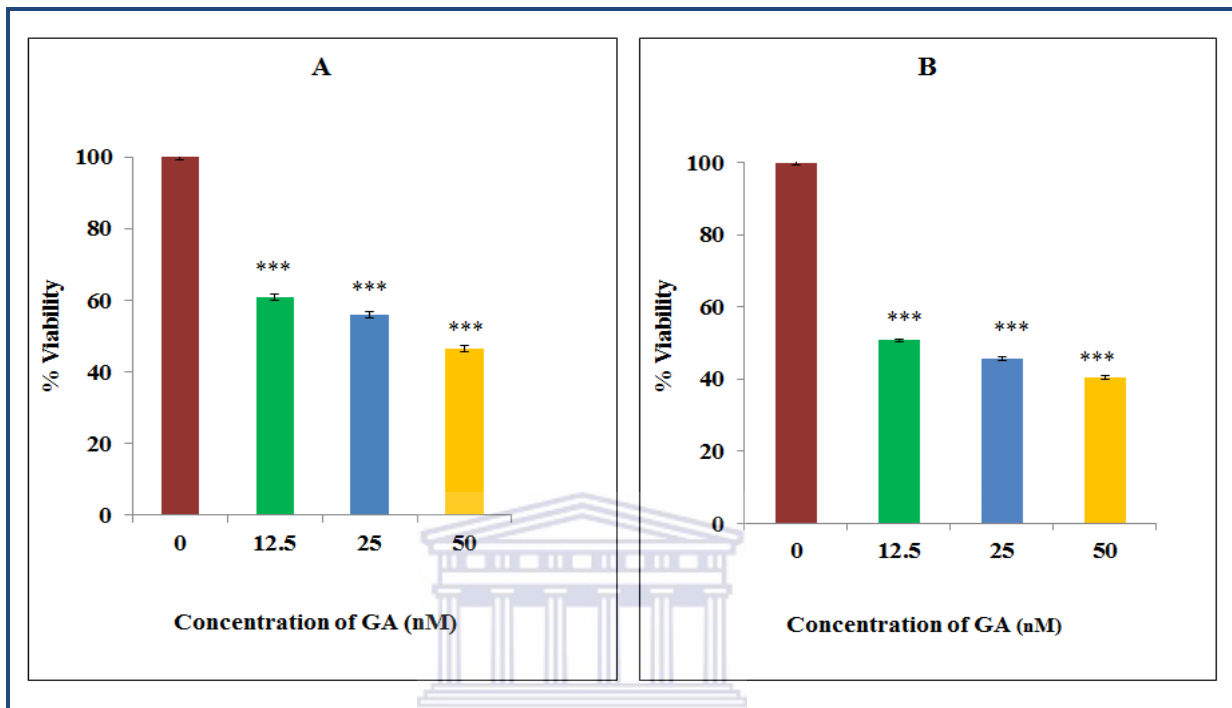
Figure 3. 18. Graph showing % viability of Caco-2 cells treated with various concentration of Gallic acid (GA).

The Caco-2 cells were treated with increased concentration of GA for 24 (A) and 48 hrs (B) The cell viability was tested using WST-1 assay. Asterisk (***) indicates statistical significance at $p < 0.0001$
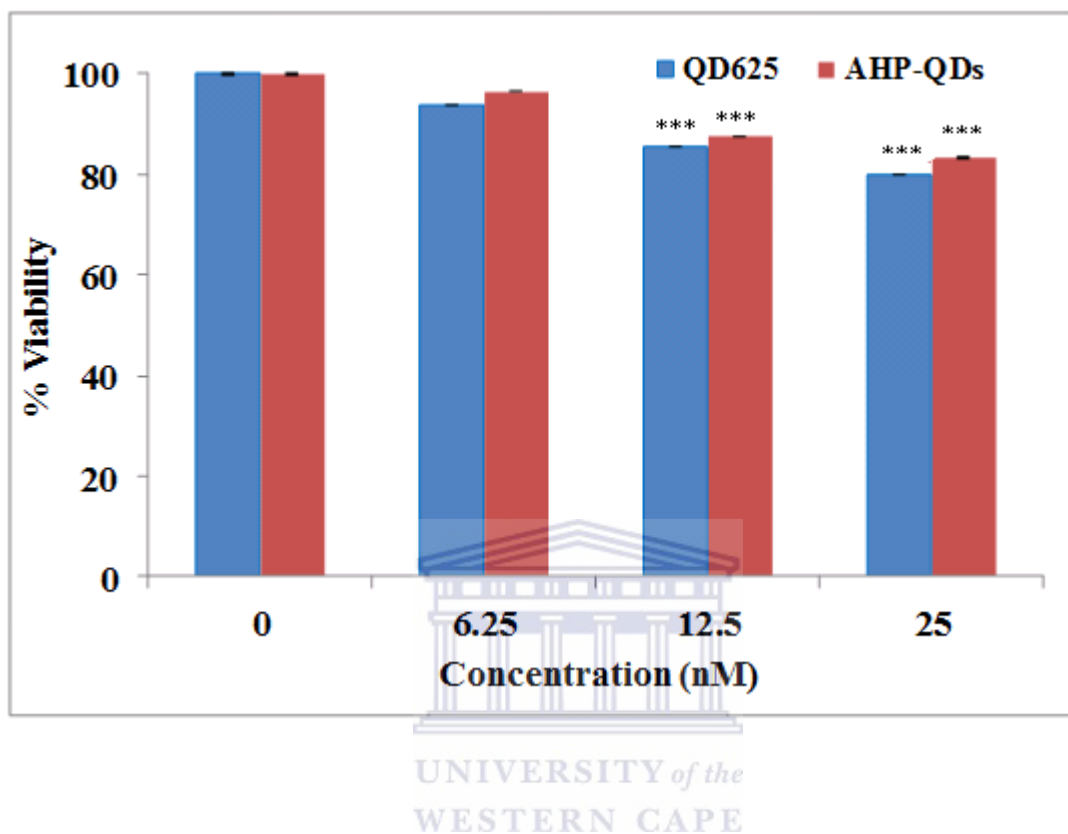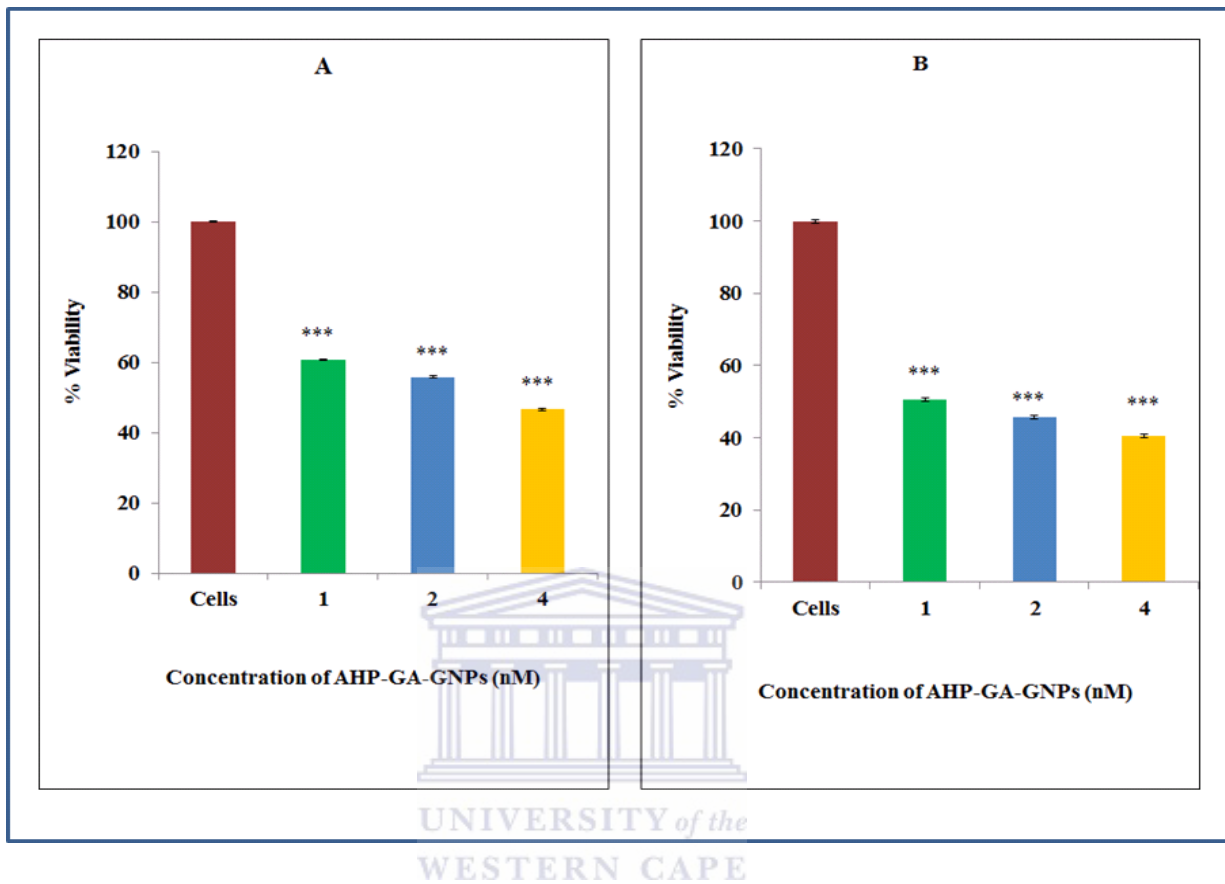
Figure 3. 19. Graph showing % viability of Caco-2 cells treated with various concentrations of AHP-GA-GNPs.

The Caco-2 cells were treated with increased concentration of AHP-GA-GNPs for 24 (A) and 48 hrs (B) The cell viability was tested using WST-1 assay. Asterisk (***) indicates statistical significance at P<0.0001
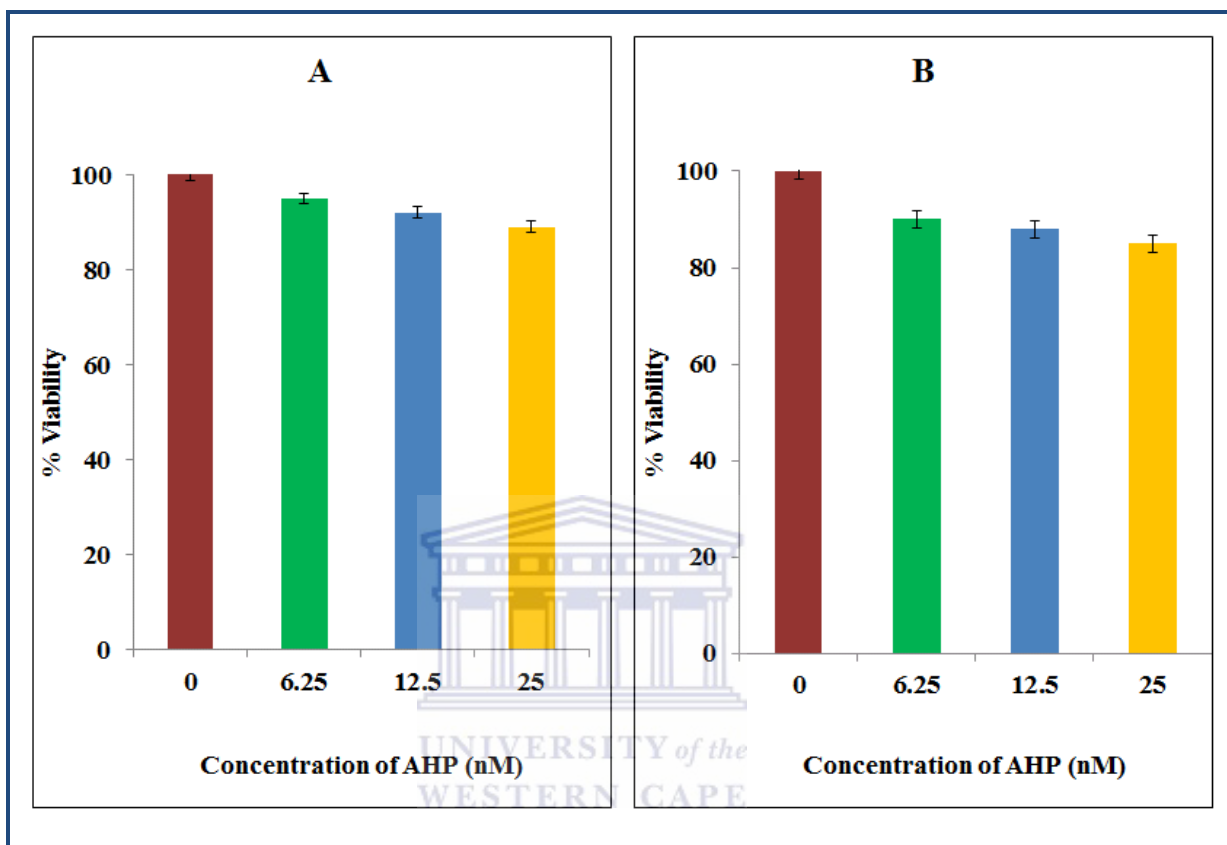
Figure 3. 20. Graph showing % viability of Caco-2 cells treated with various concentration of AHP.

The Caco-2 cells were treated with increased concentration of AHP for 24 (A) and 48 hrs (B) The cell viability was tested using WST-1 assay. The sample were not statistical significance at P<0.05.

3.8. Induction of apoptosis by GA and AHP-GA-GNPs

3.8.1. APOP*ercentage* ™ assay

To determine the apoptotic effects, cells were treated for 24 hrs with GA (25 nM), AHP-GA-GNPs (2nM) and Cisplatin (10 µM) and induction of apoptosis was assessed using the APOP*ercentage* ™ assay. Staining with the APOP*ercentage* ™ dye was quantified using FACScan ™ (Becton Dickson) instrument **(Figure 3.21),** the histograms for cells treated with GA, AHP-GA-GNPs and Cisplatin shift to the right due to increased binding of the APOP*ercentage* ™ dye, suggesting the induction of apoptosis in cells treated with GA, AHP-GA-GNPs and Cisplatin. The morphological change induced by GA and AHP-GA-GNPs was also investigated using inverted light microscopy. Morphological examination showed the typical feature of cell death, cell detachment, cell shrinkage and rounding up of the cells **(Figure 3.22.).** The cells undergoing apoptosis are stained with APOP*ercentage* ™ dye as indicated in Figure 3.22.
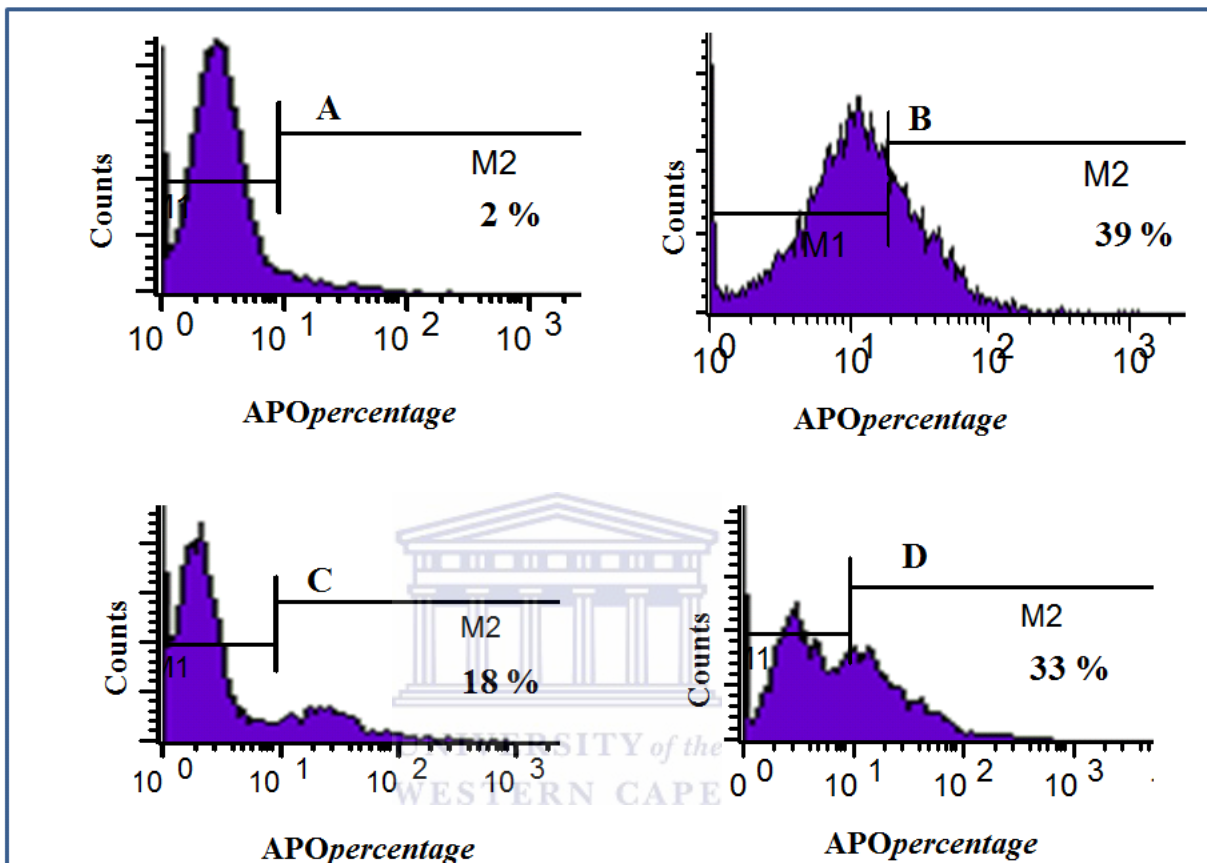
Figure 3.21. The quantification of apoptosis in Caco-2 cells by flow cytometry.

The cells were treated with Cisplatin (B), AHP-GA-GNPs (C) or GA (D), for 24 hrs. The cells were then stained with APOP*ercentage*^{TM} dye and analyzed using flow cytometry. Histogram A, indicate the untreated cells. The shift of the cells distribution to the right into the second decade (M2) indicates the cells undergoing apoptosis that is an increase in fluorescence as indicated by %.
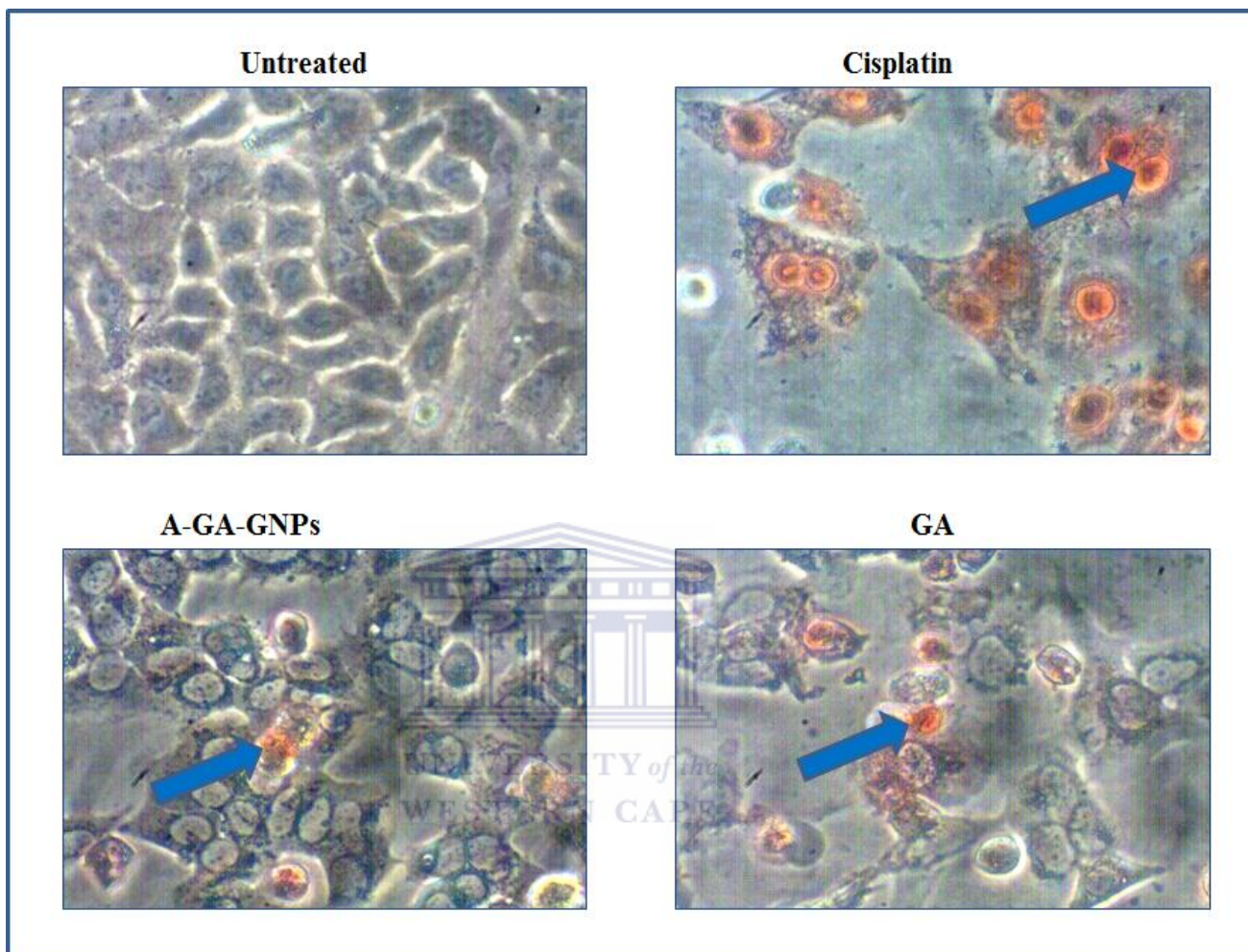
Figure 3.22. Morphological images in Caco-2 cells treated with GA, AHP-GA-GNPs and cisplatin.

The cells were incubated for 24 hrs with either Cisplatin (10 µM), AHP-GA-GNPs (2 nM) or GA (25 nM). The cells were then stained with APOP*ercentage* dye (1:120) dilution for 30 minutes and the cell morphology was observed under inverted light microscopy. The arrow on the image indicates the cells stained with APOP*ercentage* dye which indicates marker of apoptosis.

3.8.2. Caspase 3 activation of GA and AHP-GA-GNPs

To determine whether the GA, AHP-GA-GNPs activates caspase-3, cells were treated with GA or AHP-GA-GNPs or Cisplatin (as positive control) for 24 hrs and thereafter incubated with anti-active caspase-3 antibody. The cells were examined under the inverted light microscope for morphological changes and analyzed on FACScan ^{TM} (Becton Dickson) instrument to determine caspase-3 activity. Negative control cells were used to set cells in the negative quadrant before all sample were acquired. Samples were acquired and analyzed using CELLQuest PRO software (BD Biosciences). The cells treated with cisplatin, GA and AGA-GNPs undergo apoptosis after 24 hrs as compared to untreated cells, as shown by activation of caspase-3 measured by the fluorescence of active caspase-3 FITC (Figure 3.23).
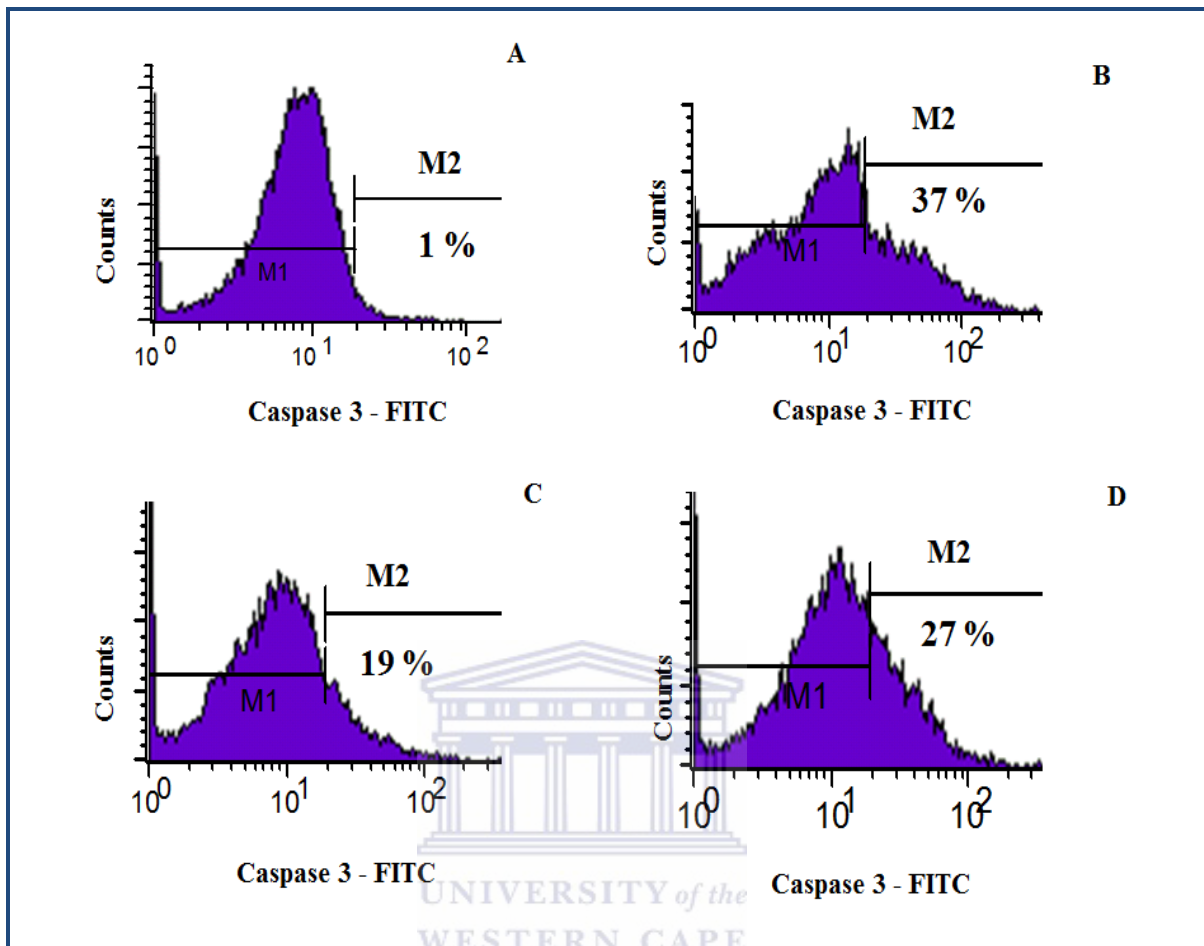
Figure 3.23. Quantification of the activation of Caspase 3 in Caco-2 cells by flow cytometry.

Caco-2 cells were treated for 24 hrs with Cisplatin 10 μM (**B**), A-GA-GNPs 2 nM, (**C**) or GA 25 μM (**D**), stained with anti-active caspase-3 antibody and analysed by flow cytometry. Histogram A, indicate untreated cells.The shift of the cells distribution to the right into the second decade (M2) indicates the cells activating caspase- 3 that is an increase in fluorescence as indicated by %.
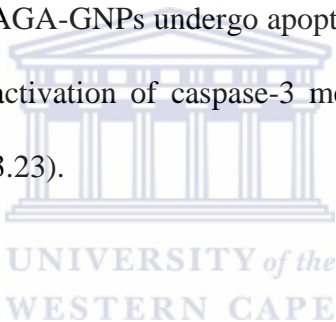
CHAPTER 4

4. Results: *In vivo* studies

4.1. Measurement of body weight, organs and adipose tissue mass

To assess the difference between the body weight of low fat (LF) (lean) and high fat (HF) (obese) fed rats, the rats were weighed weekly during the obesity induction period. This was done to see if there will be changes in their body weight. It is shown in **Figure 4.1 and Figure 4.2,** that the HF fed diet rats were heavier as compared to the LF group. The difference in groups were found to be statistically significant at $p < 0.05$, as analysed by Graph pad prism 5 statistical package.

Figure 4. 1. The body weights gain of LF and HF diet induced rats measured weekly.

The rats (HF and LF group) were measured weekly. Asterisk (*) indicates statistical significance at p<0.05.
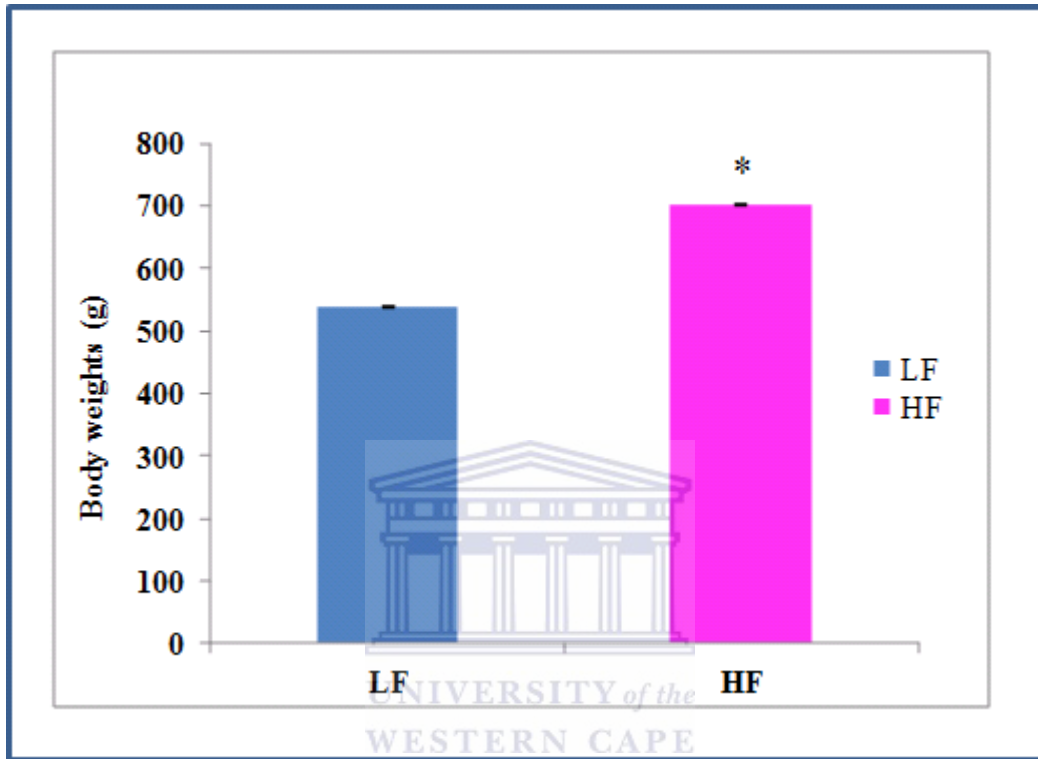
Figure 4. 2. The body weights gain of LF and HF diet induced rats measured at termination.

The rats (HF and LF group) were measured at termination. HF group were heavier than the LF group.

Asterisk (*) indicates statistical significance at p<0.05.

4.1.2. Tissues and organs weights

To determine the weights of body tissues and organs, tissues were dissected and weighed at termination as indicated in **Table 4.1**. The adipose tissue weights including, inguinal or subcutaneous (SQ), epididymal (EPI), perirenal (PERI), retroperitoneal (RETRO) and mesenteric (MES) fat pads were found to be heavier and significantly increased in the HF group as compared to those in the LF group, as shown in **Figure 4.3**. The weights of these tissue in both groups were found to be statistically significant at $p<0.05$ as analysed by Graph pad prism 5 statistical package.

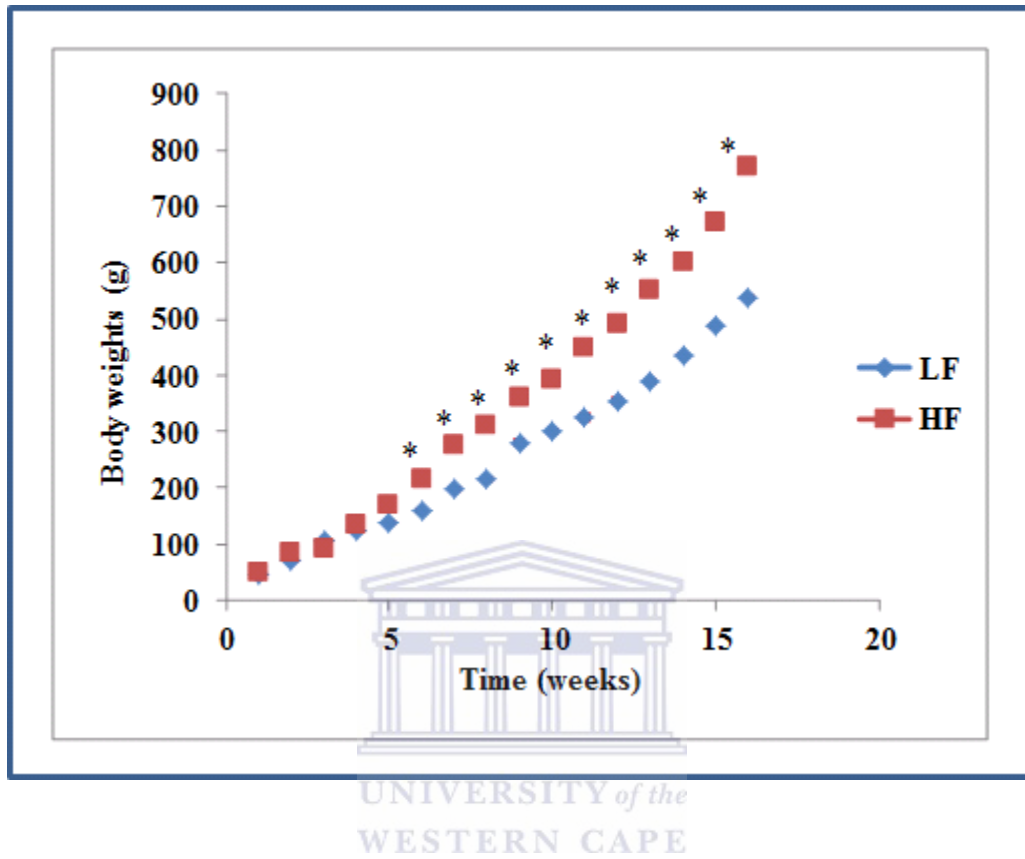**Table 4. 1.The average body and tissue weights isolated from LF and HF rats at termination**

Asterisk (***) indicates statistical significance at p<0.0001, (*) indicates statistical significance at p<0.05,

NS - not statistically significant and ↑increase. Data is presented as Means ± SD/SE, n=20

	LF	HF
BW	539.7 ± 15.9	701.2 ± 14.8 *
SQ	15.3 ± 2.05	36.2 ± 2.12 ***
EPI	8.72 ± 0.85	23.3 ± 1.09 ***
MES	8.66 ± 0.92	18.4 ± 0.87 ***
RETRO	6.33 ± 0.83	29.5 ± 0.74 ***
PERI	2.05 ± 0.45	4.25 ± 0.05 ***
Kidneys	3.10 ± 0.09	3.04 ± 0.13 NS
Lungs	1.76 ± 0.07	1.99 ± 0.16↑,NS
Liver	15.5 ± 0.84	15.8 ± 0.61 NS
Spleen	1.03 ± 0.06	0.96 ± 0.05 NS
Testes	3.77 ± 0.05	3.78 ± 0.07 NS
Heart	1.44 ± 0.06	1.48 ± 0.05 NS
Brain	2.09 ± 0.04	2.13 ± 0.02 NS
Stomach	2.31 ± 0.08	2.79 ± 0.47↑,NS
Pancreas	2.22 ± 0.24	2.58 ± 0.14↑,NS
Adrenal	0.05 ± 0.004	0.06 ± 0.005 NS
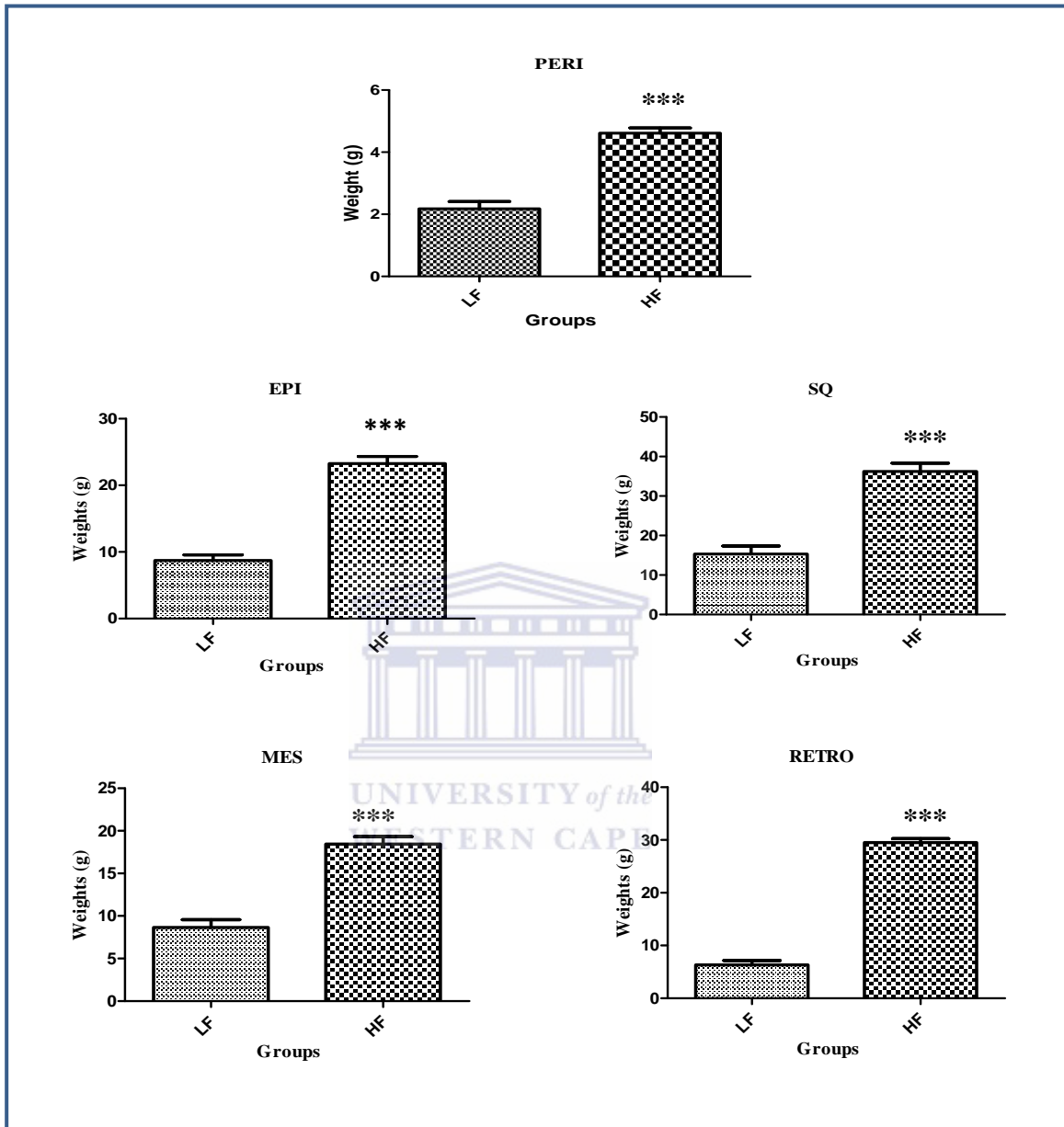
Figure 4. 3. The average weights of various adipose tissue depots.

The perirenal (PERI), epidydimal (EPI) subcutaneous (SQ), mesenteric (MES) and retroperitoneal (RETRO) weights isolated from LF and HF rats, measured at termination.   Asterisk (***) indicates statistical significance at p<0.0001

The weights of adrenals, pancreas, stomach and lungs were slightly heavier, in the HF group as compared to those in the LF group but statistically they were not significant at $P<0.05$ while the weight of the spleen, brain, testes, heart, liver and kidneys were the same in both groups, however they were not statistically significant. Between the weights of the pancreas a significance different was observed at $p<0.05$. The average tissue weights of LF and HF groups are indicated in **Table 4.1** and **Figure 4.4 & 4.5.**

UNIVERSITY *of the*
WESTERN CAPE
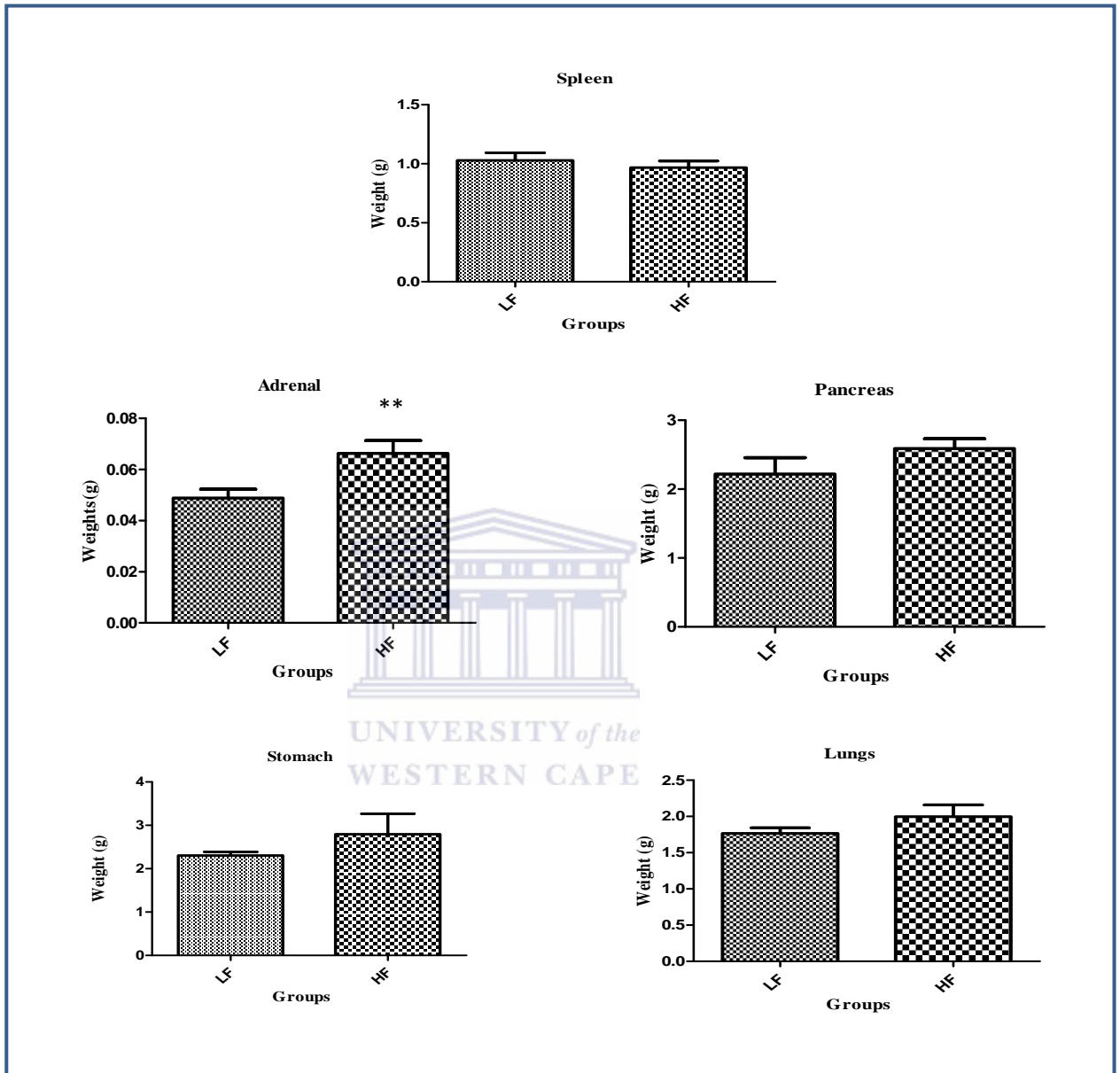
Figure 4. 4. The average weights of spleen, adrenal, pancreas, stomach and lungs isolated from LF and HF rats, measured at termination.

Asterisk (**) indicates statistical significance at p<0.0061
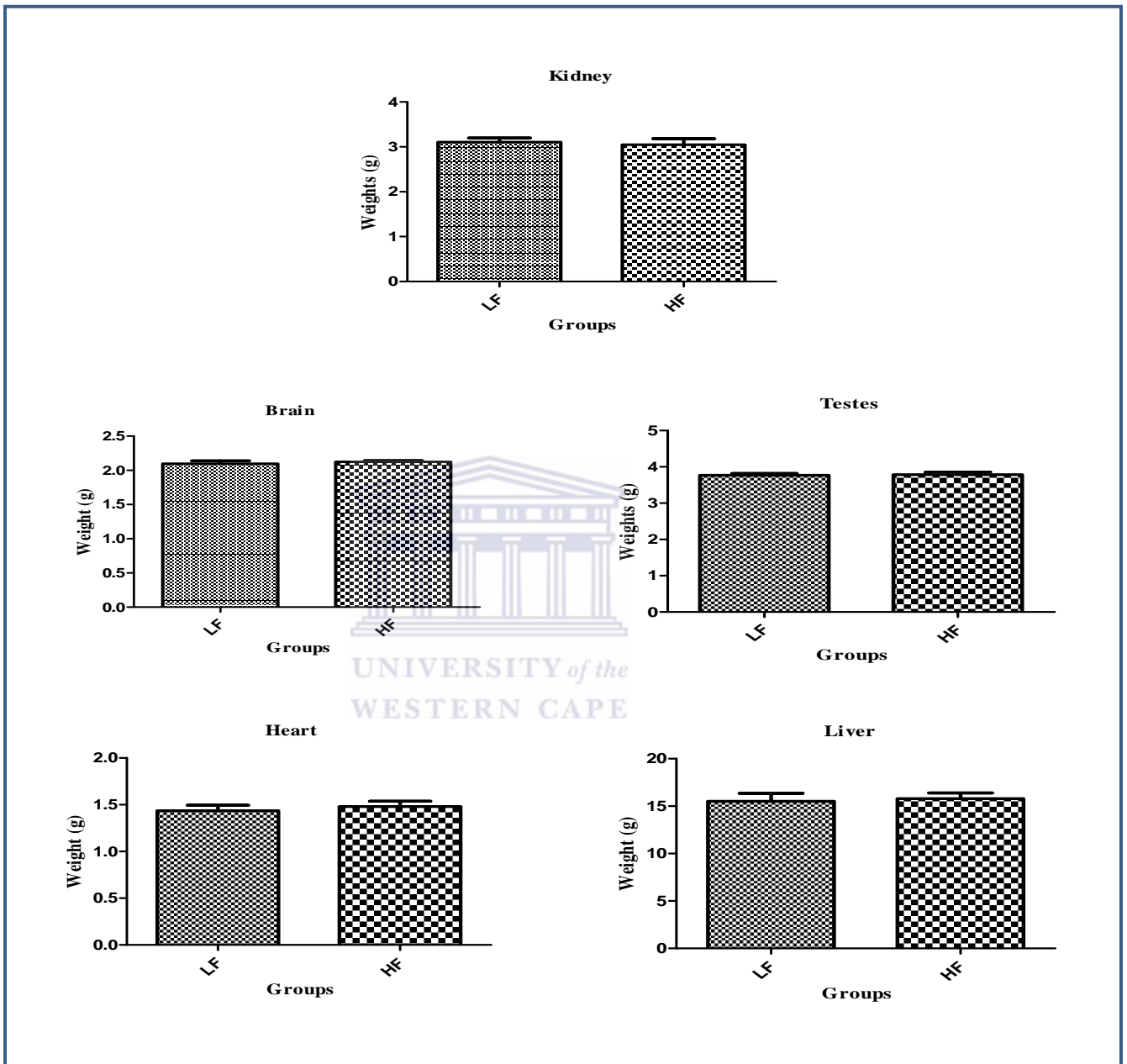
Figure 4. 5. The average weights of brain, testes, heart, liver and kidneys isolated from LF and HF

rats at termination.

4.2. Adiposity index

To determine what percentage weight each tissue contributed to the final body weight, the weight of each tissue was divided by the final body weight at termination and multiplied by 100. The adiposity index was then determined as the percentage of the sum of weights of all WAT in relation to the total body weight. This was expressed as percentage adiposity index as indicated in **Figure 4.6**. The adiposity index was found to be higher for the HF group with 15.98 ± 0.39 as compared to the LF group with 7.5 ± 0.67 as indicated in **Figure 4.6.**

UNIVERSITY *of the*
WESTERN CAPE
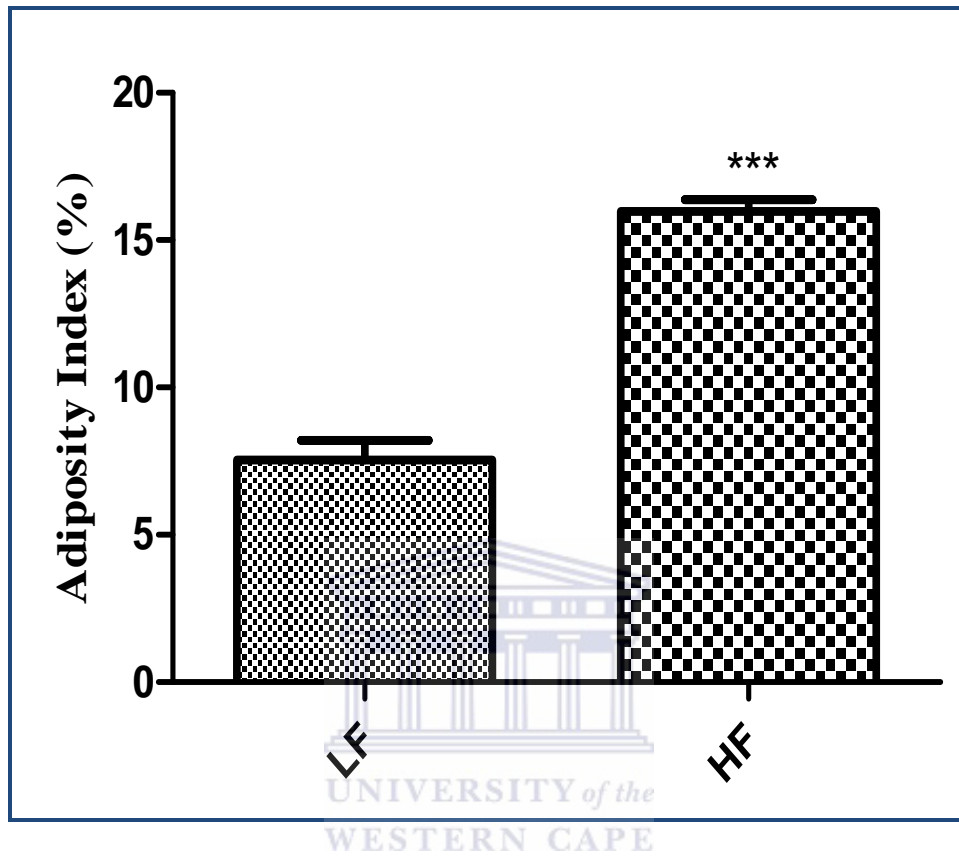
Figure 4. 6. The total percentage (%) body weight index in both LF and HF groups at termination.

Asterisk (***) indicates statistical significance at p<0.0001

4.3. Biodistribution studies of QDs after intravenous injection

4.3.1. *Ex vivo* imaging of QDs using IVIS® Lumina XR

To assess the biodistribution and localization of QDs *in vivo*, lean and obese rats (Figure 4.1) were intravenously injected with unfunctionalized and AHP-functionalized QDs. The organs and tissues were dissected out and imaged using IVIS® Lumina XR. No fluorescence was observed in organs and WATs from PBS-treated rats (control group). The unfunctionalized QDs accumulated in the liver, testes, kidney and brain, but rarely distributed in WATs. In contrast, the AHP-functionalized QDs accumulates mostly in the WAT (mesenteric, inguinal, epidydimal and retroperoteneal) but did not accumulated in the organs. The intense yellow fluorescence was observed in liver, testes, kidney and brain, but accumulated mainly in WATs of the AHP functionalized QDs as indicated in **Figure 4.7.**
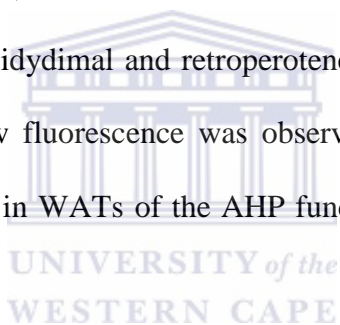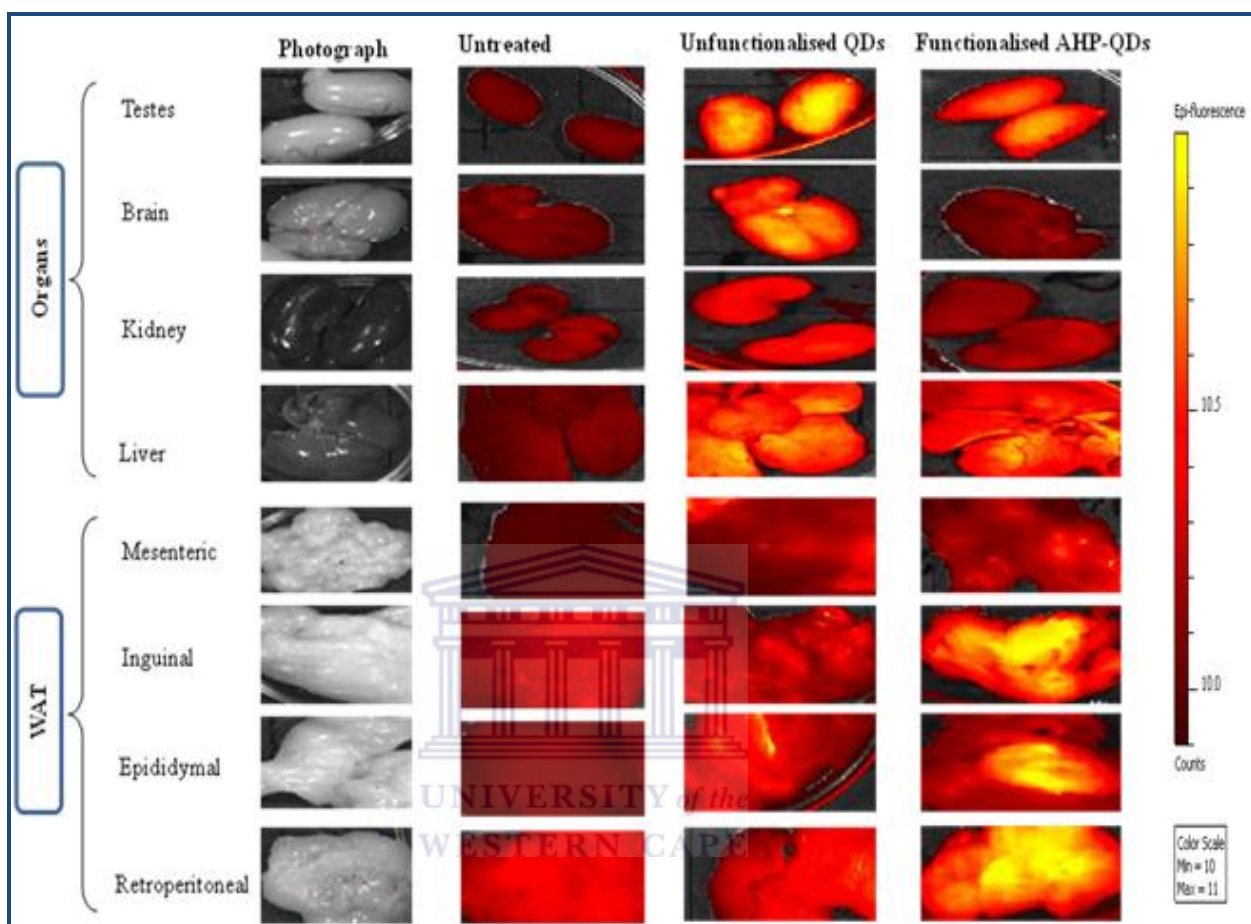
Figure 4.7. Photographs and fluorescence images of isolated organs of rats intravenously injected with unfunctionalized and AHP-functionalised QDs.

Biodistribution of QDs was determined 24 hrs after intravenous injection. Organs were dissected after 24 hrs, and imaged under IVIS® Lumina XR, using DsRed filter (Excitation wavelength ranges between 430-745 nm and Emission, 580-700nm) and results analysed using IVIS living image software.

4.3.2. The quantitative analysis of QDs and GNPs using ICP-OES

To quantitatively assess the concentrations of QDs and GNPs *in vivo*, lean and obese rats were injected intravenously with unfunctionalized and AHP-functionalised QDs and GNPs, and organs and tissues were analyzed by ICP-OES. As shown in **Figure 4.8**, high concentrations of Cd were measured mainly in the liver, lungs, spleen, kidney and testes from rats injected with unfunctionalized QDs. Low concentrations of Cd were observed in WATs, except retroperitoneal WAT. In contrast, low levels of Cd were measured in liver, lungs, spleen, kidney and testes from rats injected with AHP-functionalised QDs. High concentrations of Cd were measured in WAT. The same trend was observed in the measurement of gold in organs of rats injected with unfunctionalized and AHP-functionalized GNPs (**Figure 4.9**).
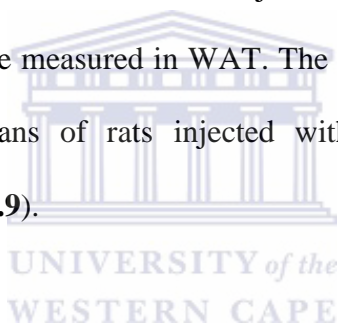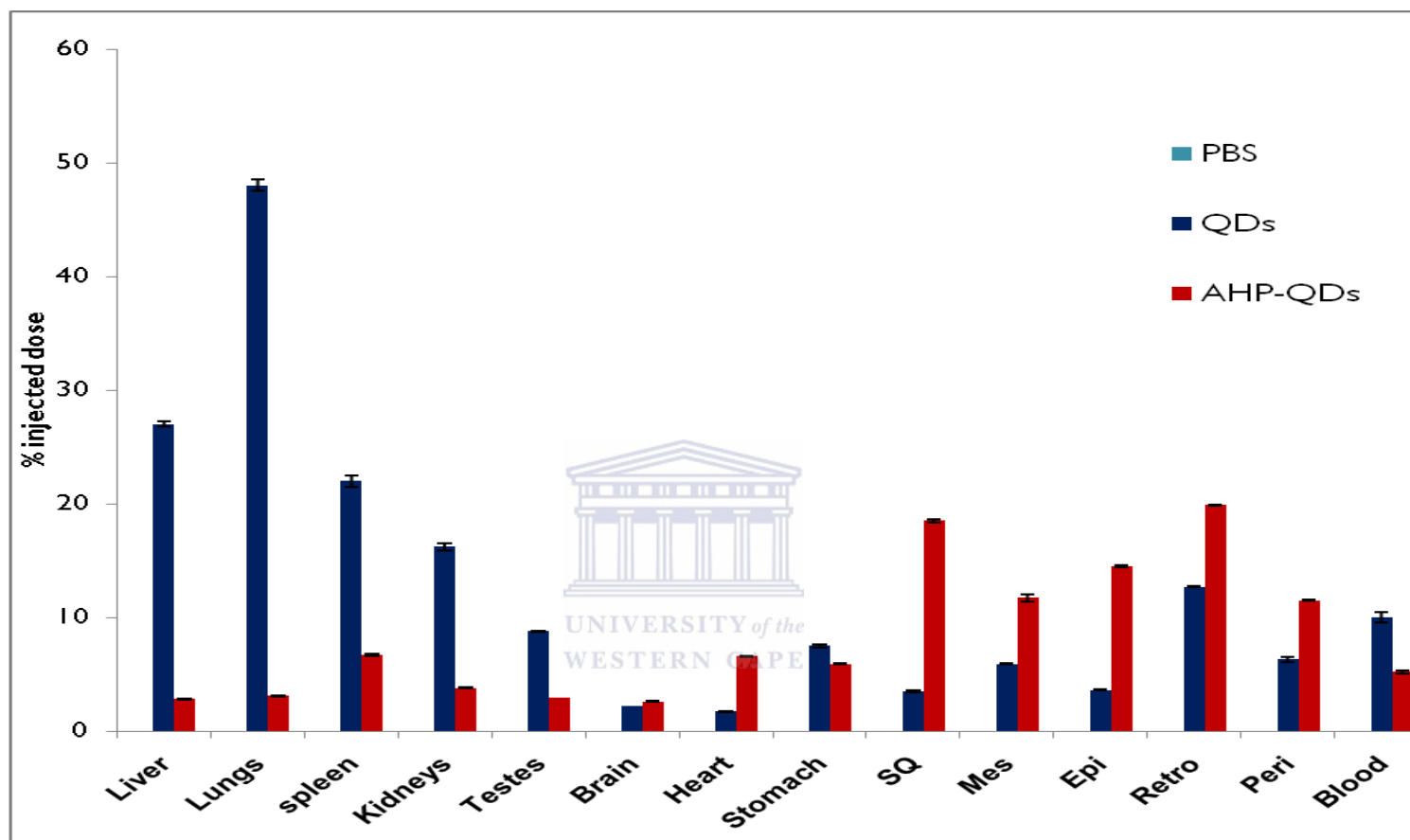
Figure 4. 8. Percentage injected dose of cadmium, in selected organs to determine biodistribution of QDs.

Rats were injected intravenously with PBS, unfunctionalized and AHP-functionalized QDs. Organs and tissues were dissected after 24 hrs. Quantification of Cadmium (Cd) in various organs was determined by ICP-OES.
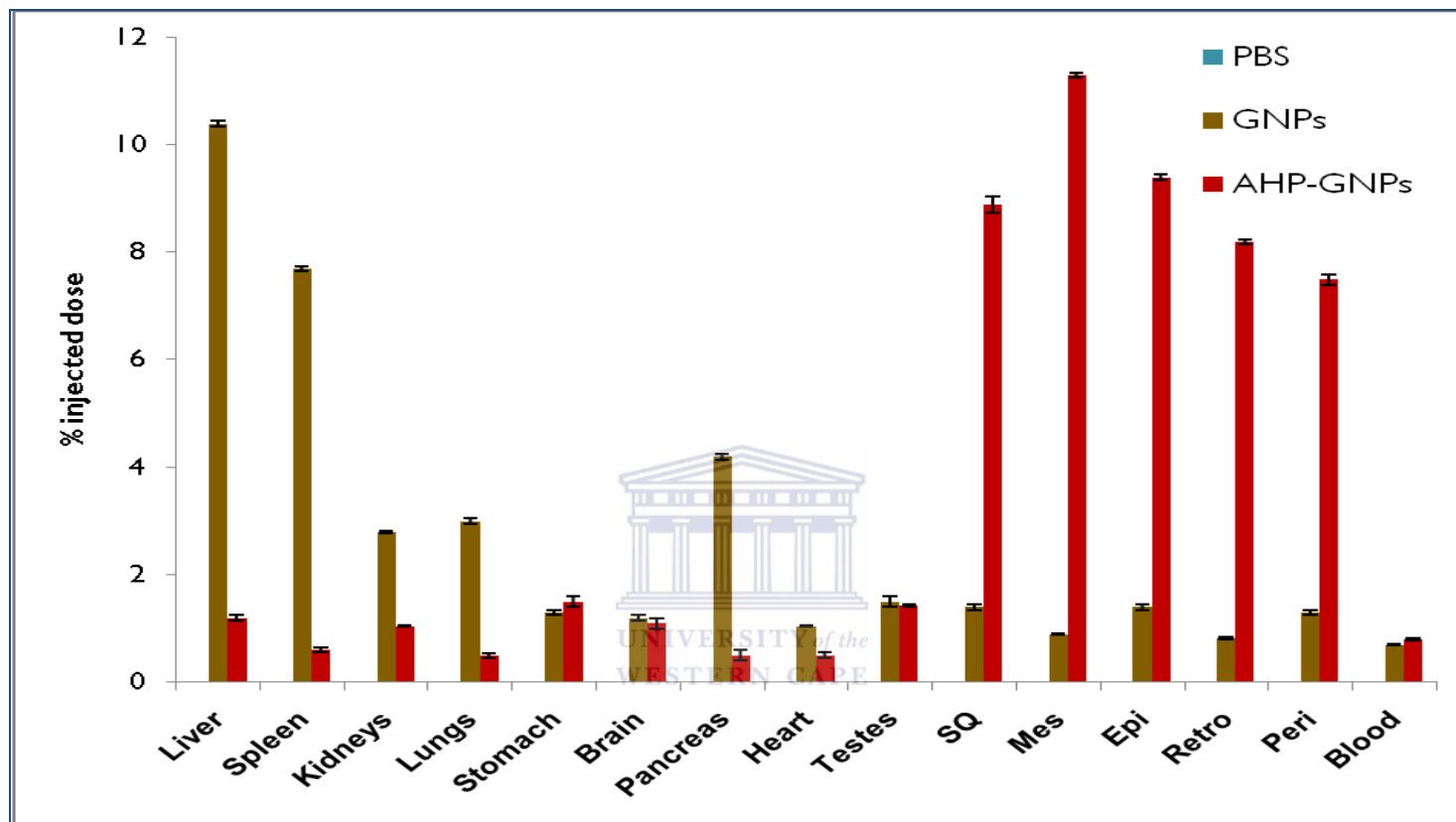
Figure 4. 9. Percentage injected dose of gold in selected organs, to determine biodistribution of GNPs.

Rats were injected intravenously with PBS, unfunctionalized and AHP-functionalized GNPs. Organs and tissues were dissected after 24 hrs.

Quantification of gold (Au) in various organs was measured by ICP-OES.

4.4. Measurement of Free fatty acid (NEFA), Insulin and glucose level

The serum samples from both lean and obese rats were analysed to determine the concentration of free fatty acid, insulin and glucose. It is shown in **Figure (4.10; 4.11; 4.12)** and **Table 4.1** that the higher concentration of NEFA, insulin and glucose were observed in the serum obtained from obese (HF) rats as compared to the lean (LF) rats. The results were statistically significant at $p < 0.05$.

UNIVERSITY *of the*
WESTERN CAPE
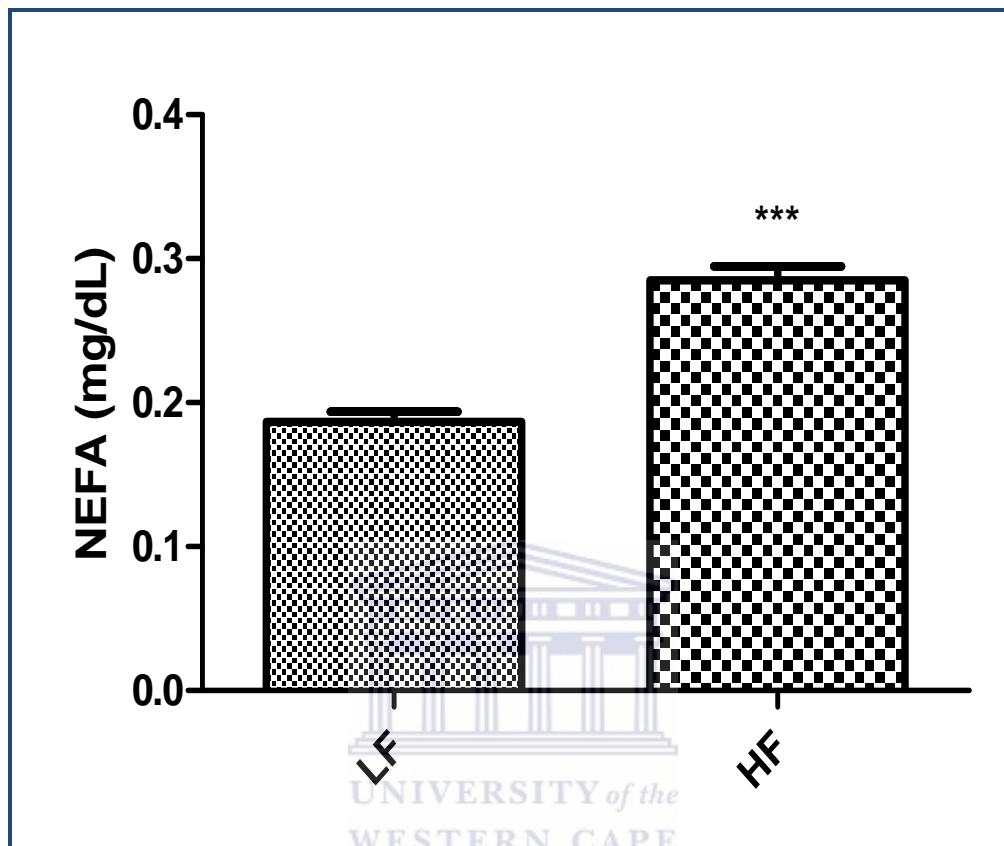
Figure 4. 10. Measurement of free fatty acid levels in the serum samples of both lean (LF) and obese (HF) groups.

Asterisk (***) indicates statistical significance at p<0.0001
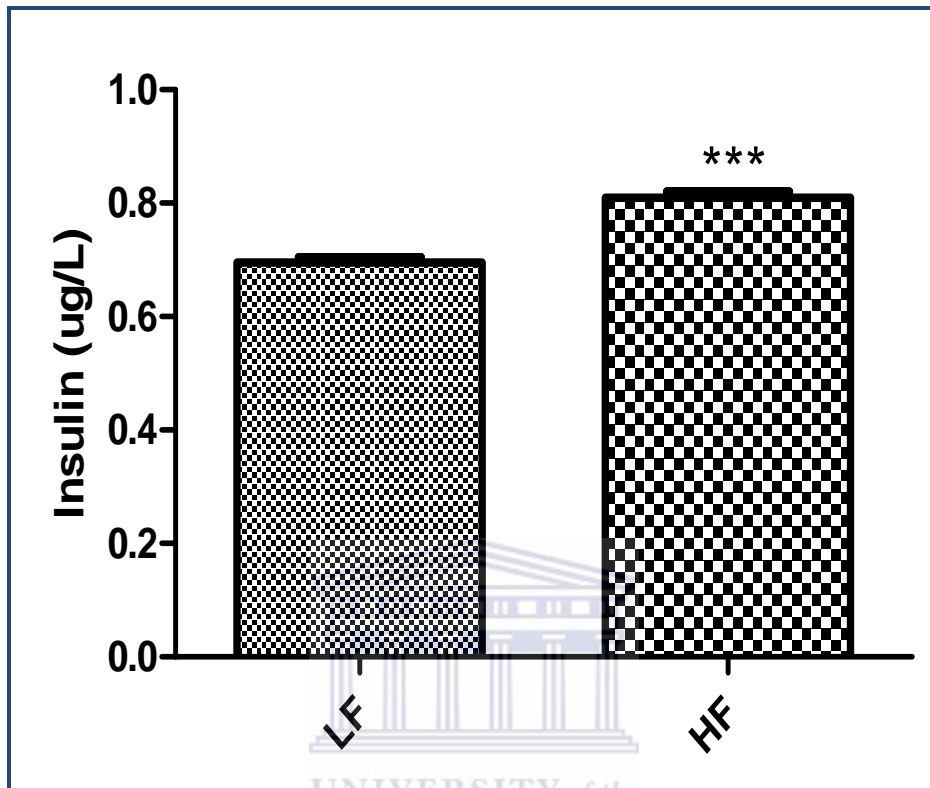
Figure 4. 11. Measurement of insulin levels in the serum samples of both lean (LF) and obese (HF) groups.

Asterisk (***) indicates statistical significance at $p < 0.0001$
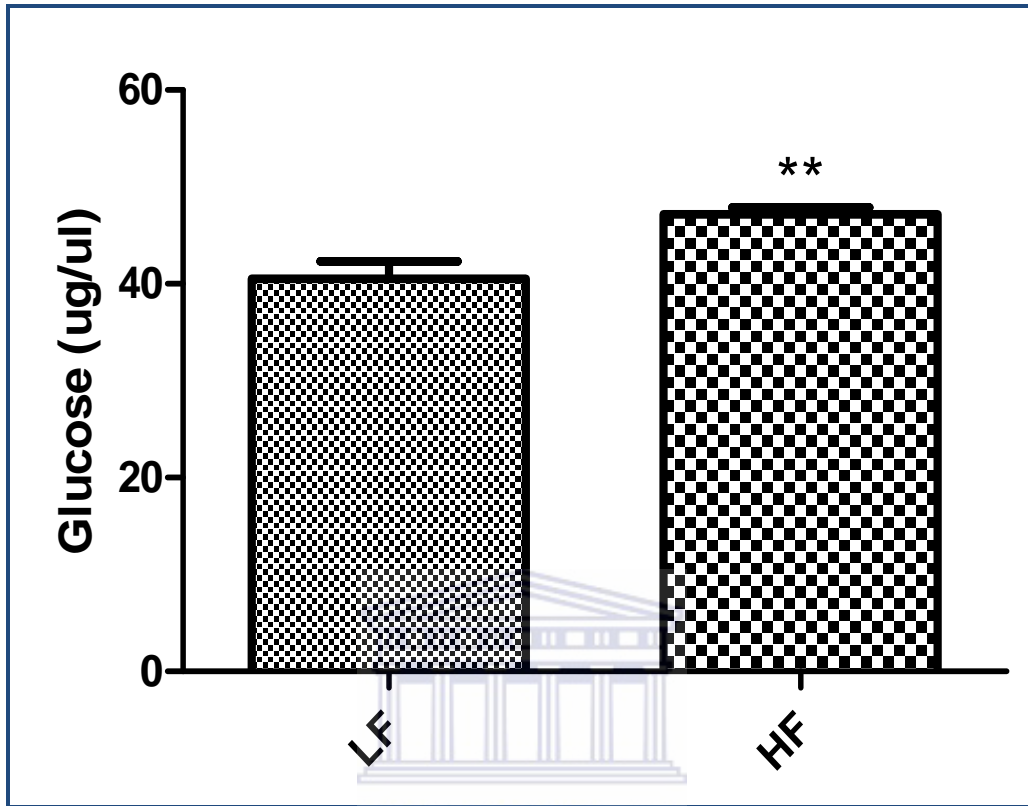
Figure 4. 12. Measurement of glucose concentration in serum samples of lean (LF) and obese (HF) groups.

Asterisk (**) indicates statistical significance at $p < 0.0014$

Table 4. 2. The concentration of serum insulin, glucose and NEFA.

This table shows the concentration of insulin, glucose and NEFA obtained from serum of lean

(LF) and obese (HF) Wistar rats.

	BW (g)	Insulin conc.(µg/L)	Glucose conc.(µg/µL)	NEFA conc.(mg/dL)
LF	539.73	0.69	40.8	0.185
HF	701.23	0.811	48.0	0.283

Abbreviations: LF (Low fat), **HF** (High fat), **BW** (Body weights), **NEFA** (Non-esterified fatty acid),

Conc (concentration)
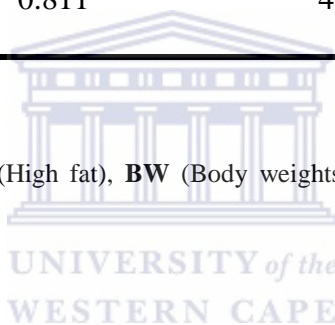
CHAPTER 5

5.1. General discussion

The study focused on the development of nanotechnology based drug delivery systems (GNPs) and imaging agents (QDs) to the white adipose tissue vasculature using obese male Wistar rats. In 2004, Kolonin *et al*, discovered a synthetic peptide motif (sequence CKGGRAKDC), which was found to be a vascular targeting peptide that homes to the white fat vasculature. Of our interest, we then named the peptide an Adipose Homing Peptide "shorten" AHP. PHB was found to be a target for AHP, which is now known as a vascular marker of adipose tissue. For the advancement of the study, the GNPs and QDs were functionalized with AHP to specifically target the white adipose tissue vasculature. Functionalization of the nanoparticles was confirmed using agarose gel electrophoresis and UV-vis spectroscopy. UV-vis spectroscopy showed a change in absorbance but not in the absorption peak, as indicated in **Figure 3.1 and 3.2.** These results correlate with other studies, showing that functionalized NPs migrate slower on agarose gel than the unfunctionalized NPs. This was attributable to surface modification (Kumar *et al*., 2012).

However, PL characterisation of QD625 and AHP-QDs did not change the emission spectrum of the QDs **(Figure 3.4).** A study by (Franchello *et al*.) also showed that functionalization of the NPs does not change the PL characteristics of QD625 (Franchello *et al*., 2013). This study is therefore in agreement with the work done by Franchello and colleaques.

In addition, several studies indicated that various NPs functionalized with different biomolecules can be used in nanotechnology, due to their versatility, ease in chemical synthesis, less toxicity and biocompatibility (McNeil, 2005; Lira *et al*., 2012). Furthermore, range of these NPs are used as imaging and drug-delivery systems and can be formulated from diverse materials with unique architectures to serve as possible drug-delivery vehicles to treat variety of diseases (Atlanta, 2005; Lira *et al*., 2012; Parveen *et al*., 2012).

To confirm PHB as a target for AHP, GNPs and QDs were functionalized with AHP and the binding specificity was tested in PHB expressing cells, the MCF-7 and Caco-2 cells. The expression of PHB in these cell lines was described in the literature (Rastogi *et al*., 2006; Sharma and Qadri, 2004). Immunofluorescence staining was performed on MCF-7 cells to confirm the expression of PHB and to investigate the localization of PHB. The anti-PHB antibody was confirmed in the mitochondrion. This is shown in **Figure 3.5.** The localization of PHB in the nucleus was also confirmed using anti-PHB antibody and DAPI as indicated in **Figure 3.6**.

The study done by Kolonin *et al*., (2004), showed that AHP specifically targets adipose tissue vasculature and binds to PHB expressed on endothelial cells. **Figure 3.7 and 3.8,** confirmed the binding of AHP-QDs to MCF-7 and Caco-2 cells, as determined by fluorescence microscopy. Cells that do not express PHB (CHO, KMST-6) did not show any binding of AHP-QDs **(Figure 3.9).**

The binding and uptake of AHP-QDs was studied in ECs generated from lean and obese Wistar rats, by quantifying the concentration of cadmium (Cd) in the cells, following exposure of the cells to AHP-QDs and QD625. The concentration of Cd in ECs isolated from lean rats was much lower compared to ECs isolated from obese rats **(Figure 3.11).** The Cd concentration for cell treated with QD625 was very low for ECs produced from both lean and obese rats.

Taken together, these data suggest that the binding of AHP was receptor-mediated and specific to a receptor that is expressed in ECs from obese WAT. We speculate that this could be due to increased PHB expression on the cell surface of ECs from obese rats as indicated by Hossen *et al*., 2010. Although it has been reported that PHB is an inner mitochondrial protein that is present in all cells and nuclear expression in some types of cells, it is also expressed on the plasma membrane of vascular endothelial cells in adipose tissue.

To determine the specificity of AHP binding Caco-2 cells (PHB expressing cells) were incubated with AHP-FITC at 4 and 37°C, in the presence or absence of AHP-GNPs as competitor to AHP-FITC. Incubation at 4°C prevented the binding and uptake of AHP-FITC by Caco-2 cells **(Figure 3.12(A)).** Also, incubation of cells with AHP-FITC in the presence of AHP-GNPs reduced the uptake of AHP-FITC by Caco-2. In contrast, cells incubated at 37°C **(Figure 3.12(B))** showed higher binding and uptake of AHP-FITC by Caco2 cells. This further suggests that the binding of AHP was receptor mediated.

To quantitatively assess the cellular uptake, Caco-2 cells were exposed to QD625; AHP-QDs, GNPs; AHP-GNPs or GA; AHP-GA-GNPs. Intracellular concentration of Cd and gold (Au) were detected in the cells using ICP-OES **(Figure 3.13 and 3.14).** Very low level of Cd and Au were detected in cells treated with unfunctionalized QDs (QD625) and GNPs.

This indicated that the particles are unable to bind or to be taken up by the PHB expressing cells, due to absence of AHP on the particles. This is in line with the work done by Kumar and colleaques (2012), where the functionalized particles were taken up by the cells as compared to unfunctionalized NPs. Neither AHP-QDs or AHP-GNPs nor GNPs and QDs were toxic to the cells, as shown in **Figure 3.15 and 3.16.** This correlates with the published studies (Choi and Frangioni, (2010); Kima *et al*., 2012), that most of the functionalized and PEGylated NPs have little effect on the cellular viability. In contrast GA, AHP-GA-GNPs reduced cellular viability in Caco-2 cells at 24 and 48 hrs treatment, **(Figure 3.18 and 3.19)** and induced apoptosis through activation of Caspase-3, as seen by the increase or shift in the fluorescence of Caspase-3 FITC, compared to untreated cells, **(Figure 3.21 and 3.23).**

In order to determine whether the observed *in vitro* effects of AHP are applicable *in vivo*, the male Wistar rats were used. These rats were either obese induced (HF) or standard chow fed rats (LF). It was observed that the obese (HF) rats were much heavier than the lean (LF) rats **(Figure 4.1 and 4.2).** The adipose tissue weights were also heavier and significantly increased in the HF group compared to those in the LF group. The adiposity

index was higher for the HF group as compared to the LF group **(Figure 4.6).** This is in line with published literature where the fat percentage on HF fed rats is higher than in the LF fed rats (Shanmugam *et al*., 2009; Jeyakumar *et al*., 2009).The biodistribution and localization of QDs *in vivo* was assessed in lean and obese rats. No fluorescence was observed in organs and WATs from control group (PBS-treated rats), **(Figure 4.7).** The QDs accumulated in the liver, testes, kidney and brain, but barely distributed in WATs. In contrast, the AHP- QDs accumulates mostly in the WAT but did not accumulate in other organs as indicated in **Figure 4.7.**

Quantitatively high concentrations of Cd was measured mainly in the liver, lungs, spleen, kidney and testes from rats treated with unfunctionalized QDs. Low concentrations of Cd were observed in WATs, except retroperitoneal WAT. In contrast, low levels of Cd were measured mainly in liver, lungs, spleen, kidney and testes from rats treated with AHP-QDs. High concentrations of Cd were measured in WAT. The same trend was observed in the measurement of gold in organs of rats injected with GNPs and AHP- GNPs **(Figure 4.8 and 4.9).** This data correlate with most of the studies reported in the literature (Sonavane *et al*., 2008; Lasagna-Reeves *et al*., 2010; Wang *et al*, 2010; Morais *et al*., 2012) where most of the NPs accumulate mostly in the liver, lungs, kidneys and spleen. Lasagna-Reeves and colleagues, (2010) and Wang and colleagues, (2010) showed that the NPs are taken up by Kupffer cells in the liver, and that the liver is unable to clear exogenous NPs easily. Also and the increasing NPs in the spleen might originate from NPs excreted from lung and kidney since the Kidney is the most important organ for excretion of waste and some metabolites (Zhang *et al*., 2012).

This is because these organs of the reticuloendothelial systems (RES), [liver, spleen and lung] internalize NPs through the action of macrophages and lymphocytes. Taken together, these results indicate that AHP-functionalized NPs accumulate preferentially in WATs, suggesting that AHP targets PHB on the WAT vasculature *in vivo*. This confirmed that PHB is selectively expressed at high levels on the white adipose tissue vasculature. This is supported by the work done by Kolonin *et al*., (2004) and Hossen *et al*., (2010).

This study showed that obese rats had higher serum concentration of NEFA, insulin and glucose compared to the lean rats, **(Figure 4.10 - 4.12).** An increase in NEFA plasma concentration is linked with insulin resistance, which plays a role in the development of diseases such as diabetes mellitus, (Karpe *et al*., 2011). Other studies reported that circulating NEFA stimulate β-cell insulin secretion which eventually contributes to the development of insulin resistance in both skeletal muscle and liver, classical features in obese individuals (Mohamed-Ali *et al*., 1998). In this study, the increase in glucose level in the presence of high insulin level indicate that the obese rats were insulin resistant, that insulin action in the disposal of glucose was limited in insulin sensitive tissues. Elevated NEFA concentrations in obesity could result from the process of fatty acid mobilization from adipose tissue through lipolysis. This then leads to a vicious cycle increasing insulin resistance (Karpe *et al*., 2011).

5.2. Conclusions

NPs suffer from the problem of uptake by the RES (Lasagna-Reeves *et al*., 2010; Choi and Frangioni, 2010; Liu *et al*., 2010; Zhang *et al*., 2012). In addition to NPs size, surface charge plays a key role in RES uptake. This is because the filtration barrier is covered with a layer of polyanionic glycoproteins that repel most large anions, (Choi and Frangioni, 2010). However, surface charge and hydrophobicity promote adsorption or opsonization by serum proteins present in the blood, which bind to foreign particles and increase recognition by phagocytic cells, (Choi and Frangioni, 2010; Liu *et al*., 2010). The binding of these proteins result in an effective increase in hydrodynamic density and can prevent renal clearance of NPs. Therefore, surface modification of NPs using hydrophilic biologically inert, neutral polymers such as PEG will slow the rate of clearance from the blood and retention in the RES (Choi and Frangioni, 2010; Zhang *et al*., 2012).

Therefore, the development of nanotechnology based drug delivery and imaging agents to the WAT vasculature was successful. Figure 5.1 illustrate the potential mechanism by which targeted drug loaded nanoparticles can be delivered to the cells and induce apoptosis. This study shows successful selective delivery of AHP-QDs and AHP-GNPs to WAT vasculature *in vivo*. It also demonstrates that GA and AHP-GA-GNPs induced cell viability and apoptosis *in vitro*. Unfortunately the *in vivo* applications of GA and AHP-GA-GNPs was not done due to time constraits. Moreover, while this study was ongoing. Hossen *et al*., (2012), published the work on vascular-targeted nanotherapy for

obesity using liposomes. Hossen's work support the data obtained in this study and the specificity of prohibitin as a target for the WAT. The success in targeting WAT vasculature has reached the clinical trial stage using proapoptotic peptide $_D$(KLAKLAK)$_2$ (Kolonin *et al*., 2004; Hossen *et al*., 2012). On the other hand the use of $_D$(KLAKLAK)$_2$ might be expensive compared to GA. Therefore there is a need to screen different anti-obesity conjugated nanoparticles. This study represents a potential approach for targeted drug delivery systems to the adipose tissue and also improves the body of knowledge in obesity treatment.

UNIVERSITY *of the*
WESTERN CAPE

5.3. Future work

This study showed a plausible mechanism for treatment of obesity, and a promise of the drug-loaded AHP functionalized GNPs (GA-AHP-GNPs) *in vivo*. This construct needs to be tested in the near future for its anticipated effects in the reduction of body weight of obese rodents. Much of the forecasted promise of nanotechnology in medicine is premised around development of smart technologies, such as theranostic platforms that can target, diagnose and administer treatment to different diseased areas in the body. Therefore, this study forms the basis for a theranostic platform on which other proapototic agents or drugs could be screened for treatment of obesity. For example, antiobesity drugs that have been removed from the market could be revived by attaching them to GNPs functionalized with AHP.
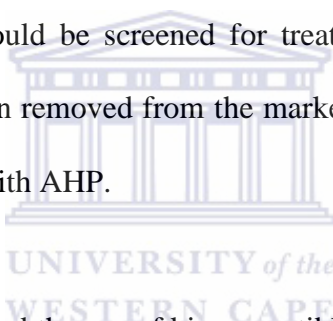
Although this study demonstrated the use of biocompatible nanoparticles, both GNPs and QDs, their potential toxicity remains a concern. The literature is flooded with references indicating GNPs to be non-toxic, and cadmium-based QDs to be toxic. However, the durations of experiments used could not answer whether persistence in the body may produce longer-term toxicities. Therefore, it will be important to study whether longterm exposure to the nanoparticles used in this study have any toxic effects to normal tissues over a long period of time. The use of other less toxic QDs for imaging purposes must be considered in the future to reduced exposure toxic nanoparticles. Moreover, future studies must be setup to determine whether the route of administration of nanoparticles can affect the therapeutic efficancy of the drug-loaded nanoparticles.

And finally, the advancement of biomarker discoveries in obesity and its associated chronic diseases will be key to the development of novel theranostics for obesity treatment. These biomarkers will render new targets for the diseased tissues and reduce bystander toxicity effects of nanoparticles. Continued development and combination of these applications will lead to revolutionary advances in the treatment of obesity, and those foreseen in nanomedicine.
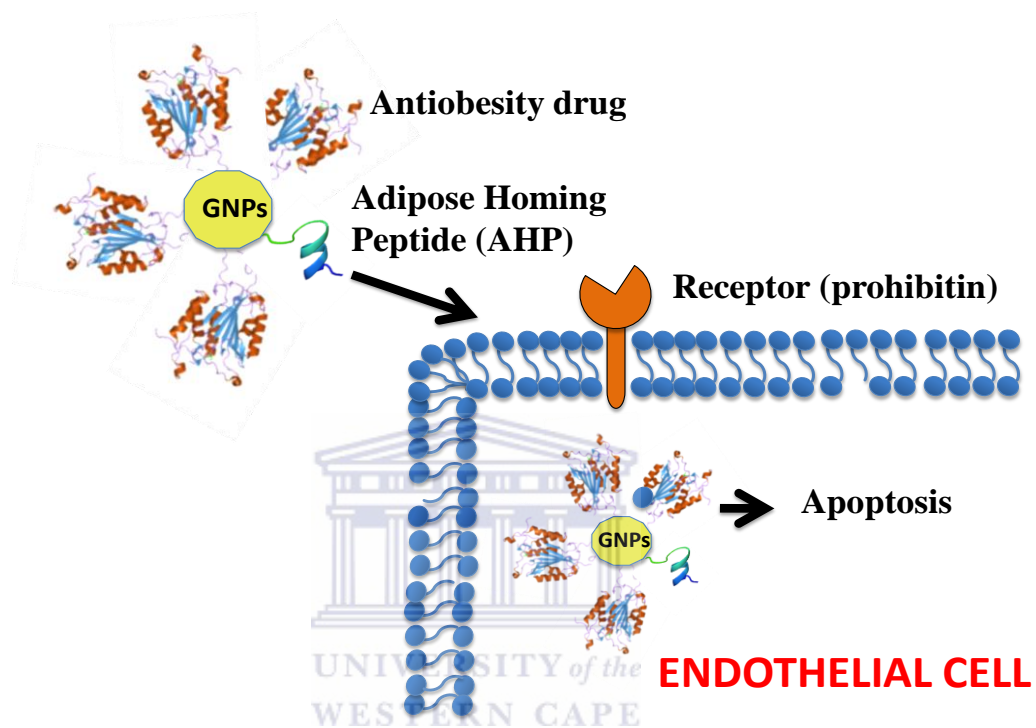
Figure 5.1. The possible mechanism of targeted drug delivery to the endothelial cells for obesity treatment.

REFERENCES

Abdelhalim MAK and Mady MM. 2011. Liver uptake of gold nanoparticles after intraperitoneal administration in vivo: A fluorescence study. *Lipids in Health and Disease*. **10**:195.

Abdelhalim MAK and Moussa SAA. 2013. The gold NPs size and exposure duration effect on the liver and kidney function of rats: *In vivo. Saudi Journal of Biological Sciences.* S1319-562X (13) 00011-9, http://dx.doi.org/10.1016/j.sjbs.2013.01.007.

Absher M. 1973. Hemacytometer counting in Tissue Culture Methods and Applications, Eds. Kruse, P.F. and Patterson, M.K., *Jr. Academic Press*, *NewYork*. 355-397.
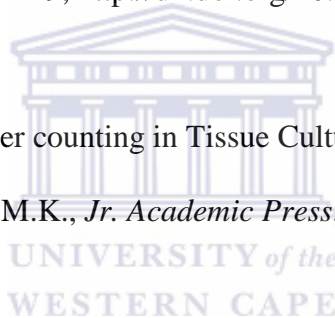
Akerman ME, Chan WCW, Laakkonen P, Bhatia SN, Ruoslahti E. 2002. Nanocrystal targeting, i*n vivo*. *Proceedings of the National Academy of Sciences of the United States of America.* **99**:12617–12621.

Alivisatos, P, Gu, W and Larabell, C. 2005. Quantum dots as fluorescent n probes, *Annual Review of Biomedical Engineering.* **7:** 55–76.

Arap W, Pasqualini R, Ruoslahti E. 1998a. Chemotherapy targeted to tumor vasculature. *Current Opinion in Oncology*. **10**: 560-565.

Arap W, Pasqualini R, Ruoslahti E. 1998b. Cancer treatment by targeted drug delivery to tumor vasculature. *Science.* **279**: 377-380.

Arvizo R, Bhattacharya R, Mukherjee P. 2010. Gold NPs:opportunities and challenges in nanomedicine. *Expert Opinion on Drug Delivery.* **7** (6):753-763.

Atkinson RL. 1997. Use of drugs in the treatment of obesity. *Annual Review of Nutrition.* **17**: 383-403.

Atlanta .2005. Gold NPs may simplify cancer detection. Georgia Institute of Technology and University of California. *Science daily.*

Balasubramanian SK, Jittiwat J, Manikndan J, Ong C, Yu LE, Ong W. 2010. Biodistribution of goldNPs and gene expression changes in the liver and spleen after intravenous administration in rats. *Biomaterial.* **31**:2034-2042.

Balogh L, Nigavekar SS, Nair BM, Lesniak W, Zhang C, Sung LY *et al*. 2007. Significant effect of size on the in vivo biodistribution of gold composite nanodevices in mouse tumor models. *Nanomedicine.* **3**(4):281–296.

Balwierz A, Czech U, Polus A, Filipkowski RK B. Mioduszewska B. 2008. Human adipose tissue stromal vascular fraction cells differentiate depending on distinct types of media. *Cell Proliferation.* **41**, 441-459.

Barteneva N and Vorobjev I. 2010. Quantum dots in microscopy and cytometry: immunostaining applications. *Microscopy: Science, Technology, Applications and Education.* **53**:1-4.

Bays HE, Gonzalez-Campoy JM, Bray GA, Kitabchi AE, Bergman DA, Schorr AB *et al*. 2008. Pathogenic potential of adipose tissue and metabolic consequences of adipocyte hypertrophy and increased visceral adiposity. *Expert Review of Cardiovascular Therapy.* **6**:343e368.

Belsing TZ and Rasmusson UF. 2004. Obesity; the new worldwide epidemic threat to general health and our complete lack of effective treatment. *Endocrinology*. **145940**: 1501-1502.
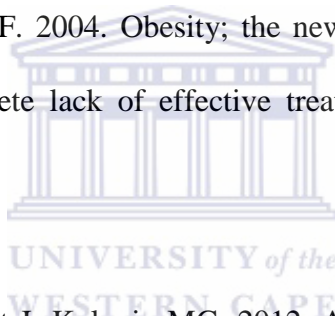
Bertolini F, Lohsiriwat V, Petit J, Kolonin MG. 2012. Adipose tissue cells, lipotransfer and cancer: A challenge for scientists, oncologists and surgeons, *Biochimica et Biophysica Acta*. **1826**: 209-214.

Blüher M.2009. Adipose tissue dysfunction in obesity. *Experimental and Clinical Endocrinology and Diabetes*.**117**: 241-250.

Blüher M. 2013. Adipose tissue dysfunction contributes to obesity related metabolic diseases. *Best Practice and Research Clinical Endocrinology & Metabolism.* 1-15.

Brannon-Peppas L and Blanchette JO. 2004. Nanoparticle and targeted systems for cancer therapy. *Advance Drug Delivery Review*. **56**: 1649-1659.

Bray GA and Greenway FL. 2007. Pharmacological treatment of the overweight patient. *Pharmacological Reviews*. **59,** 151-184.

Bruchez M, Moronne M, Gin P, Weiss S, Alivisatos AP.1998. Semiconductor Nanocrystals as Fluorescent Biological Labels. *Science*. **28** (1):2013-2016.

Buchwald H, Avidor Y, Braunwald E, Jensen MD, Pories W, Fahrbach K, Schoelles K. 2004. Bariatric surgery: a systematic review and meta-analysis. *Journal of the American Medical Association*. **292** (14):1724-37.
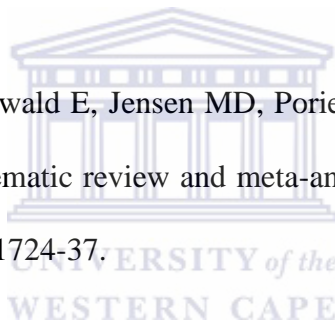
Budihardjo I, Oliver H, Lutter M, Luo X, Wang X. 1999. Biochemical Pathways of Caspase Activation During Apoptosis. *Annual Review of Cell and Developmental Biology*. **15:** 269-90.

Buettner R, Scholmerich J, Bollheimer LC. 2007. High-fat diets: modeling the metabolic disorders of human obesity in rodents. *Obesity (Silver Spring)*. **15**: 798-808.

Byers RJ, Hitchman ER. 2011. Quantum Dots Brighten Biological Imaging. *Progress in Histochemistry and Cytochemistry*. **45**: 201-237.

Cai W, Shin DW, Chen K, Gheysens X, 2006, Peptide-labeled near-infrared quantum dots for imaging tumor vasculature in living subjects. *Nano Letters*. **6**: 669-676.

Cai W and Chen X. 2008. Preparation of peptide-conjugated quantum dots for tumor vasculature-targeted imaging. *Nature Protocols*. **3**: 89-96.

Calle EE, Calle EE, Rodriguez C, Walker-Thurmond K, Thun MJ. 2003. Overweight, obesity, and mortality from cancer in a prospectively studied cohort of U.S. adults. *New England Journal of Medicine.* **348**: 1625-1638.

Campfield LA, Smith FJ, Guisez Y, Devos R, Burn P.1995. Recombinant mouse OB protein: evidence for a peripheral signal linking adiposity and central neural networks. *Science*. **269**:546-549.

Cao Y. 2010. Adipose tissue angiogenesis as a therapeutic target for obesity and metabolic diseases. *Nature Reviews - Drug discovery*. **9**: 107-115.

Chalmers NJ, Palmers RJ, Du-thumm L. 2007. Use of quantum dots luminescent probes to achieve single-cell resolution of human oral Bacteria in Biofilms, Department of Biomedical Science, *American Society for Microbiology.* **739**(20): 630-636.

Chanda, N, Kattumuri, V, Shukla, R, Zambre, A, Katti K, Kulkarni RR, Kan P, Fent GM, Chen PC, Mwakwari SC, Oyelere AK. 2008. Gold NPs from nanomedicine to nanosensing. *Nanotechnology, science and application*. **1**:45-56.

Chanda N, Kattumuri V, Shukla R., Zambre A, Katti K, Upendran A, Kulkarni RR, Kan P, Fent GM, Casteel SW, Smith CJ, Boote E, Robertson JD, Cutler C, Lever, JR, Katti KV, Kannan R. 2010. Bombesin functionalized Gold nanoparticles show *in vitro* and *in vivo* cancer receptor specificity. *Proceedings of the National Academy of Sciences of the United States of America*. **107** (9): 8760-8765.

Chen LM, Zurita AJ, Ardelt PU, Giordano RJ, Arap W, Pasqualini R. 2004. Design and validation of a bifunctional ligand display system for receptor targeting. *Chemical Biology*. **11**:1081-91.
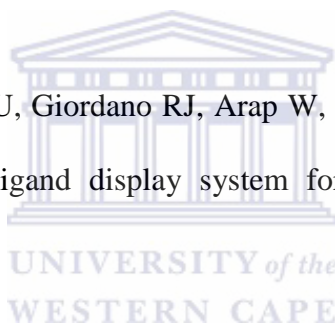
Chen Z, Chen H, Meng H, Xing G, Gao X, Sun B, Shi X, Yuan H, Zhang C, Liu R, Zhao F, Zhao Y, Fang X. 2008. Bio-distribution and metabolic paths of silica coated CdSeS quantum dots. *Toxicology and Applied Pharmacology*. **230**: 364-371.

Chirra HD, Sexton T, i Biswal D, Hersh LB, Hilt JZ. 2011. Catalase-coupled gold NPs: Comparison between the carbodiimide and biotin–streptavidin methods. *Acta Biomaterialia*. **7**: 2865-2872.

Cho WS, Kim S, Han BS, Son WC, Jeong J. 2009. Comparison of gene expression profiles in mice liver following intravenous injection of 4 and 100 nm-sized PEG-coated gold NPs. *Toxicology Letters*. **191**: 96-102.

Choi HS and Frangioni JV. 2010. NPs for Biomedical Imaging: Fundamentals of Clinical Translation. *Molecular Imaging.* **9** (6): 291-310.

Christiaens V and Lijnen HR. 2010. Angiogenesis and development of adipose tissue. *Molecular and Cellular Endocrinology*. **318**: 2-9.

Claphan CJ, Arch JRS, Tadayyon M. 2001. Antiobesity drugs: critical review of current therapies and future opportunities. *Pharmacology and therapeutics*. **89**:81-121.

Clarke SJ and Sharma R. 2006. Angiogenesis inhibitors in cancer mechanisms of Action. *Experimental and Clinical pharmacology*. **29**:9-12.

Connor EE, Mwamuka J, Gole A, Murphy CJ, Wyatt MD. 2005. Gold NPs are taken up by human cells but do not cause acute cytotoxicity. *Small*. **1**:325–327.

Cypess AM. 1999. Identification and important of Brown Adipose tissue in Adult Humans, *Humans*. **360**: 1509-1517.

Daquinag AC, Zhang Y, Kolonin MG, 2011, Vascular targeting of adipose tissue as an anti-obesity approach. *Trends in Pharmacological Sciences*. **32** (5).

De Jong WH, Hagens WI, Krystek P, Burger MC, Sips AJ, Geertsma RE. 2008. Particle size-dependent organ distribution of gold NPs after intravenous administration. *Biomaterials*. **29**:1912-1919.

Despres JP, Lemieux I, Prud'homme D. 2001. Treatment of obesity: need to focus on high risk abdominally obese patients. *British Medical Journal*. **322**: 716-720.

Dizdar O and Alyamac E. 2004. Obesity: an endocrine tumor?. *Medical Hypotheses*. **63**: 790-792.
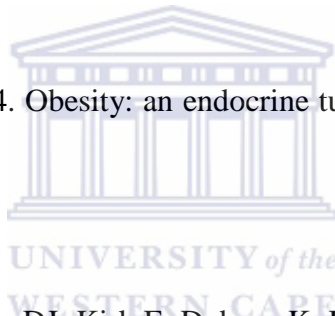
Donnelly JE, Smith B, Jacobsen DJ, Kirk E, Dubose K, Hyder M *et al*.2004. The role of exercise for weight loss and maintenance. *Best Practice and Research, Clinical Gastroenterol*ogy. **18**:1009-1029.

Dubnov G, Brzezinski A, Berry EM. 2003. Weight control and the management of obesity after menopause: the role of physical activity. *Maturitas*. **44**:89-101.

Elangbam CS. 2009. Review paper: current strategies in the development of anti-obesity drugs and their safety concerns. *Veterinary Pathology*. **46**:10-24.

Farokhzad CO and Langer R. 2009. Impact of nanotechnology on drug delivery. *American Chemical Society Nano*. **3**(1): 16-20.

Fent GM, Casteel SW, Kim DY, Kannan R, katti k, Chanda N and Katti K. 2009. Biodistribution of maltose and gum Arabic hybrid goldnanoparticles after intravenous injection in juvenile swine. *Nanomedicine.* **5**:128-135.

Flegal KM, Grauband BI, Williamson DF, Gail MH. 2007. Cause-specific excess deaths associated with underweight, overweight, and obesity. *Journal of the American Medical Association*. **298**:2028-2037.

Formiguera X and Canton A. 2004. Obesity: epidemiology and clinical aspects. *Best Practice & Research Clinical Gastroenterology*.**18** (6): 1125-1146.

Franchello F, deSouza LD, Laureto E, Quivy AA, Dias IFL, Duarte JL. 2013. Influence of bimodal distribution and excited state emission on photoluminescence spectra of InAs self-assembled quantum dots. *Journal of Luminescence*. **137**: 22-27.

Galic S, Oakhill JS, Gregory R. Steinberg GR. 2009. Adipose tissue as an endocrine organ. *Molecular and Cellular Endocrinology*. **316**: 129-139.

Gao X, Yang L, Petros JA, Fray F Marshall FF Jonathan W Simons JW and Nie S. 2005. *In vivo* molecular and cellular imaging with quantum dots. *Current Opinion in Biotechnology.* **16**: 63-72.

Garon EB. Marcu L, Luong Q, Tcherniantchouk O, Gay M, Crooks GM, Koeffler HP. 2007. Quantum dot labeling and tracking of human leukemic, bone marrow and cord blood cells. *Leukemia Research.* **31**: 643-651.

Gaumet M, Vargas A, Gurny R, Delie F. 2008. NPs for drug delivery: particles size parameters. *European journal of Pharmaceutics and Biopharmaceutics.* **69**:1-9.

Ghosh P, Han G, De M, Kim CK, Rotello MV. 2008. Gold nanoparticles in delivery application. *Advanced drug delivery application.* **60** (11): 1307-1315.

Gill RS, Sharma AM, Gill SS, Daniel W. Birch DW, Karmali S. 2011. The impact of obesity on diabetes mellitus and the role of bariatric surgery. *Maturitas.* **69**: 137-140.

Goedecke JH, Jennings CL, lambert. 2005. Obesity in South Africa. *Chronic disease of lifestyle in South Africa* since. 1995-2005.

Goodman CM, McCusker CD, Yilmaz T, Rotello VM. 2004. Toxicity of gold NPs functionalized with cationic and anionic side chains. *Bioconjugate Chemistry*. **15**: 897-900.

Goralski, BK., McCarthy, CT and Hanniman, AE. 2007. Chemerin, a Novel Adipokine That Regulates Adipogenesis and Adipocyte Metabolism. *Journal of Biological Chemi*stry. **282** (38): 28175-28188.

Han LH, Sumiyoshi M, Zhang J, Liu MX, Zhang XF, ZhengYN, Okuda H and Kimura Y. 2003. Anti-obesity action of Salix matsudana leaves (Part 1). Anti-obesity action by polyphenols of Salix matsudana in high fat-diet treated rodentanimals. *Phytotherapy Research*. **17**:1188-1194.
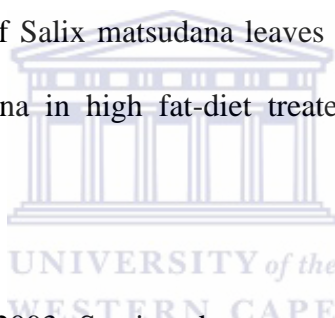
Hanaki K, Momo A, Oku T. 2003. Semiconductor quantum dot/albumin complex is a long-life and highly photostable endosome marker. *Biochemical and Biophysical Research Communications*. **302**: 496-501.

Ho H, Chang C, Ho W, Liao S, Wu C, Wang C. 2010. Anti-metastasis effects of Gallic acid on gastric cancer cells involves inhibition of NF-JB activity and down regulation of PI3K/AKT/small GTPase signals. *Food and Chemical Toxicology*. **48**: 2508-2516.

Hossen MN, kajimoto k, Akita H, Hyodo M, Ishitsuka T, Harashima. 2010. Ligand-based targeted delivery of a peptite modified nanocarrier to endothelial cells in adipose tissue. *Journal of Controlled Release*. **147**: 261-268.

Hossen MN, Kajimoto K, Akita H, Hyodo M, Harashima H. 2012. Vascular-targeted nanotherapy for obesity: Unexpected passive targeting mechanism to obese fat for the enhancement of active drug delivery. *Journal of Controlled Release.* **163**:101-110.

Hsu CL, Huang SL, Yen GC. 2006. Inhibitory effect of phenolic acids on proliferation of 3T3-L1 pre-adipocytes in relation to their antioxidant activity. *Journal of Agricultural and Food Chemistry*. **54**:4191-4197.

Huxley R, Zheleznyakov SME, Reddy,S, Chan,J. 2010. Body mass index, waist circumference and waist hip ratio as predictors of cardiovascular risk, a review of the literature. *European Journal of Clinical Nutrition*. **64**:16-22.

Jain KK. 2005. Nanotechnology in clinical laboratory diagnostics. *Clinica Chimica Acta*. **358**:37-54.

Jaiswal JK, Mattoussi H, Mauro JM, Simon SM. 2003. Long-term Multiple Color Imaging of Live Cells Using Quantum Dot Bioconjugates. *Nature Biotechnology.* **21**:47-51.

Jamieson, T, Bakhshi R, Petrova. 2007. Biological application of Quantum Dot, Review. *Biomaterial*. **28**: 4717-4732.

Jiang W, Papa E, Fischer H. 2004. Semiconductor Quantum dots as contact agent for whole animal imaging. *TRENDS in Biotechnology*. **22.**

Jiao PF, Zhou HY, Chen LX Yan B. 2011. Cancer-Targeting Multifunctionalized Gold NPs in Imaging and Therapy. *Current Medicinal Chemistry*. **18**: 2086-2102.

Jeyakumar SM, Lopamudra P, Padmini S, Balakrishna N, Giridharan3 NV,Vajreswari A. 2009. Fatty acid desaturation index correlates with body mass and adiposity indices of obesity in Wistar NIN obese mutant rat strains WNIN/Ob and WNIN/GR-Ob. *Nutrition and Metabolism*. **6**:27.
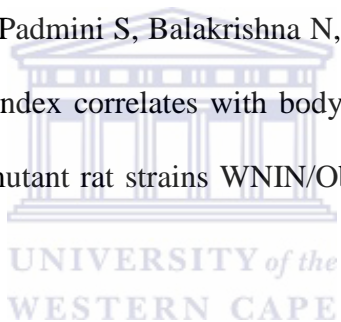
Kahn BB and Flier JS. 2000. Obesity and insulin resistance. *Journal of Clinical Investigation*. **106** (4):473-481.

Kamat PV. 2002. Photophysical, Photochemical and Photocatalytic Aspects of Metal NPs. *Journal of Physical Chemistry B*. **106**:7729-7744.

Karpe F, Dickmann JR, Frayn KN. 2011. Fatty Acids, Obesity, and Insulin Resistance: Time for a Reevaluation. *American Diabetes Association*. **60**(10): 2441-2449. *diabetes.diabetesjournals.org*.

Kasashima K, Ohta E, Kagawa Y. 2006. Mitochandrial Function and Estrogen receptor-dependent, Nuclear Translocation of pleiotropic Human prohibitin 2. *The Journal of Biological Chemistry.* **281947:** 36401-36401.

Katsikari A, Patronidou Chr, Kiparissides C, Arsenakis M. 2009. Uptake and cytotoxicity of poly(d,l-lactide-co-glycolide) NPs in human colon adenocarcinoma cells. *Materials Science and Engineering B.* **165**: 160-164.

Kershaw EE and Flier JS. 2004. Adipose tissue as an endocrine organ. *Journal of Clinical Endocrinology and Metabolism.* **89** (6): 2548-56.

Kim S, Lim YT, Soltesz EG, De Grand AM. 2004. Near infrared fluorescent type II quantum dots for sentinel lymph node mapping. *Nature Biotechnology.* **22:**93-97.

Kim KY. 2007. Nanotechnology platforms and physiological challenges for cancer therapeutics. *Nanomedicine: Nanotechnology, Biology and Medicine.* **3**:103-110.

Kim JH, Kim JH, Kim KW, Kim MH, Yu YS. 2009. Intravenously administered gold NPs pass through the blood-retinal Barrier depending on the particle size, and induce no retinal toxicity. *Nanotechnology.* **20**:505101.

Kima T, El-Saidb WA, Choi J. 2012. Highly sensitive electrochemical detection of potential cytotoxicity of CdSe/ZnS quantum dots using neural cell chip. *Biosensors and Bioelectronics*. **32**: 266-272.

Kirchner C, Liedl T, Kudera S, Pellegrino T, Javier AM, Gaub HE, Stölzle S , Fertig N, Parak WJ. 2005. Cytotoxicity of colloidal CdSe and CdSe/ZnS NPs. *Nano Letters*. **5**: 331-338.

Kissler HJ, Settmacher U. 2013. Bariatric Surgery to Treat Obesity. *Seminars in Nephrology*. **33** (1): 75-89.

Klein S, Zolk O, Fromm MF, Schrödl F, Neuhuber W, Kryschi C. 2009. Functionalized silicon quantum dots tailored for targeted siRNA delivery. *Biochemical and Biophysical Research Communications*. **387**:164-168.

Kolonin MG, Saha PK, Chan L, Pasqualini R, Arap W. 2004. Reversal of obesity by targeted ablation of adipose tissue. *Natural Medicine*. **10** (6): 625-632.

Kamat PV. 2002. Photophysical, Photochemical and Photocatalytic Aspects of Metal Nanoparticles. *Journal of Physical Chemistry B*. **106**:7729-7744.

Kong WH, Bae KH, Jo SD, Kim JS and Park TG. 2011. Cationic lipid-coated GoldNPs Efficient and non-cytotoxicity intracellular siRNA delivery vehicle. *Pharmacal Research.* **29**: 362-374.

Konyanda K, Chen G, Lee Y. 1997. Tissue triglycerides, insulin resistance, and insulin production: implication for hyperinsulinemia of obesity. *Giffort laboratory*. **273940**: E708-E713.

Koo OM, Rubinstein I, Onyuksel H. 2005. Role of nanotechnology in targeted drug delivery and imaging:concise review. *Nanomedicine: Nanotechnology, Biology, and Medicine*. **1:** 193-212.
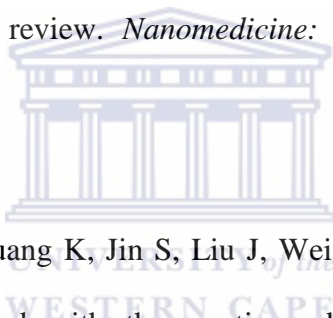
Kumar A, Ma H, Zhang X, Huang K, Jin S, Liu J, Wei T, Cao, W, Zou G, Liang X. 2012. Gold NPs functionalized with therapeutic and targeted peptides for cancer treatment. *Biomaterials*. **33**: 1180-1189.

Langin D. 2006. Adipose tissue lipolysis as a metabolic pathway to define pharmacological strategies against obesity and the metabolic syndrome. *Pharmacological Research*. **53**:482-491.

Larson DR, Zipfel WR, Williams RM, Clark SW, Bruchez MP, Wise FW *et al*.2003. Water-soluble quantum dots for multiphoton fluorescence imaging *in vivo*. *Science*. **300**:1434-6.

Lasagna-Reeves C, Gonzalez-Romero D, Barria MA, Olmedo I, Clos A, Ramanujam VMS, Urayama A, Vergara L, Kogan MJ, Soto C. 2010. Bioaccumulation and toxicity of gold nanoparticles after repeated administration in mice. *Biochemical and Biophysical Research Communications*. **393**: 649-655.

Lavie CJ, Milani RV, Ventura HO. 2009. Obesity and Cardiovascular Disease. *Journal of the American college of Cardiology*. **53** (21): 1925-32.

Leitzmann M, Brinton LA, Lubin JH, Sherman ME, Schatzkin A, and Schairer C. 2006. Weight, Height, and Body Mass Index and Risk for Ovarian Cancer in a Cohort Study. *Association of Educational Psychologists*.**16** (12):869-876.

Li J, Wu D. 2010. Zhengrui Miao and Yan Zhang, Preparation of Quantum Dot Bioconjugates and their Applications in Bio-Imaging. *Current Pharmaceutical Biotechnology*. **11**: 662-671.

Liang Z, Zhang J, Wang L, Shiping W, Fan C, Li G. 2007. A Centrifugation-based Method for Preparation of Gold NPs and its Application in Biodetection. *International. Journal of Molecular Science*. **8**:536-532.

Lim YT, Kim S, Nakayama A, Stott NE, Bawendi MG, Frangioni JV. 2003. Selection of quantum dot wavelengths for biomedical assays and imaging. *Molecular Imaging*. **2**:50–64.

Lira RB, Cavalcanti MB, Seabra MABL, Silva DCN, Amaral AJ, Santos BS, Fontes A. 2012. Non-specific interactions of CdTe/Cds Quantum Dots with human blood mononuclear cells. *Micron*. **43**: 621-626.

Liu Y and Deisseroth A. 2006. Tumor vascular targeting therapy with viral vectors. *The American Society of Heamatology*. **107** (8): 3027-3033.

Liu Y, Meng L, Zhang K, Wu X, Zhang Li, Li B, Chen C. 2010. Characterization of gold nanorods *in vivo* by integrated analytical techniques: their uptake, retention, and chemical forms. *Analytical and Bioanalytical Chemistry*. **396**:1105-1114.

Liu C, Zhang P, Zhai X, Tian F, Li W, Yang J, Liu Y, Wang H, Wang, Liu W. 2012. Nano-carrier for gene delivery and bioimaging based on carbon dots with PEI-passivation enhanced fluorescence. *Biomaterials*. **33**: 3604-3613.

Loos RJF and Bouchard C. 2003. Obesity – is it a genetic disorder?. *Journal of Internal Medicine*. **254** (5):401-425.

Lu F, Doane T L, Zhu J, Burda C. 2012. Gold nanoparticles for diagnostic sensing and therapy. *Inorganica Chimica Acta*. **393:** 142-153.

Mahtab R, Harden HH, Murphy CJ. 2000. Temperature and salt dependent binding of long DNA to protein-sized quantum dots: thermodynamics of "inorganic protein" DNA interactions. *Journal of the American Chemical Society*. **122**: 14-17.

Manish G and Vimukta S. 2011. Targeted drug delivery system: A Review. *Research Journal of Chemical Sciences*. **1**:2.

Mattousi H, Mauro JM, Goldman ER, Anderson AP, Sunder VC, Bawendi MG. 2000. Self-assembly of CdSe-ZnS quantum dots bioconjugates using an engineered recombinant protein. *Journal of the American Chemical Society.***122**: 12142-12150.

Maurya DK, Nandakumar N and Devasagayam TPA. 2011. Anticancer property of gallic acid in A549, a human lung adenocarcinoma cell line and possible mechanisms. *Journal of Clinical Biochemical Nutrition.***48** (1):85-90.

McNeil ES. 2005. Nanotechnology for the Biologist. *Journal of Leukocyte Biology*. **78**. (10:1189/jlb.0205074).

Meyer M, Essack M, Kanyanda S, Rees JG, 2008. A low-cost flow cytometric assay for the detection and quantification of apptosis using an anionic halogenated fluorescein dye. *BioTechniques*. **45**: 317-320.

Mishra S, Murphy LC, Nyomba G, Murphy LJ 2005. Prohibitin: a potential target for new therapeutic. *Trends in Molecular Medicine.* **10**: 1016.

Misra R, Acharya S, Sahoo SK. 2010. Cancer nanotechnology: application of nanotechnology in cancer therapy. *Drug Delivery Today*. **15:** (19/20).

Mohamed-Ali V, Pinkney JH, Coppack SW. 1998. Adipose tissue as an endocrine and paracrine organ. *International Journal of Obesity*. **22**: 1145-1158.

Mokdad AH, Ford ES, Bowman BA, Dietz WH, Vinicor F, Bales VS, Marks JS. 2003. Prevalence of obesity, diabetes, and obesity-related health risk factors. *Jama*. **289**: 76-79.

Morais T, Soares ME, Duarte JA, Soares L, Maia S, Gomes P, Pereira E, Fraga S, Carma H and Bastos M. 2011. Effects of surface coating on the biodistribution profile of gold NPs in rats. *European Journal of Pharmaceutics and Biopharmaceutics*. **80**: 185-193.

Morrison RF and Farmer SR.2000. Hormonal signaling and transcriptional control of adipocyte differentiation. *Journal of Nutrition*. **130**: 3116S-3121S.

Ngamwongsatit P, Banada PP, Panbangred W, Bhunia AK. 2008. WST-1-based cell cytotoxicity assay as a substitute for MTT-based assay for rapid detection of toxigenic Bacillus species using CHO cell line. *Journal of Microbiological Methods*. **73:** 211-215

Niidome T, Yamagata M, Okamoto Y, Akiyama Y, Takahashi H, Kawano T, Katayama Y,Niidome Y. 2006. PEG-modified gold nanorods with a shealth character for *in vivo* application. *Journal of Control Release*.**114**: 343-347.

OwensIII DE and Peppas NA. 2006. Optimization, biodistribution and pharmacokinetics of polymeric NPs. *Journal of Pharmaceutics*. **307**: 93-102.

Paciotti GF, Kingston DGI, Tamarkin L. 2006. Colloidal gold NPs: a novel nanoparticle platform for developing multifunctional tumor-targeted drug delivery vectors. *Drug Development Research*. **67** (1): 47-54.

Pandya NM, Dhalla NS, Santani DD. 2006. Angiogenesis-a new target for future therapy. *Vascular Pharmacology*. **44**: 265-274.
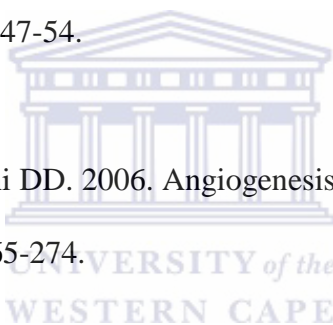
Papasani MR, Wang G, Hill RA. 2012. Gold NPs: the importance of physiological principles to devise strategies for targeted drug delivery. *Nanomedicine: Nanotechnology, Biology, and Medicine*. **8**: 804-814.

Parimal PM, Shah Y, Sen DJ. 2010. Gold NPs: A new approach for cancer detection. *Journal of Chemical and Pharmaceutical Research.* **2**(1): 30-37.

Park K. 2007. Nanotechnology: what it can do for drug delivery. *Journal Control Release*. **120**: 1-3.

Parveen S and Sahoo SK, 2008, Polymeric NPs for cancer therapy. *Journal of Drug Targeting.* **16**: 108-123.

Parveen S, Misra R, Sanjeeb K. Sahoo SK. 2012. NPs: a boon to drug delivery, therapeutics, diagnostics and imaging. *Nanomedicine: Nanotechnology, Biology, and Medicine.* **8**:147-166.

Pathak S, Davidson MC, Silva GA. 2007. Characterization of the Functional Binding Properties of antibody Conjugated Quantum Dots. *Nano Letters.* **7**:1839-1845.

Paull J. 2008, Nanotechnology: The next challenge for organic. *Journal of organic system.* **3** (1).
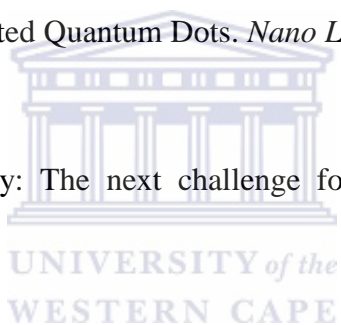
Pellegrina CD, Padovani G, Mainente F, Zoccatelli G, Bissoli G, Mosconi S, Veneri G, Peruffo A Andrighetto G, Rizzi C, Chignola R. 2005. Anti-tumour potential of a gallic acid-containing phenolic fraction from Oenothera biennis. *Cancer Letters.* **226**: 17-25.

Phan-Hug F, Beckmann JS, Jacquemont S. 2012. Genetic testing in patients with obesity. *Best Practice & Research Clinical Endocrinology & Metabolism*. **26**: 133-143.

Pinaud F, King D, Moore HP, Weiss S. 2004. Bioactivation and cell targeting of semiconductor CdSe/ZnS nanocrystals with phytochelatin-related peptides. *Journal of the American Chemical Society*. **126**: 6115-6123.

Popovtzer R, Agrawal A, Kotov AN, Popovtzer A, Balter J. 2008. Targeted Gold NPs Enable molecular CT imaging of cancer. *International Journal of Nanomedicine*. **8** (9120): 4593-4596.

Prieto-Hontoria PL, Pérez-Matute P, Fernández-Galilea M, Bustos M, Martínez JA, Moreno-Aliaga MJ. 2011. Role of obesity-associated dysfunctional adipose tissue in cancer: A molecular nutrition approach. *Biochimica et Biophysica Acta*. **1807**: 664-678.

Qatanani M and Lazar MA. 2007. Mechanisms of obesity-associated insulin resistance: many choices on the menu. *Genes and Development*. **21**: 1443-1455.

Qiu Y, Liu Y, Wang L, Xu L, Bai R, Ji Y, Wu X, Zhao Y, Li Y, Chen C. 2010. Surface chemistry and aspect ratio mediated cellular uptake of Au nanorods. *Biomaterials*. **31**: 7606-7619.

Racette SB, Deusinger SS, Deusinger R. 2003. Obesity: Overview of prevalence, etiology, and treatment. *Physical Therapy*. **83** (3):276-88.

Rastogi S, Joshi B, Fusaro G, Chellappan S. 2006. Camptothecin Induces Nuclear Export of Prohibitin Preferentially in Transformed Cells through a CRM-1-dependent Mechanism. *The Journal of Biological Chemistry*. **281** (5): 2951-2959.

Rastogi S, Joshi B, Dasgupta P, Morris M, Wright K, Chellappan S. 2006. Prohibitin Facilitates Cellular Senescence by Recruiting Specific Corepressors to inhibit E2F target genes. *Molecular and Cellular Biology*. **26** (11): 4161-4171.

Ravi Kumar MNV. 2008. Handbook of Particulate Drug Delivery (2-Volume Set), *American Scientific Publishers*. ISBN 1-58883-123-X.

Raynal I, Prigent P, Peyramaure S,*et al.* 2004. Macrophage endocytosis of superparamagnetic iron oxide NPs: mechanisms and comparison of ferumoxides and ferumoxtran-10. *Investigative Radiology*. **39**: 56-63.

Reuveni T, Motiei M, Romman Z, Popovtzer A, Popovtzer R. 2011. Targeted gold nanoparticles enable molecular CT imaging of cancer: an *in vivo* study. *International Journal of Nanomedicine*. **6**: 2859-2864.

Roger WJ and Basu P. 2005. Factors regulating macrophage endocytosis of nanoparticles: implications for targeted magnetic resonance plaque imaging. *Atherosclerosis*. **178**:67-73.

Rosmond R and Bjorntorp. 2000. The role of antidepressants in the treatment of abdominal obesity. *Medical Hypotheses*. **54** (6): 990-4.

Rosenthal SJ, Chang JC, Kovtun O, McBride JR, Tomlinson ID. 2011. Tomlinson ID, Biocompatible Quantum Dots for Biological Applications. *Chemistry and Biology*. **18**(1):10-24.

Sahin H, Betul Cicek B, Yılmaz M, Ongan D, Inanc N,Aykut M, Elmali F. 2011. Obesity prevalence, waist-to-height ratio and associated factors in adult Turkish males. *Obesity Research & Clinical Practice*. **5**: e29-e35.

Sahoo SK, Parveen S, Panda JJ. 2007. The present and future of nanotechnology in human health care. *Nanomedicine: Nanotechnology, Biology, and Medicine*. **3**: 20-31.

Savla R, Taratula , Garbuzenko O, Minko T. 2011. Tumor targeted quantum dot-mucin 1 aptamer-doxorubicin conjugate for imaging and treatment of cancer. *Journal of Controlled Release*. **153**: 16-22.

Scherer PE. 2006. Adipose tissue: from lipid storage compartment to endocrine organ. *Diabetes*. **55**: 1537-1545.

Schleicher M, Shepered BR, Suarez Y. 2008. Prohibitin-1 maitas the angiogenic capacity of endothelial cells by regulating mitochondrial function and senescence. *The Journal of Cell Biology*. **18091** : 101-112.

Shaffer C. 2009. *In vivo* imaging technology spotlight. *Biocompare*. (http://www.biocompare.com/Editorial-Articles/41639-in-vivo-Imaging).

Sharma A and Qadri A. 2004. Vi polysaccharide of Salmonella typhi targets the prohibitin family of molecules in intestinal epithelial cells and suppresses early inflammatory responses. *Proceedings of the National Academy of Sciences.* **101**(50): 17492-17497.

Shulman GI. 2000. Cellular mechanisms of insulin resistance. *Journal of Clinical Investigation*. **106**: 171-176.

Sidik MS and Ahmad R. 2004. Childhood obesity; contributing factors consequences and intervention. *Malaysian Journal of Nutrition*. **10** (10): 13-22.

Sirin O and Kolonin MG. 2012. Treatment of obesity as a potential complimentary approach to cancer therapy. *Drug discovery today*. **18** (11-12): 567-73.

Sonavane G, Tomoda k and makino K. 2008. Biodistribution of colloidal gold NPs after intravenous administration: effect of particles size. *Biointerfaces*. **66**: 274-280.

Sul HS and Wang D. 1998. Nutritional and hormonal regulation of enzymes in fat synthesis: studies of fatty acid synthase and mitochondrial glycerol-3-phosphate acyltransferase gene transcription. *Annual Review Nutrition*. **18**: 331-351.

Sun L, Liu D, Wang Z. 2008. Functional gold nanoparticle-peptide complexes as cell targeting agents. *Langmuir*. **24**: 10293-10297.

Swinburn BA, Sacks G, Hall KD, McPherson K, Finegood DT, Moodie ML, Gortmaker SL. 2011. The global obesity pandemic: shaped by global drivers and local environments. *Lancet*. **378:** 804-14.

Tapiero H, Tew KD, Ba GN, Mathe G, 2002, Polyphenols: do they play a role in the prevention of human pathologies?. *Biomedicine & Pharmacotherapy*. **56**: 200-207.

Tiwari Pm, Vig K, Dennis VA, Singh SR. 2011. Functionalized gold NPs and the biomedical application. *Nanomaterial.* **1**(1): 31-61.

Trayhurn P and Beattie JH. 2001. Physiological role of adipose tissue: white adipose tissue as an endocrine and secretory organ. *Proceedings of the Nutrition Society*. **60**: 329-339.

Trayhurn P, Bing C, Wood IS. 2006. Adipose Tissue and Adipokines Energy Regulation from the Human Perspective. *American Society for Nutrition*. (0022-3166/06 $8.00).

Turkevitch J, Stevenson PC, Hillier J. 1951. A study of the nucleation and growth process in the synthesis of colloidal gold. *Faraday Society.* **11**, 55-75.

Van Kruijsdijk RC, van der Wall E, Visseren FL. 2009. Obesity and cancer: the role of dysfunctional adipose tissue. *Epidemiology, Biomarkers & Prevention.***18**: 2569-2578.

Vazquez-Vela MEF, Torres N and Tovar AR. 2008. White adipose tissue as endocrine organ and its role in obesity. *Archives of Medical Research*. **39**: 715-728.

Walling AM, Novat JA, Shepard EJR. 2009. Quantum dots for live cell and *In vivo* imaging. *International. Journal of Molecular Sciences.* **10** (2): 441-491.

Wang L, Zhang J, Wang X, Huang Q, Pan D, Song S, Fan C. 2008. Gold nanoparticle-based optical probes for target- responsive DNA structures. *Gold Bulletin*. **41**: 37-41.

Wang L, Li Y, Zhou L, Liu Y, Meng L, Zhang K, Wu X, Zhang L, Li B, Chen C. 2010. Characterization of gold nanorods *in vivo* by integrated analytical techniques: their uptake, retention, and chemical forms. *Analytical Bioanalytical Chemistry*. **396**: 1105-1114.

Weissleder R. 2001. A clearer vision for *in vivo* imaging. *Nature Biotechnology*.**19**: 316-317.

Wickline SA, Gregory MD, Lanza M. 2003. Nanotechnology for molecular imaging and Targeted therapy. *Circulation, Journal of the American Heart Association*. **10**:1161/01.

World Health Organization (WHO). 2006. Obesity and Overweight. (http://www.who.int/ media centre/factsheets/fs311/en/index.html).

World Health Organization. 2010. WHO global infobase. Data for saving lives. *International comparisons,* Accessed 4 August 2012. (https://apps.who.int/infobase/Comparisons.aspx).

Wosnitza M, Hemmrich K, Groger A, Graber S, Paulla N. 2007. Plasticity of human adipose stem cells to perform adipogenic and endothelial differentiation. *Differentiation*. **75**: 12-23.

Xiao Y and Barker PE. 2004. Semiconductor nanocrystal probes for human metaphase chromosomes. *Nucleic Acids Research*. **32**: e28.

Xing Y and Rao J. 2008. Quantum dots bioconjugate *in vitro* diagnostic and *in vivo* imaging. *Cancer Biomarkers*. **4**: 307-319.

Xing Y, Chaudry Q, Shen C, Kon KY, Zhau HE, Nie S. 2007. Bioconjugated quantum dots for multiplexed and quantitative immunohistochemistry. *Nature Protocols*. **2**: 1152-1165.

Yang P, Zhang A, Sun H, Liu F, Jiang Q, Cheng X. 2010. Highly luminescent quantum dots functionalized and their conjugation with IgG. *Journal of Colloid and Interface Science*. **345**: 222-227.

Yezhelyer MV, Qi L, O'Regan RM, Ni S, Gao X. 2001. Proton-sponge-coated Quantum dots for siRNA delivery and intracellular imaging. *Advanced Biomaterials*. **130928**: 9006-9012.
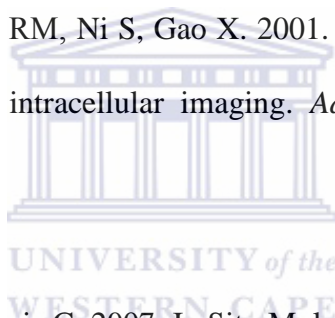
Yezhelyev MV, Al-Hajj A, Morris C. 2007. In Situ Molecular Profiling of Breast Cancer Biomarkers with Multicolor Quantum Dots. *Advanced Biomaterials*. **19**: 3146-3151.

Yin L, Wei Y, Wang Y, Xu Y, Yang Y. 2013. Long Term and Standard Incubations of WST-1 reagent reflect the same inhibitory trend of cell viability in rat airway smooth muscle cells. *International Journal of Medical Science*. **10**(1): 68-72.

You BR, Moon HJ, Han YH, Park WH. 2010. Gallic acid inhibits the growth of HeLa cervical cancer cells via apoptosis and/or necrosis. *Food and Chemical Toxicology*. **48**: 1334-1340.

Zhang B, MacNaul K, Szalkowski D.1999. Inhibition of adipocytes differentiation by HIV protease inhibitors. *Journal of Clinical Endocrinology and Metabolism*. **84**: 4274-77.

Zhang X, Wu D, Shen X, Liu P, Fan F; Fan S. 2012. *In Vivo* Renal Clearance, Biodistribution, Toxicity of Gold nanoclusters. *Biomaterial*. **33**: 4628-4638.

Zhu X-X, Cao Y-C, Jin X, Yang J. 2008. Optical Encoding of Microbeads Based on Silica Particle Encapsulated Quantum Dots and Its Applications. *Nanotechnology*. **19**: 1-8.

Zrazhevskiy P, Gao X. 2009. Multifunctional quantum dots for personalized medicine. *Nano Today*. **4**: 414-428.

http://sharnyandjulius.com/healthy-food-pyramid-is-making-you-fat/

http://www.pathologyoutlines.com/topic/softtissueadiposebrownfat.html

http://health-care-org.blogspot.com/2013/01/being-modest-obese-might-not-present.html

http://stevegallik.org/sites/histologyolm.stevegallik.org/htmlpages/HOLM_Chapter04_Page01.html.